

3D SIMULATION OF MAGNETOTELLURIC DATA USING FINITE DIFFERENCE EIGENMODE METHOD

Ph.D. THESIS

by

KRISHNA KUMAR



**DEPARTMENT OF EARTH SCIENCES
INDIAN INSTITUTE OF TECHNOLOGY ROORKEE
ROORKEE - 247 667 (INDIA)
AUGUST, 2009**

3D SIMULATION OF MAGNETOTELLURIC DATA USING FINITE DIFFERENCE EIGENMODE METHOD

A THESIS

*Submitted in partial fulfilment of the
requirements for the award of the degree
of*

DOCTOR OF PHILOSOPHY

in

EARTH SCIENCES

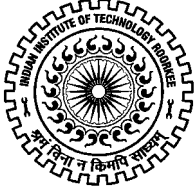
by

KRISHNA KUMAR



**DEPARTMENT OF EARTH SCIENCES
INDIAN INSTITUTE OF TECHNOLOGY ROORKEE
ROORKEE-247 667 (INDIA)
AUGUST, 2009**

**©INDIAN INSTITUTE OF TECHNOLOGY ROORKEE, ROORKEE, 2009
ALL RIGHTS RESERVED**



INDIAN INSTITUTE OF TECHNOLOGY ROORKEE ROORKEE

CANDIDATE'S DECLARATION

I hereby certify that the work which is being presented in the thesis entitled **3D SIMULATION OF MAGNETOTELLURIC DATA USING FINITE DIFFERENCE EIGENMODE METHOD** in partial fulfilment of the requirements for the award of the Degree of Doctor of Philosophy and submitted in the Department of Earth Sciences of the Indian Institute of Technology Roorkee, Roorkee is an authentic record of my own work carried out during a period from July, 2004 to August, 2009 under the supervision of Dr. Sri Niwas, Professor and Dr. Pravin K. Gupta, Professor, Department of Earth Sciences, Indian Institute of Technology Roorkee, Roorkee.

The matter presented in the thesis has not been submitted by me for the award of any other degree of this or any other Institute.

(KRISHNA KUMAR)

This is to certify that the above statement made by the candidate is correct to the best of our knowledge.

(Pravin K. Gupta)
Supervisor

(Sri Niwas)
Supervisor

Date:

The Ph.D. Viva-Voice Examination of **Mr. KRISHNA KUMAR**, Research Scholar, has been held on _____

Signature of Supervisors

Signature of External Examiner

ABSTRACT

Magnetotelluric method is used to delineate the subsurface conductivity structure of earth using natural electromagnetic waves in the frequency range 10^{-5} Hz – 10^5 Hz as source field. These natural fields are generated mainly by thunderstorm activity (>1 Hz) and the interaction of solar wind with the earth's magnetosphere (<1 Hz) (Kaufman and Keller, 1981). The horizontal electric and magnetic field components are measured at the earth's surface and analyzed to infer electrical resistivity distribution in the earth's interior. The two orthogonal horizontal electric field components are linearly related to the two horizontal magnetic field components through appropriate transfer function (Tikhonov, 1950 and Cagniard, 1953). The depth of penetration of electromagnetic (EM) wave depends upon its frequency and conductivity distribution of medium.

The EM fields are studied using Maxwell's equations, coupled in electric (**E**) and magnetic field (**B**) vectors. These equations are transformed into vector Helmholtz equation for decoupled E-field or B-field. The vector Helmholtz equation is used to solve for the response of a given earth model. Typical model parameters are geometry of the target and spatial distribution of conductivity. The estimation of model parameters from the physical fields, measured on earth surface, is termed as an inverse problem, while the mapping of model parameters to measured fields is known as a forward problem. For a good inversion algorithm, an efficient forward modeling code is needed. This work deals with the development of an efficient 3D forward modeling algorithm.

The popular numerical modeling schemes can be broadly classified into Integral Equation Methods (IEM) and Differential Equation Methods (DEM) (Finite Difference Method (FDM), Finite Element Method (FEM)). While IEM can be efficiently used only

for computing the responses of confined targets buried in a layered earth, the DEMs are capable of modeling arbitrary complex distributions of conductivity. The coefficient matrix in case of IEM is full but small in size, while in case of DEM it is large but grossly sparse. In DEMs use of staggered grid is popular, particularly in 3D case, because its use analytically incorporates the divergence equation of magnetic field. FDM with staggered grid is used in the present study.

Instead of using FDM to solve the complete Boundary Value Problem (BVP) with sources, we have first studied fundamental nature of the eigenvalue problem obtained in case of source free BVP. Eigenvalues and eigenvectors, collectively known as eigenmodes, exhibit the basic characteristics of the response to a given physical property distribution in the model. After estimating the eigenmodes for a given geometry and physical property distribution, the EM response for a given source frequency can be obtained through superposition of the eigenvectors. In geophysical applications, similar approach was implemented by Druskin et al. (1994, 1999) and Stuntebeck (2003).

In the eigenmode method, the responses for additional frequencies can be obtained in negligible time. In contrast, in case of traditional use of FDM to generate multifrequency responses, one has to re-run the code for each frequency. During evaluation of superposition coefficients, the eigenvalues appear in the denominator, implying that the smaller eigenvalues contribute more significantly to the field. Therefore, one need compute only a subset of the smallest eigenvalues and corresponding eigenvectors for a given degree of accuracy of field values. For evaluation of this subset, the iterative methods serve better than the direct methods, particularly in case of 3D problems where the matrix size is extremely large.

The most widely used methods for evaluating a subset of eigenmodes are Krylov subspace projection methods. In these methods, only product of the matrix with a vector is needed and, therefore, only non-zero elements of the sparse coefficient matrix need be stored. Lanczos and Arnoldi methods are two popular Krylov subspace methods. Former is used for symmetric matrices while the latter is used for non-symmetric matrices.

Before launching the development of 3D code, we gained experience of eigenmode method by developing 1D and 2D forward modeling codes. The FDM coefficient matrix is symmetric. In case of 3D, the symmetric coefficient matrix is of large size, which is reduced in size by using the current divergence equation, to eliminate the z-component of electric field from expressions. This step transforms the symmetric coefficient matrix to a nonsymmetric one, albeit of much smaller size. So, Lanczos method is used to obtain the eigenmodes in 1D and 2D case while Arnoldi method is used in case of 3D. The eigenmode evaluation subprogram of our algorithm is adapted from the routines of ARPACK (1997) software which is based on Implicit Restarted Lanczos/Arnoldi Method (IRLM/IRAM) given by Sorensen et al. (1992). ARPACK works in different modes such as 'regular', 'shift and invert' etc. The regular mode is efficient in obtaining largest magnitude eigenvalues while invert mode is efficient in obtaining smallest magnitude ones. Since we are interested in the smallest eigenvalues, shift and invert mode is used. Further, to circumvent the problem of loss of Lanczos vector orthogonality in case of degenerate eigenvalues, their complete reorthogonalization has been employed.

The development of 3D algorithm was carried out on a PC. As a result, we had to introduce several I/O detours and had to work under severe limitations imposed on the size

of the grid. Therefore, we designed several appropriate experiments using the coarse grid to validate the 3D algorithm.

The organization of seven chapters in the thesis is presented next.

In **chapter one**, the literature review is presented.

In **chapter two**, the theory for 3D Magnetotellurics using electric field vector Helmholtz equation, obtained from Maxwell's equations, is discussed. Different types of boundary conditions such as domain and interface boundary conditions are described. The eigenmode problem is formulated and the eigenmodes are used to obtain the EM response for multi-frequency case. The derivations of response functions, i.e. apparent resistivity and phase corresponding to both 2D-TE and 2D-TM modes are discussed.

In **chapter three** implementation of FDM on staggered grid is described. The domain is discretized into a grid comprising cuboids. We have followed the convention that electric field components are defined on midpoints of edges while magnetic field components are defined at the centers of surfaces. The derivation of matrix equation from the governing partial differential equation and boundary conditions is presented next. The coefficient matrix obtained is symmetric and about one third of its eigenvalues are zero. These spurious zero eigenvalues do not contribute to field synthesis. This knowledge is made use of in reducing the coefficient matrix size to the number of non-zero eigenvalues by eliminating the vertical component of electric field and working only with the horizontal components. This step transformed the symmetric coefficient matrix to a non-symmetric one. A brief review of ARPACK subprograms adapted to determine the eigenmodes is presented.

In **chapter four**, the details of various stages of development of algorithm, MT_3D_EA, are discussed. Starting with symmetric matrix eigenmode evaluation using Singular Value Decomposition (SVD), the Lanczos and Arnoldi methods in ‘regular’ and in ‘shift and invert’ modes are presented. In invert mode a matrix equation need be solved so efficient matrix solvers based on Conjugate Gradient Method and various preconditioners used are described next. Finally, the algorithm is presented along with flow charts of important subprograms.

In **chapter five**, the synthetic experiments designed to test and validate the algorithms MT_2D_EA and MT_3D_EA are discussed. First we performed different tests such as grid convergence and no contrast case to check the consistency and accuracy. Then, we compared the results of 2D version of our algorithm with published results. We studied two 2D models (simple and complex) taken from COMMEMI (Zhdanov et al., 1997) and obtained good match with the average values given in the paper. The RMS errors for simple and complex models are 0.01 and 0.06 respectively. Next we studied the impact on the field values of using different percentages of eigenmodes. We observed that for obtaining accurate field values, 5% eigenmodes were sufficient for the conductive block model whereas for the resistive block 20% eigenmodes were needed for same accuracy. In the multi-frequency experiment, we studied Weaver (1976) model. We used two grids for time periods 1s and 10s and generated the responses (true) for these grids. Next we generated the response at 1s using 10s eigenmodes and vice versa and found excellent fit with the corresponding true responses. In case of 3D, additional experiment conducted was to verify that 3D apparent resistivity values converge to corresponding 2D values as the strike length in one direction is extended. We compared our 3D response with the

published apparent resistivity values of the model described as 3D-2 in COMMEMI report and found a good fit.

In **chapter six**, we have used MT_3D_EA algorithm to generate 3D models whose responses are commensurate with the MT field data acquired by Israil et al. (2008) in Garhwal Himalaya. Tyagi (2007) and Israil et al. (2008) analyzed this data using WingLink software, and proposed the first 2D geoelectric model. We used this model as base model for our study. Using MT_2D_EA algorithm, we generated responses of this model at two time periods and found excellent match with the corresponding WINGLINK responses. Due to limited computer resources, we could not run the complex model using MT_3D_EA algorithm. So, for 3D study we designed a simplified 3D model retaining the dominant feature of conducting block. We generated the 3D responses for 4 strike length values (20 km, 50 km, 70 km and 100 km) of the conducting body. At 100 km strike length the 3D response of the model matches well with the 2D response. Finally, we experimented with the strike-length and the depth of burial of the block and generated equivalent 3D models that would explain the conducting anomaly in the observed data. The 3D geometry of the conductive block, buried under the Roorkee-Gangotri profile near MCT, can be taken as 70 km strike, 20-26 km width and 4 km depth and its resistivity is estimated as 8 Ω -m. However, the detailed 3D study suggests that the conductive block can be approximated as a 2D one.

In **chapter seven**, we have discussed the strategies for further improvement of our algorithm.

LIST OF PUBLICATIONS

a) Conference/ Symposia

1. **Krishna Kumar**, Pravin K. Gupta and Sri Niwas, 2007. 3D Finite Difference Scheme for magnetotelluric data using the Implicitly Restarted Lanczos Algorithm. National seminar on “Mapping and modeling of deep crustal features using geoelectromagnetic and other geophysical methods”, Department of Applied Geophysics, ISM University, Dhanbad, India.
2. **Krishna Kumar**, Pravin K. Gupta and Sri Niwas, 2008. Efficient 2D modeling using Implicitly Restarted Lanczos Method. 7th International conference and exposition on petroleum geophysics “Hyderabad 2008”, Bi-annual conference of Society of Petroleum Geophysicists (SPG), an affiliate society of SEG, January, 14-16, HICC Hyderabad, India.
3. **Krishna Kumar**, Pravin K. Gupta and Sri Niwas, 2008. Efficient geomagnetic modeling using Implicitly Restarted Lanczos Method. International conference on tectonics of the Indian subcontinent, March, 3-6, IIT Bombay, Mumbai, India.
4. **Krishna Kumar**, Pravin K. Gupta and Sri Niwas, 2008. 3D Finite Difference Scheme for MT data using eigenmodes. 1st Indo-German Workshop on electromagnetic induction studies for complex geological problems, March, 14-18, Lonavala, Mumbai, India.

ACKNOWLEDGEMENTS

Having an opportunity to acknowledge the help I have had, in completing the research work towards the doctoral degree, is really the thing I have been waiting for. And here the names first come to my mind are that of my learned supervisors **Prof. Pravin K. Gupta** and **Prof. Sri Niwas**, Department of Earth Sciences, Indian Institute of Technology Roorkee, who have guided me in real sense. I wish to express my deep sense of gratitude and appreciation to them for their stimulating supervision with invaluable suggestions, keen interest, constructive criticisms and constant encouragement during the course of the present study. I learned a lot from them not only in the academic area but in other spheres of life also. I wholeheartedly acknowledge their full cooperation that I received from the very beginning of this work up to the completion in the form of this thesis.

During this research, the department has had two heads; *Prof. R. P. Gupta* and *Prof. V. N. Singh* and most fortunately they encouraged me by extending every sort of help as and when sought for.

The author is especially thankful to *Prof. M. Israil*, Department of Earth Sciences for their invaluable help and advice from time to time as when needed. The author is also thankful to *Dr. Navneet Gupta* and *Mr. Tarun*, Computer Centre, IIT Roorkee, for providing the computation facility.

The author would like to make a special note of thank to all faculty members of the Department of Earth Sciences for their co-operation. Thanks are also to *Prof. Deepak Kashyap*, Department of Civil Engineering for their constant encouragement during my research work. The author also acknowledge his deep sense of gratitude to *Late Prof. P. Weidelt*, Institute of Geophysics and Meteorology, TU Braunschweig, Germany, *Prof. B.*

Tezkan, Institute for Geophysics, Gottingen, Germany, *Dr. K. M. Strack* and *Dr. Wei Qian*, KMS Technologies, Huston , USA whose critical and timely suggestions proved to be helpful.

The author is highly obliged and wishes to express my sincere thanks to the technical staff of the Department of Earth Sciences, especially to *Mr. Nayar*, *Mr. Rakesh*, *Mr. V. K. Saini*, *Mr. S. K. Sharma*, who have helped him in all possible ways during the official work.

The financial support provided by Ministry of Human Resources and Development (MHRD), New Delhi and KMS Technologies, Huston, USA to complete the present work is highly acknowledged.

When hurdles appeared insurmountable and target unachievable, the encouragement and camaraderie of friends helped keep things in perspective. Author wishes special thank to his lovely friends, who helped lighten the burden, especially to *Sandy*, *Vikram*, *Parmanand*, *Arun*, *Navin*, *Birju*, *Mukesh*, *Azad*, *Suneet*, *Dr. D. K. Tyagi*, *Dr. Anurag Gaur*, *Vishal*, *Yogesh*, *Kuldeep rana*, *Vijay (Mota bhai)*, *Dr. Pundeer*, *Dr. Neer*, *Dr. Tiwari*, *Deepak (Tinnu)*, *Nagesh*, *Nigmanand ojha*, *Dr. Parminder*, *Dr. Ajay Kumar*, *Dr. Amrish*, *Dr. Sandeep*, *Dr. Nitin*, *Dr. Sapan*, *Dr. Aman Pal*, *Dr. Nirpendra*, *DR. R. K. Rai.*, *Dr. R. K. Chauhan*, *P. K. R. Gautam*, *Ritesh*, *Pankaj*, *Nitil*, *Anuj*, *Rahul*, *R. B. S. yadav*, *Rajiv Rana*, *Ankit*, *Raghu*, *Yashpal*, *Sonu Dhiman*, *Dikku*, *Anil Boyal*, *Rajiv*, *Najim*, *Varun*.

I also want to thank to *Dr. Manoj*, *Dr. Gaurav*, *Mrs. Rama*, *Dr. Niti*, *Aditya*, and *Nandini*. The help provided by *Mr. Ramesh Chand* during write up of the thesis is especially acknowledged.

The ever enthusiastic help of my family members, uncles, *Shri Parmal Singh, Shri Giriraj Singh*, aunties, *Smt. Savitri Devi, Smt Rajbala Devi* , brothers *Shiv Hari, Pravin, Vipin, Pawan*, and sister *Pavitra* , bhabhi, *Santosh and Nirmesh* who were distant to me but were always by his side whenever the need so arrived and accompany for me to work peacefully during the study period. I am in dearth of proper words to express my abounding feelings and affection for my lovely Jiju *Devendra Yadav* and sister *Reena*. The author is also thankful to my lovely and cute nephews and nieces *Aman, Abhishek, Mayank, Taksha, Ayush* and *Ayushi*.

I express my heartily gratitude to *Smt. Shashi Pandey, Smt. Mamta Gupta* and *Smt. Saeeda* as time spent occasionally during tea ,dinner was very pleasant.

Finally, I express my heartfelt gratitude to my highly respectable and adorable father, *Shri Dharam Veer Singh* and mother, *Smt. Kamlesh Devi* for their unconditional love, encouragement and blessings. Words can never express my feelings for them. They have been a guiding force all his life and he tried to measure up to their expectations. I also express my abounding feelings of gratitude to all those who helped me in this course but have not been listed here.

At last thanks to the almighty god who has given the author spiritual support and courage to carry out this work.

I.I.T. Roorkee

(Krishna Kumar)

August, 2009

CONTENTS

	Page No.
CANDIDATE'S DECLARATION	i
ABSTRACT	iii
LIST OF PUBLICATIONS	ix
ACKNOWLEDGEMENTS	xi
CONTENTS	xv
LIST OF FIGURES	xix
LIST OF TABLES	xxiii
CHAPTER 1 INTRODUCTION	1-19
1.1 Applications of Electromagnetic Methods	2
1.1.1 Crustal studies	2
1.1.2 Geothermal studies	3
1.1.3 Marine EM studies	4
1.2 Interpretation of EM Data	4
1.3 Numerical Modeling	9
1.4 Krylov Methods	13
1.4.1 Lanczos/Arnoldi methods	14
1.5 About the Present Work	17
CHAPTER 2 THEORY OF MAGNETOTELLURIC METHOD	21-34
2.1 Introduction	21
2.2 Electromagnetic Theory	22
2.3 About Origin of MT Source	24
2.4 Boundary Value Problem	25
2.4.1 Interface boundary conditions	26
2.4.2 Domain boundary conditions	27
2.5 Eigenmode Formulation of EM Problem	28
2.6 MT Response Function	31
2.6.1 MT apparent resistivity and phase	32

CHAPTER 3 FINITE DIFFERENCE IMPLEMENTATION	35-51
3.1 Introduction	35
3.2 Finite Difference Implementation	36
3.2.1 Implementation of staggered grid	37
3.3 Description of System Matrix	41
3.4 Elimination of Spurious Eigenmodes	43
3.5 Reduced System Matrix	45
3.6 Eigensolver for the Matrix	46
3.6.1 Implicitly restarted Lanczos/Arnoldi method	48
3.6.1.1 Regular mode	49
3.6.1.2 Shift and invert mode	49
3.7 Synthesis of Full Eigenvector	50
CHAPTER 4 DEVELOPMENT AND DETAILS OF ALGORITHM	53-64
4.1 Introduction	53
4.2 Sequence of Development	53
4.2.1 Development of MT_2D_EA algorithm	54
4.2.2 Development of MT_3D_EA algorithm	55
4.3 Salient Features of MT_3D_EA algorithm	56
4.3.1 Response functions	56
4.3.2 Source term	56
4.3.3 BiCGStab method	57
4.3.4 Multi-frequency response	57
4.4 Description of MT_3D_EA Algorithm	57
4.5 Structure of MT_3D_EA Algorithm	58
CHAPTER 5 RESULTS AND ISCUSSION	65-87
5.1 2D Experiments	65
5.1.1 Simple model	65
5.1.2 Complex model	67
5.2 3D Experiments and Results	69
5.2.1 Comparison with analytical solution	69
5.2.2 Convergence of electric field with the refinement of	70

grid	
5.2.3 No contrast study	73
5.2.4 Electrically similar models	73
5.2.5 Reduced and full version	74
5.2.6 Effect of working with different percentage of eigenmodes	76
5.2.7 Multi-frequency response computation	82
5.2.8 Extension of strike length	84
5.2.9 Comparison with 3D-2 model of COMMEMI report	86
CHAPTER 6 EXPERIMENT WITH FIELD DATA	89-102
6.1 General	89
6.2 2D Experiment	93
6.2.1 Study with different basement depths	95
6.2.2 Study with different block resistivities	96
6.2.3 Multi-frequency responses	97
6.2.4 Comparison with and without salient features	98
6.3 3D Experiment	99
6.3.1 Effect of varying the strike length	99
6.3.2 Effect of changing depth to top of the conductive block	101
6.3.3 Effect of varying the thickness and width of the block	102
6.4 Conclusion	102
CHAPTER 7 SUMMARY AND CONCLUSION	103-108
7.1 Conclusion	106
7.2 Limitations of the Algorithm	107
7.3 Suggestions for Future Work	107
APPENDIX A1 INTEGRAL BOUNDARY CONDITION	109-111
A1.1 Integral Boundary Condition at the Air-Earth Interface	109
APPENDIX A2 MATRIX COEFFICIENTS AND SIGMA ORTHONORMALIZATION	113-117

A2.1	Matrix Coefficients	113
A2.2	Sigma Orthogonality of Eigenvectors	116
APPENDIX A3	ALGORITHM PARAMETERS AND	119-124
	SUBPROGRAMS	
APPENDIX A4	SAMPLE INPUT AND OUTPUT FILES	125-141
	Input.dat	125
	Output_main.dat	127
	Output_response.dat	137
	Output_time.dat	141
REFERENCES		143-165

LIST OF FIGURES

Figure No.	Title	Page No.
1.1	(a) Block diagram of interpretation.	5
1.1	(b) extended block diagram of interpretation.	6
1.2	Functional diagram (a) forward modeling, (b) inverse modeling.	6
1.3	Logic diagram for numerical solution of forward problem.	7
2.1	Presentation of interface boundary condition	27
2.2	Anomalous conductive block in a half space	30
3.1	3D Finite Difference grid.	37
3.2	Arrangement of electric and magnetic field components on Yee's grid	38
3.3	The grid cells and associated electric (red colour) and magnetic (blue colour) components required for the FD equation of $e_x(i,j,k)$. The shaded prism is of averaged conductivity $\bar{\sigma}_x(i,j,k)$.	40
3.4	The eigenvalue plot for uniformly discretized half space.	42
3.5	Representation of reduced matrix structure	46
4.1	Algorithm in nutshell.	58
4.2	Flow chart of main program.	60

4.3	Flow chart of EIGENMODE_3D subprogram.	62
4.4	Flow chart of EIGENSTEP subprogram.	63
5.1	(a) Simple model (Model 2D-1 of COMMEMI, distance in km and resistivity in Ω -m), (b) eigenvalue plot; Comparison of COMMEMI (Zhdanov et al., 1997) and MT_2D_EA at 0.1s (c) electric field and (d) apparent resistivities.	66
5.2	(a) Complex model (Model 2D-4 of COMMEMI, distances in km and resistivity in Ω -m), (b) eigenvalue plot and (c) comparison between apparent resistivities of COMMEMI and MT_2D_EA at 1s.	68
5.3	(a) 3D Test model (distances in km); Eigenvalue plot (b) coarse grid, (c) medium grid, (d) fine grid.	71
5.3	Plots for different grids at 1s (e) electric field and (f) apparent resistivities	72
5.4	Plots corresponding to 2D TE mode for electrically similar models (a) real Ey field, (b) apparent resistivities,	73
5.4	Plots corresponding to 2D TM mode for electrically similar models (c) Re Ex field and (d) apparent resistivities.	74
5.5	Plots for reduced and full versions corresponding to 2D TE mode (a) Ey field, (b) apparent resistivities; and Plots corresponding to 2D TM mode (c) Re Ex field, (d) apparent resistivities.	75
5.6	Electric field plots for different percentages of eigenmodes (a) real part and (b) imaginary part.	76
5.7	(a) 2D Test model (distances in km); Eigenvalue plot (b) skin-depth based grid, (c) coarse grid,	78
5.7	Plots for different percentage of eigenmodes; For skin depth based grid (d) Re-electric field and (e) apparent resistivities and for coarse grid (f) Re-electric field, (g) apparent resistivity.	79
5.8	(a) 2D-3 model of COMMEMI, (b) eigenvalue plot,	80

5.8	Plot for different percentage of eigenmodes at 10s (c) Real e-field (d) apparent resistivity.	81
5.9	(a) Electric field plots for different frequencies in 3D; 2D apparent resistivity curves using 1s and 10s grid eigenmodes (b) at 1s, (c) at 10s.	83
5.10	(a) Test model (distances are in km); Plots for different strike lengths (b) eigenvalues, (c) Re electric fields, and (d) apparent resistivities.	85
5.11	(a) 3D-2 model of COMMEMI (distances in km and resistivities in Ω -m),	86
5.11	(b) eigenvalue plot and (c) plots of apparent resistivity for COMMEMI and MT_3D_EA at 100s.	87
6.1	Location map of Himalayan region. NB: Namche Barwa; GT: Gangdese Thrust; HKS: Hazara-Kashmir Syntaxis; ITSZ: Indus Tsangpo Suture Zone; KOH: Kohistan Island arc; LB: Ladakh Batholith; MBT: Main Boundary Thrust; MCT: Main Central Thrust; HFT: Himalayan Frontal Thrust; MMT: Main Mantle Thrust; NP: Nanga Parbat; NS: Northern Suture; SR: Salt Range; SDTZ: South Tibetan Detachment Zone; UK: Uttarakhand (Najman, 2006) (after Tyagi, 2007).	90
6.2	Geological map of the study area (compiled from Viridi, 1988; Sorkhabi et al., 1999; Kumar et al., 2002). 1- MT Sites; 2- Thrust; 3- Cities; 4- Dehra Dun Reentrant; 5- Blaini-Infrakrol-Krol; 6- DaMTha; 7- Garwhal Nappe; 8- Jaunsar-Simla (Undifferentiated); 9- Sunder Nagar-Berinag Groups; 10- Undifferentiated Metamorphics; 11- Undifferentiated Tertiaries; 12- Piedmont zone. MT data collected in the Indo-Gangetic Plains, Siwalik, Lesser and Higher Himalayan region in Garhwal Himalaya. (after Tyagi, 2007).	91
6.3	Depth section showing local earthquakes recorded in Garhwal-Kumaon Himalaya (Khattri, 1992) (after Tyagi, 2007).	92
6.4	2D resistivity models of the crust derived from inversion of joint TE, TM mode MT data (Tyagi, 2007).	94

6.5	Gangotri simplified model (distances in km and resistivity in Ω -m).	94
6.6	2D plot with different basement (a) at 11.61s, (b) at 90.45s.	95
6.7	2D plot with resistivity variation of conductive block (a) at 11.61s, (b) 90.45s.	96
6.8	Response curves for multifrequency using eigenmodes of 11.61s and 90.45s grid (a) at 11.61s (b) at 90.45s.	97
6.9	Curves with and without the features other than conductor.	98
6.10	Strike variation curves for different depth to the top (a) at 2 km, (b) 4 km and (c) 6 km.	100
6.11	Plot for depth to the top of block.	101
6.12	Variation in the block in other horizontal direction	102

LIST OF TABLES

Table No.	Title	Page No.
3.1	Comparison of different methods with preconditioners for best invert matrix solver	50
5.1	RMS errors for different percentage of eigenmodes in case of 3D	77
5.2	RMS errors for different percentages using skin depth based grid	82
5.3	RMS errors for different percentages using coarse grid	82
A3.1	Description of control parameters.	119
A3.2	Grid parameters description	120
A3.3	Various subprograms and their purpose	121

INTRODUCTION

The geoelectromagnetic method is an important branch of applied geophysics, in addition to seismic, gravity and magnetic etc. The cardinal objective of applied geophysics is to add a third dimension to geological maps. This is achieved by efficiently interpreting the measured anomalies using scientific instruments whose function is to detect changes in the physical properties of rocks concealed beneath the surface of the earth. Subsurface geology – the third dimension of the geological map – is unfolded somewhat obscurely through the pattern of anomalies observed above, on or under the air-earth interface. The geological picture is only vaguely adumbrated in lines of equal anomaly and the professional job of geophysicist is to interpret these observations in geological terms.

The conductive rocks affect the geoelectromagnetic response to artificially or naturally simulated electric and magnetic fields. The artificially simulated source field methods are also called Controlled Source Methods that include Controlled Source EM Method, Direct Current Resistivity Method and Induced Polarization Methods. In contrast, the naturally simulated methods are Magnetotelluric, Telluric, Geomagnetic Depth Sounding and Self Potential methods.

The Magnetotelluric method uses natural electromagnetic waves in the frequency range 10^{-5} Hz – 10^5 Hz as source field. These fields are generated mainly by thunderstorm activity (>1 Hz) and the interaction of solar wind with the earth's magnetosphere (<1 Hz) (Kaufman and Keller, 1981). The orthogonal horizontal components of electric and magnetic fields are measured at the earth's surface and analyzed in terms of electrical resistivity distribution in the earth's interior. The two orthogonal horizontal electric field

components are linearly related to the two horizontal magnetic field components through an appropriate transfer function (Tikhonov, 1950; Cagniard, 1953). The depth of penetration of electromagnetic (EM) wave depends upon its frequency and conductivity distribution of the medium.

1.1 Applications of Electromagnetic Methods

Electromagnetic methods can be used in two forms as Controlled source EM (CSEM) and natural source EM (MT). In CSEM applications an active source is used while in magnetotelluric method, naturally generated EM waves are used. MT is primarily used to delineate the crustal structure of the earth as in MT we can get information upto several hundreds of kilometers. Now a days, MT along with CSEM is also used in marine environment to detect hydrocarbons. MT is also used in geothermal exploration, ground water exploration (Petrick, 2005; Rao, 2008) and detection of waste hazards sites (Lima et al., 1995; Tezkan, 2000). A brief literature review of salient EM field case studies where 3D modeling algorithms have been successfully employed follows.

1.1.1 Crustal studies

Magnetotellurics is widely used to determine the depth of crust in different regions of the world. Most of the current field data interpretation exercises are carried out using 2D/3D modeling algorithms. Adam (1997) studied Neocene Pannonian Basin and observed deep Bakes Graben at 7 kms. Above this structure a strong magnetotelluric (MT) phase anisotropy (phase-deviation in two orthogonal directions) has been observed indicating upwelling of the partially molten asthenosphere validating deep mantle structure. Wei et al. (2001) detected wide spread presence of high conductivity fluid at a depth 15-20 km in

southern Tibet and at a depth of 30-40 km in the northern Tibet. Unsworth et al. (2005) also observed crustal melting in Himalayas from northern Tibet side. Pous et al. (2007) observed conductive feature in Pyrenees related to the subduction of the Iberian plate beneath Europe. In central Taiwan, Chen et al. (2007) observed a low resistive zone representing reduced viscosity zone that controls deformation of this active orogen. Tezken (1994) also observed a highly conductive layer in the upper mantle beneath the Black forest crystalline. Mauro et al. (1999) carried out MT investigations in seismically active region of northwest Bohemia and observed a conductive structure at a depth range from 0.5 km to 3 km related to paliofluids in the gigantic massif. Rao et al. (2003) used EM technique to study seismically active peninsular Indian region. Semenov et al. (2008) conducted the project CEMES along the south–west margin of the east European Craton using long period MT and their results indicate systematic trends in the deep electrical structure of the two European tectonic plates. Tyagi (2007) and Israil et al. (2008) studied the Garhwal Himalaya and observed a conductive feature near MCT.

1.1.2 Geothermal studies

Geothermal studies using MT were started in 80's (Hoover et al., 1978; Wright et al., 1985; Pellerin et al., 1996). In Jammu and Kashmir 1D geothermal study was done by Harinarayana (2002). In Punga valley, Ladakh, India, the 2D geothermal MT investigations were done by Abdul Azeez and Harinarayana (2007). They reported a ~ 400 m extent conductive zone of 10-30 Ω -m resistivity at 2 km depth and related it to a hot spring, In Kos island, Greece, Lagios et al. (1998) reported a 3.5-7 Ω -m conductor at 250-3000 m depth. Patricia et al. (2002) performed geothermal investigations in Brazil. 3D Magnetotellurics was used for geothermal exploration by Asaue et al. (2006) and they

found 1 km to 3 km conducting pillar at the hot spring site in the West Side Mt. Aso, Japan. Lee et al. (2007) studied in Pohang, Korea and observed a conductor at 3 km and also confirmed five layers resistivities with drilling results.

1.1.3 Marine EM studies

Marine Magnetotellurics (MMT) is mainly used as a complement to MCSEM (Marine Controlled Source Electromagnetic) to provide the background resistivity of the sub-bottom sediments, that is, to constrain the inversions (resistivity vs. depth models) produced from MCSEM data. First sea floor MT study was reported by Cox et al. (1980). The recent developments in instrumentation for Marine MT were presented by Constable et al. (1998). MCSEM is also used for studies of oceanic lithosphere (Cox, 1981; Constable and Cox, 1996), Midocean ridges (MacGreger et al., 2001) and sea floor gas hydrate (Yuan and Edwards, 2000). Recently, marine controlled source electromagnetic has shown great potential in hydrocarbon exploration to detect thin resistive layers at depth below the sea floor (MacGreger and Sinha, 2000; Ellingsurd et al., 2002; Eidsmo et al., 2002; Kong et al., 2002, Johansen et al., 2005; Constable and Weiss, 2006; Constable and Srnka, 2007; Fox and Ingerov, 2007; Weidelt, 2008; Weitemeyer, 2008).

1.2 Interpretation of EM Data

The whole operation of deducing a picture of the geology at depth from geophysical measurements is termed as interpretation, a word which aptly implies its indeterminate nature. The measurement of magnetotelluric anomaly is generally taken at the ground surface and from these data one tries to outline the disturbing regions. This part of work is closely controlled by well established physical and mathematical laws and is known as

quantitative interpretation (Figures 1.1(a) and 1.1(b)). Although the quantitative interpretation may often be ambiguous, the nature of ambiguity is well understood. The next step is termed as geological interpretation, the step to translate the quantitative interpretation into reasonable geological picture and the success in the endeavor depends upon a proper appreciation and balancing of all the physical and geological factors.

The subject matter of this thesis is very largely concerned with the quantitative interpretation of geoelectromagnetic data. The quantitative interpretation with confidence level is synonymous with the solution of inverse problem. However, to obtain a solution of inverse problem the solution of the forward problem is prerequisite. Therefore, the quantitative interpretation is explained as a cascade of solution of forward problem as well as the solution of inverse problem.

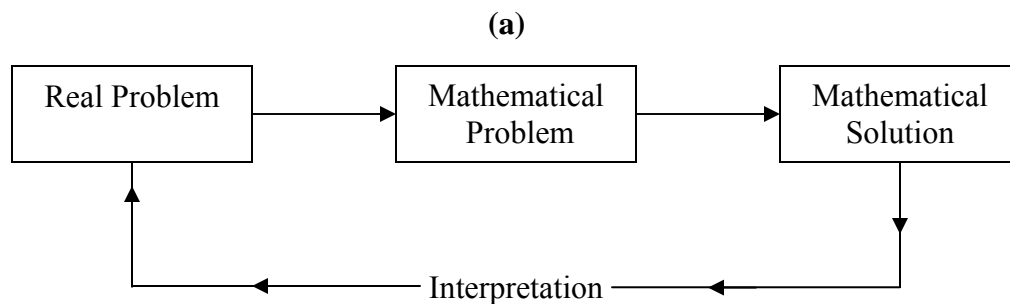


Figure 1.1: (a) Block diagram of interpretation,

(b)

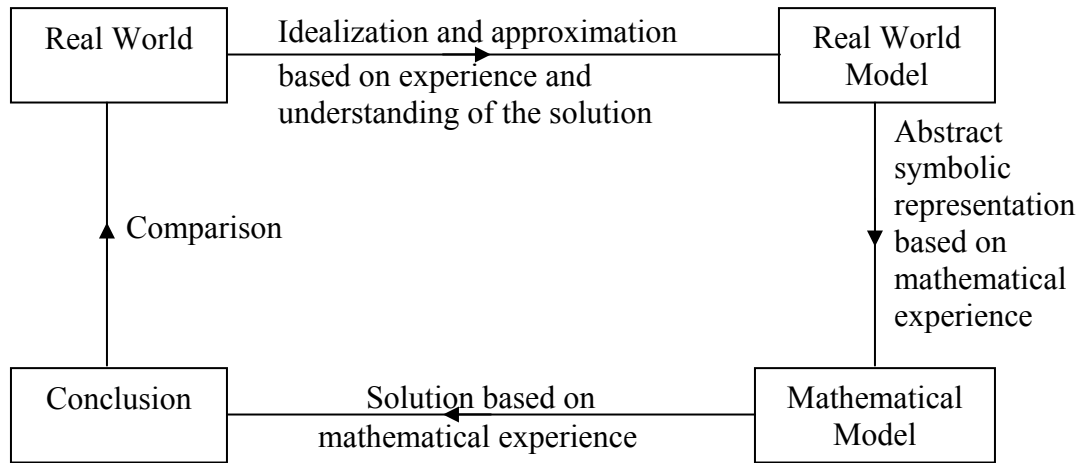


Figure 1.1continued: (b) extended block diagram of interpretation.

The mapping of model to measurable field response is known as forward problem. Typical parameters defining the model are the geometrical distribution and magnitude of the physical properties of target. The difference between the observed field values and the computed response values, obtained by forward modeling, is minimized in some optimal sense iteratively to obtain a reliable model. Functional diagram for forward modeling and inversion (Figure 1.2(a), 1.2(b)) is given below;

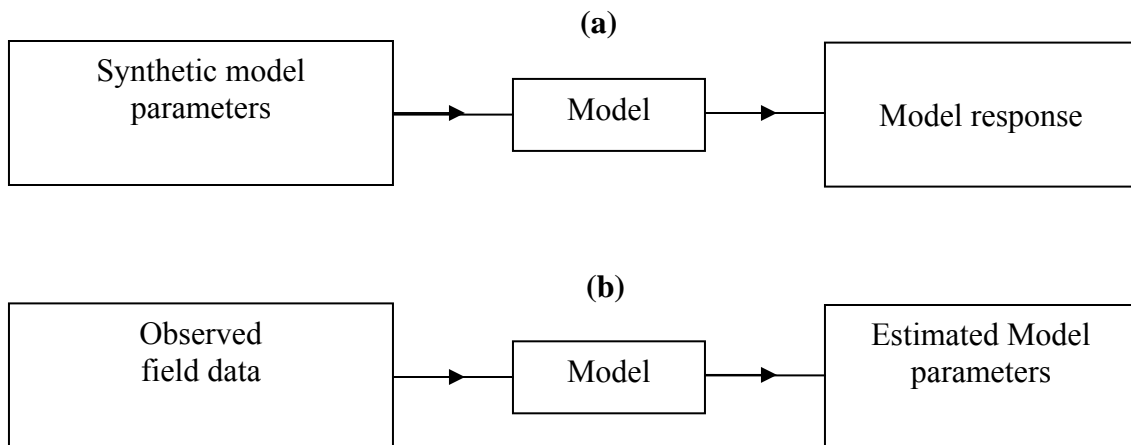


Figure 1.2: Functional diagram (a) forward modeling, (b) inverse modeling.

As described above, forward modeling is an essential part of inversion. Using trial and error method, forward modeling itself can be used to find the solution for given field data. The present work deals with the development of forward modeling algorithm for Magnetotelluric problem. Logical flow diagram of forward problem can be sketched as given below in Figure 1.3.

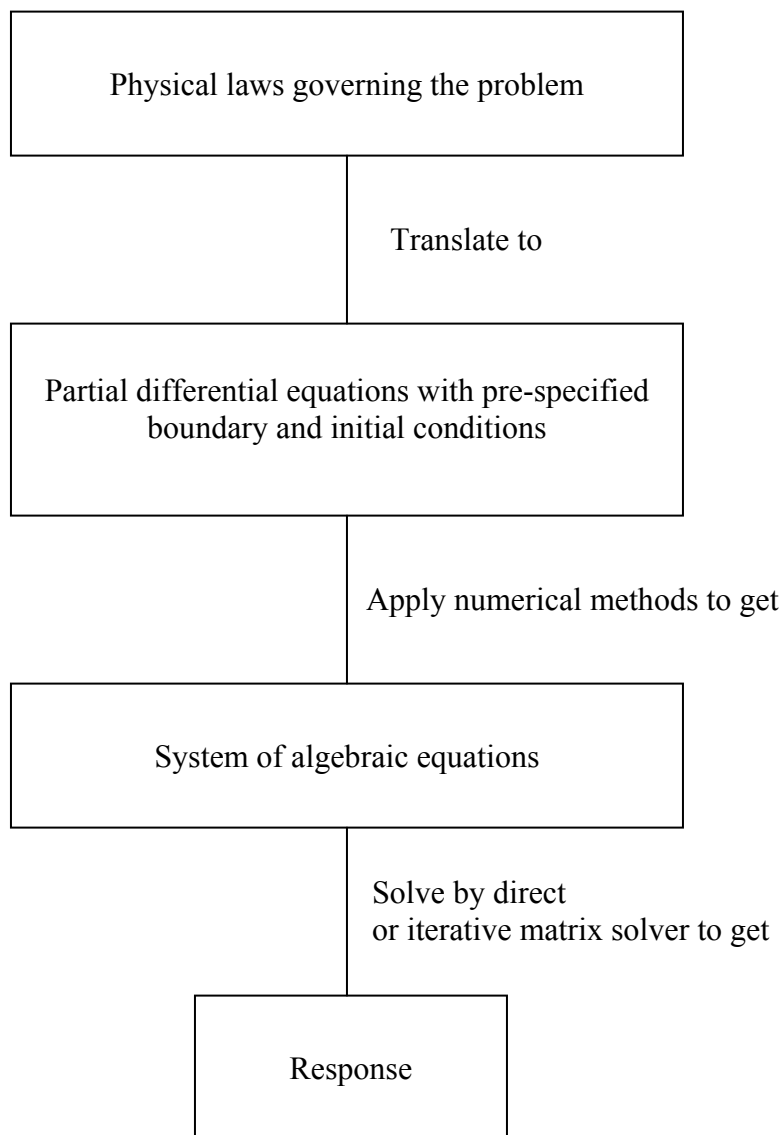


Figure 1.3: Logic diagram for numerical solution of forward problem.

EM fields are studied using Maxwell's equations, coupled in electric (**E**) and magnetic field (**B**). These equations are transformed into vector Helmholtz equation for **E**-field and/or **B**-field. The vector Helmholtz equation is used to solve the response for a given model.

The first set of modeling problems attempted pertained to a uniform conductivity half space or the conductivity variation in a layered earth. The half space problems were solved by Sommerfield (1909, 1926), Price (1962), Weaver (1971a, 1971b). Later, some characteristics of EM waves as reflection and wave tilt were studied by Singh and Lal (1980 a, 1980b) over a half space. To estimate the conductivity in a layered earth, people solved one-dimensional problems. Several one-dimensional, conductivity variation in vertical direction, algorithms were presented by Srivastava et al. (1963), Vozoff et al. (1963), Backus and Gilbert (1970), Parker (1977), Dmitriev and Berdichevsky (1979), Oldenburg (1979), Weidelt (1995) and Gupta et al. (1996).

After 1D problems, the next set of problems pertained to 2D models, in which conductivity varies only in one horizontal direction and in the vertical direction. Jones and Pascoe (1971) and Coggon (1971) presented the first two-dimensional algorithms for MT response computation. Other two-dimension algorithms were given by Brewitt-Taylor and Weaver (1976), Pek (1985), Oldenburg (1993), Weaver (1994), Rastogi et al. (1997), de Groot hedlin et al. (1990, 2004) and Pedersen et al. (2005).

The physical properties vary in all three directions i.e. both the horizontal directions and the vertical direction. The most appropriate model to obtain the exact fit of its response to data is three-dimensional. Thus, to obtain a good model from data, efficient 3D forward modeling is the need of time as emphasized by Park and Torres-Verdin (1988) "3-D

modeling simply can not be avoided in complex geological environment". Keeping this in mind, we undertook the task of developing an efficient algorithm for 3D modeling of the Magnetotellurics response.

The analytical solution for computation of responses is possible only for the simple resistivity variation models, where the geometry of the modeling domain and of the interfaces demarcating regions of different resistivity can be represented by a simple expression that eases the implementation of necessary boundary conditions, e.g. the layered earth one-dimensional problem can be solved analytically. To compute the response of arbitrary resistivity variation models only way out is to undertake numerical 3D modeling. A brief review of literature on 3D MT modeling is given next.

1.3 Numerical Modeling

The workers who initiated the study for 3D MT response simulation are Jones and Pascoe (1972), Raiche (1974), Weidelt, (1975), Hohmann (1975, 1983), Hohmann and Ting (1978), Reddy et al. (1977), Jones and Vozoff (1978).

Initially, electromagnetic methods were used in mining industry where one seeks confined conductive bodies in a half space or layered structure. To compute the response of such confined targets, the Integral Equation Methods (IEM) were used. In eighties, the 3D algorithms were based on body in a layered earth (Das and Verma, 1981, 1982; Ting and Hohman, 1981; Tabbagh, 1985; Wannamaker et al., 1984a; Wannamaker et al., 1984b; Wannamaker, 1991; Xiong et al., 1986; Xiong 1992).

IEMs can efficiently compute the responses of confined targets. However, for general conductivity structure, the Differential Equation Methods (DEM) are preferred. In IEM only the target is discretised, resulting in a small but full coefficient matrix, while in

DEM the whole domain is discretised, resulting in a large but highly sparse coefficient matrix. There are two classes of DEM's: Finite Element Method (FEM) and Finite Difference Method (FDM). Because of the efficient handling of curved boundaries, for sometime the FEM became popular in geophysical literature after IEM, however, since nineties FDM has become the most favored choice

In FEM, the matrix equations are derived using one of the several approaches, popular one being use of either the weighted residual approach or the minimum theorem. Both tetrahedral and hexahedral elements have been used for the modeling. Pridmore et al. (1981) suggested that only hexahedral elements can give satisfactory results. Livelybrooks (1993) developed 3Dfeem (3D finite element electromagnetic modeling) algorithm and compared its results with 2D analytical solution. Xu et al. (1997) applied FEM to implement Terrain corrections to MT problems. Shi et al. (2004) applied divergence correction in their solution and observed that their algorithm is comparable with IEM in computational speed. Now a days, people are using staggered grid to find accurate solution (Mitsuhata and Uchida, 2004; Naam et al., 2007; Changsheng et al., 2008; Blome et al., 2009).

Staggered grid was first introduced by Yee (1966) in his FDM algorithm developed to solve electrical engineering problems. Later, it became popular in geophysics also. Now, this approach is used in almost all algorithms due to implicit application of magnetic field divergence correction. Monk and Suli (1994) observed that this scheme is also second order convergent on a non-uniform mesh as it is on a uniform mesh.

Now one can handle curved boundaries even with FDM and it is easier to implement than with FEM. The first 3D FDM code for electromagnetic problems in

geophysics was given by Jones and Pascoe (1972) for general conductivity structure buried in a layered earth. Brewitt-Taylor and Weaver (1976) not only used central difference but also modified to weighted average the simple average conductivities that were used in the code of Jones and Pascoe (1972) and Farquharson and Oldenburg (2002) used harmonic average of conductivities. For E-polarization, asymptotic boundary condition was introduced by Weaver and Brewitt-Taylor (1978) to improve accuracy. The 3D FDM code given by Madden and Mackie (1989) used relaxation procedure as matrix solver rather than the direct methods because although direct methods are quick for 1D and 2D yet these become inordinately inefficient for 3D problems. Smith et al. (1990) used Taylor series expansion and his results agree with the Jones and Pascoe (1972). Mackie et al. (1993) used impedance propagator algorithm to solve 3D MT response. Their solution converges slowly as frequency approaches zero. Other programs were reported by Newman and Alumbaugh (1997), Chen et al. (1998) for topographic responses. Siripunvaraporn et al. (2002) formulated the problem for electric field and magnetic field. They observed that electric field formulation is less sensitive to grid resolution than the magnetic field formulation. For sufficiently fine grid, both electric and magnetic field formulations gave the same solution. However, for coarser grid, the electric field solution tends to be closer to the exact solutions. We have also used Finite Difference Method with a staggered grid.

Hybrid methods, amalgamation of DEM and IEM, were developed by Lee et al. (1981), Gupta et al. (1987) and Cerv et al. (1990). Discrete convolution method was used by Porsani and Ulrych (1989).

In numerical methods, ultimately a matrix equation is obtained which need be solved using either a direct or an iterative matrix solver. Direct solvers give satisfactory

results in 1D or 2D environment but for 3D environment iterative solvers serve better because of the large matrix size and its sparse nature.

Of the various classes of iterative methods, those based on Conjugate Gradient (CG) methods have become the popular choice. There are different variants of CG type methods such as simple Conjugate Gradient (CG), Bi Conjugate Gradient (BiCG) and Bi-Conjugate Gradient Stabilized (BiCGSTAB). Generally, CG is used to solve symmetric coefficient matrix problems while BiCG and BiCGSTAB are used to solve non-symmetric coefficient matrix problems.

Now several workers are using CG methods in 3D modeling. The 3D algorithm given by Smith (1996a, 1996b) is based on BiCG (Bi-Conjugate Gradient) method with Cholesky decomposition preconditioner. Xiong (1999) indicates BiCGSTAB (Bi-Conjugate Gradient Stabilizer) offers best convergence for the solution. Other efficient algorithms based on BiCG solver were proposed by Sasaki (2001), Xiong et al. (2000), Fomenko and Mogi (2002), Farquharson and Oldenburg (2002).

In all these traditional methods, one has to re-run the code for each frequency. While in the approach, based on eigenvalues and eigenvectors, there is no need to re-run the algorithm for each frequency. Eigenvalues and eigenvectors, collectively known as eigenmodes, represent the basic characteristics of the matrix and, in turn, of the model. After estimating the eigenmodes for given geometry and physical property distribution, the solution for multi-frequencies can be obtained using these eigenmodes within seconds. Since eigenvalues have the basic characteristics of the physical properties irrespective of source, we used this approach.

The popular method to find the eigenmodes is Singular Value Decomposition (SVD). In SVD, eigenvalues and eigenvectors (eigenmodes) are used to obtain the solution. Park and Chave (1984) used SVD to estimate magnetotelluric response functions. In SVD the matrix is needed explicitly and it is very difficult to store the matrix in 3D problems. Hence, the iterative methods are widely used to solve for the eigenmodes. The classic iterative method to find eigenvalue is power method. In addition to its role as an algorithm, the method played a key role in the development, understanding, and convergence analysis of all of the iterative methods. This method was used to find the largest eigenvalue of the system matrix. Krylov subspace projection methods are based upon the intricate structure of the sequence of vectors naturally produced by the power method. Since we have used Krylov space based method to obtain the eigenmodes, a brief survey of the literature on this topic is given below.

1.4 Krylov Methods

Krylov methods are generalization of Conjugate Gradient methods. In these methods, the coefficient matrix is not needed explicitly, rather, an algorithm yielding product of the coefficient matrix with a vector is sufficient. Saad (1980) used Krylov method to find the eigenvalues of unsymmetric matrices. Krylov methods are particularly efficient when all eigenmodes are not desired, rather only a few, either largest or smallest, eigenvalues and corresponding eigenvectors are needed. The set of eigenvectors determined constitutes the basis of Krylov subspace. The constructed approximate eigenpairs from this subspace are known as Ritz vector with corresponding Ritz value.

This method was implemented by Druskin et al. (1994, 1999) in geophysical applications with the name Spectral Lanczos Decomposition Method (SLDM). Recently,

Stuntebeck (2003) used eigenmode method in air-borne applications of EM methods. To find the eigenmodes, there are several variants of Krylov subspace method such as Jacobi-Davidson, Lanczos and Arnoldi. We have used Lanczos and Arnoldi because of their easy implementation.

1.4.1 Lanczos/Arnoldi methods

The Lanczos and Arnoldi algorithms are iterative algorithms invented by Cornelius Lanczos (1950) and W. E. Arnoldi (1951) respectively. Both are adaptations of power method to find eigenvalues and eigenvectors of a square matrix or the singular value decomposition of a rectangular matrix. In Lanczos one deals only with (Hermitian) symmetric matrices; while in Arnoldi method one finds the eigenvalues and eigenvectors of general (possibly non-Hermitian) non-symmetric matrices. After Lanczos (1950), main work on these methods was done by Paige (1970). He solved several extreme eigenvalues and eigenvectors of large symmetric matrices. His work strengthened significantly the Lanczos type methods. Band Lanczos methods were tested by Ruhe (1979), Ericsson and Ruhe (1980) to improve the computation cost.

In all these variants, the Krylov vectors are stored column-wise in a two-dimensional array. In exact arithmetic, these columns form an orthonormal basis for the Krylov subspace. These columns are referred to as the Lanczos vectors or Arnoldi vectors respectively. However, in finite precision arithmetic, care must be taken to ensure that the computed vectors are orthogonal within working precision. This operation gives rise to a tridiagonal matrix for symmetric cases and upper Heisenberg for nonsymmetric cases, from which the eigenvalues or Ritz values are estimated.

To find out the desired subset (either largest or smallest) of eigenvalues and corresponding eigenvectors restarting techniques were introduced. Using these techniques, the desired eigenvalues were obtained using a very small number of Krylov vectors in comparison to the dimension of the matrix. There were two ways of restarting, explicit and implicit restarting.

The explicit restarting technique for non-symmetric system of equations was proposed by Saad (1984). It was based upon the polynomial acceleration scheme developed by Manteuffel (1978) for the iterative solution of linear systems. In this approach, starting vector is preconditioned so that it nearly lies in the invariant subspace of interest. This preconditioning takes the form of a polynomial applied to the starting vector to damp the unwanted components from the eigenvector expansion. Parlett and Scott (1979) observed slow convergence of Lanczos for Tchebychev distribution for diagonal matrices. Duff (1991) tried to solve the rightmost or left most eigenvalues of a real non-symmetric matrix by using subspace iteration method with Chebychev acceleration. Meerbergen (2000) developed a program based on explicit restarting named as 'EA16' in FORTRAN having capabilities of ARPACK (1995). Tong et al. (1999) analyzed BiCG in finite precision arithmetic and observed that loss of biorthogonality does not necessary deter convergence of the residuals provided the polynomial acceleration factor is bounded. Emad et al. (2005) developed an algorithm named Multiple Explicitly Restarted Arnoldi Method (MERAM) and compared it with the Explicitly Restarted Arnoldi Method (ERAM) to discover acceleration in convergence. For multiple eigenvalues, harmonic restarted Arnoldi algorithm was proposed by Morgan et al. (2006) and their method avoids the need of block methods but it needs explicit restart. Hernandez et al. (2007) studied the impact of re-

orthogonalization in finite precision arithmetic in explicitly restarted Lanczos in terms of parallel efficiency.

Another approach to restarting, that offers a more efficient and numerically stable formulation, is known as implicit restarting. In this approach truncated form of implicitly shifted QR iteration is used. In their landmark paper Sorensen et al. (1992) discussed Arnoldi process using implicitly shifted QR iteration. They also studied loss of orthogonality of eigenvectors and storage requirement and used exact shifts to update the starting vector. Calvetti (1994) used Leja points to update the starting vector. However, Baglama et al. (1998) find Leja points quite time consuming for large problems and they modified it to Fast Leja points for faster computation. Subspace iteration methods were used by some workers such as Meerbergen et al. (1994), Brizenski (2001), Hochstenbach (2003) and Beattie (2005). The work of Lehoucq et al. (1996) on QR algorithms revealed that these are the best choice for Schur decomposition of the matrix. They studied truncated QR algorithm and observed that it is a generalization of Rayleigh-Ritz procedure on a block krylov subspace for a non-Hermitian matrix and showed that it may be viewed as truncated form of implicitly QR algorithm. Based on these works of Sorenson, Lehoucq and others, a public domain code ARPACK was presented in FORTRAN to aid development of complex professional softwares. Sorensen et al. (1995) described the details of implementation of Implicitly Restarted Arnoldi Method (IRAM) in the ARPACK user's guide (1996). Lehoucq et al. (1996) introduced the deflation procedure to improve convergence of IRAM. Scott et al. (1997) and Morgan et al. (1996) observed that Arnoldi method is more efficient than the subspace iteration method. Beattie et al. (2005) describe exact shifts as best in implementation and Hetmanuik et al. (2006) showed that shift and

invert method in Lanczos gave best result for determination of few eigenvalues as well as eigenvectors. Tremblay et al. (2007) proposed unsymmetric Lanczos algorithm with modification to resonance lifetimes and suggests how there is no need of storage of large number of vectors. Joubert (1992) observed the phenomenon of breakdown and loss of orthogonality of eigenvectors in a nonsymmetric system. Several workers have developed strategies to overcome this loss of orthogonality. Firstly, DGKS (1976) method was given to improve the orthogonality of eigenvectors. Problems related to orthogonalization are also discussed in Cullum and Willoughby (1985). A good work was done by Langou (2003) in his Ph. D. thesis. He suggests two improvements in classical Gram-Schmidt procedure (a) modified Gram-Schmidt generates well-conditioned set of eigenvectors, (b) Gram-Schmidt algorithm iterated twice gives an orthogonal set of vectors. Giraud et al. (2003) also suggested selective reorthogonalization to compute orthogonal set of vectors.

1.5 About the Present Work

The objective of study is fulfilled with the development of softwares MT_2D_EA (Magnetotelluric 2D Eigenmodes Algorithm) and MT_3D_EA (Magnetotelluric 3D Eigenmodes Algorithm) which are capable of generating MT responses for arbitrarily distributed 3D electrical conductivity models. The thesis writeup has been organized into seven chapters briefly summarized below.

In the present chapter 1, literature review is presented.

In chapter 2, the basic theory for 3D Magnetotellurics is discussed. Theoretical development of eigenmodes determination and application of eigenmodes for multi-frequency response computations is described. Various types of boundary conditions

employed are discussed. The apparent resistivity computations are presented for both the modes, one corresponding to 2D TE and the other corresponding to 2D TM.

In chapter 3, Finite Difference implementation on 3D staggered grid is presented. It is discussed how the electric and magnetic fields are arranged on staggered grid. The structure of the coefficient matrix, in various cases, is described and corresponding implementation of Lanczos and Arnoldi Methods for evaluation of eigenmodes is presented. Application of preconditioner with conjugate gradient methods is also discussed.

In chapter 4, several stages of development of the algorithms MT_2D_EA and MT_3D_EA are discussed, starting from all eigenmode solution using SVD to Lanczos for symmetric matrix and Arnoldi method for non-symmetric matrix.

In chapter 5, testing of the algorithms MT_2D_EA and MT_3D_EA are described. It includes tests like (i) Response of electrically same models, (ii) Effect of different percentage of eigenmodes on resistive and conductive bodies, (iii) Effect of coarseness of grid on the solution, (iv) Multi-frequency response computation and (v) Comparison with some published results.

In chapter 6, we applied our algorithm to field data. The data was acquired from Roorkee to Gangotri in Garhwal Himalaya by our department and a robust 2D inverted model, obtained using WingLink, was proposed by Tyagi (2007). Using our 2D algorithm, first we obtained the response of the proposed complex model and found excellent match. Next we designed a simple 3D model from the complex 2D model and computed its responses for large strike length at two periods and found good fit with data. Due to limited computer resources in 3D we could not run the complex version of 3D models so we compared responses at large period and found acceptable match with data.

In chapter 7, we discuss further improvement steps that need be taken to make the algorithm more accurate, efficient and versatile.

Finally, the Appendix A1 presents the integral boundary condition formulation. The generation of matrix coefficients for e_x , e_y and e_z components and sigma orthogonality of eigenvectors are presented in Appendix A2. In Appendix A3, the tables of algorithm parameters for control and grid and various subprograms along with their purpose are described. Sample input and output files are presented in Appendix A4.

THEORY OF MAGNETOTELLURIC METHOD

2.1 Introduction

The Magnetotelluric (MT) method deals with the observation and analysis of natural electromagnetic (EM) fields with a goal to derive pertinent information about the geoelectric structure of the subsurface. The observed field can be calculated as total field or it can be viewed as a superposition of the primary and secondary fields. Primary fields are generated by an external source, while the secondary fields are generated by the induced secondary currents in the earth. If the Earth model is a uniform half space, then the induced currents and the resulting secondary fields follow a regular pattern. Inhomogeneities present in the real earth invariably disturb this regular pattern of secondary currents and of the secondary fields leading to perturbation of the total EM fields. These perturbed fields, measured on the earth surface, provide an insight into the resistivity distribution within the earth. This provides information about the structure of the earth and also helps in understanding the ongoing physical processes.

The mechanism of perturbed fields can be understood only when the capability of generating responses of arbitrary resistivity distributions is fully developed. The computation of EM response of a given earth model, with prescribed resistivities, is known as the forward problem of EM induction.

An exhaustive knowledge of EM theory, based on the fundamental Maxwell's equations, is essential for solving the forward problem. In literature there exists a vast pool of texts on EM theory differing in their emphasis on mathematical background,

computational aspects and applications. One can refer to Stratton(1941), Smythe (1950), Morse and Feshbach (1953), Jackson (1975), Born and Wolf (2005, 7th edition) for fundamentals, to Mitra (1973, 1975), Morgan (1990), Zhou (1993) and Taflove (1995) for computational aspects and to Grant and West (1965), Rikitake (1966), Ward (1967), Prostendorfer (1975), Rokityansky (1982), Wait (1982), Kaufman and Keller (1981), Berdichevsky and Zhdanov (1984), Nabighian (1988, 1991) and Zhdanov (2009) for geophysical applications. A brief description of EM theory is presented here.

2.2 Electromagnetic Theory

The EM phenomenon is governed by Gauss law for electrostatics, Gauss law for magnetostatics (i.e. non existence of monopoles), Faraday's law of induction and Ampere's law for magnetic induction. Maxwell's equations, are the mathematical forms of these laws and are given below for a source free case,

$$\nabla \cdot \mathbf{D} = q_f, \quad (2.1)$$

$$\nabla \cdot \mathbf{B} = 0, \quad (2.2)$$

$$\nabla \times \mathbf{E} = -\frac{\partial \mathbf{B}}{\partial t}, \quad (2.3)$$

$$\nabla \times \mathbf{B} = \mu \mathbf{J} + \mu \frac{\partial \mathbf{D}}{\partial t}, \quad (2.4)$$

where, $\nabla = \hat{i} \frac{\partial}{\partial x} + \hat{j} \frac{\partial}{\partial y} + \hat{k} \frac{\partial}{\partial z}$.

Here, \mathbf{D} is dielectric displacement vector in coulomb/meter² (C/m²), \mathbf{B} is magnetic induction vector in tesla (T), \mathbf{E} is the electric field intensity vector in volt/meter (V/m) and \mathbf{J} is the electric current density vector in ampere/meter² (A/m²). q_f is the free electric

charge density in coulomb/meter³ (C/m³) and μ is the magnetic permeability in henry/meter (H/m).

Equations (2.1) and (2.4) lead to the equation of continuity

$$\nabla \cdot \mathbf{J} + \frac{\partial q_f}{\partial t} = 0. \quad (2.5)$$

Equations (2.3) and (2.4) involve five vectors, making it an underdetermined system. To make the system of vector equations deterministic, the following constitutive relations are employed,

$$\mathbf{J} = \sigma \mathbf{E}, \quad (2.6)$$

$$\mathbf{D} = \varepsilon \mathbf{E}, \quad (2.7)$$

and

$$\mathbf{H} = \frac{1}{\mu} \mathbf{B}. \quad (2.8)$$

Here, σ is the electrical conductivity in siemens/meter (S/m) and ε is the medium dielectric permittivity in farad/meter (F/m). \mathbf{H} is the magnetic field intensity vector in ampere/meter (A/m). Equation (2.6) may be recognized as Ohm's law. The μ and ε can be respectively expressed as

$$\mu = \mu_r \mu_0$$

and

$$\varepsilon = \varepsilon_r \varepsilon_0.$$

Here μ_r is the relative permeability and ε_r is relative electrical permittivity. Since the primary physical property of interest in magnetotellurics is conductivity σ , the

magnetic permeability and dielectric permittivity of the medium are assumed to be equal to corresponding free space values μ_0 and ε_0 , as;

$$\mu_0 = 4\pi \times 10^{-7} \text{ H/m}$$

and

$$\varepsilon_0 = 10^{-9} / 36\pi \text{ F/m.}$$

2.3 About Origin of MT Source

The magnetotelluric method is a passive electromagnetic technique that involves measuring fluctuations in the natural electric and magnetic field at the surface of the earth. The primary source field has its origin in the electric currents blowing in and beyond the ionosphere which, in turn, arise from the complex interactions of solar radiations and plasma flux with the earth's magnetosphere and ionosphere. The external inducing field due to source, is horizontal and laterally uniform and therefore the signals can be treated as a plane wave incident normally on the earth. The domain of study can be treated as source free and the effect of source is accounted through the boundary conditions. The respective boundary conditions for solving \mathbf{E} or \mathbf{B} are presented in section 2.4.

The magnetotelluric analysis is carried out in frequency domain. Taking time dependence to be $\exp(i\omega t)$, i.e. $\tilde{\mathbf{e}}(\mathbf{r}) \cdot \exp(i\omega t)$ equations (2.3) and (2.4) become

$$\nabla \times \tilde{\mathbf{e}} = -i\omega \tilde{\mathbf{b}}, \quad (2.9)$$

$$\nabla \times \tilde{\mathbf{b}} = \mu \tilde{\mathbf{j}} + i\omega\mu \tilde{\mathbf{d}}, \quad (2.10)$$

where ω is the angular frequency (hertz).

It can be easily established that when $\tilde{\mathbf{b}}$ and $\tilde{\mathbf{d}}$ having continuous first and second order derivatives, equation (2.1) can be derived from equations (2.5) and (2.10) while

equation (2.2) can be derived from equation (2.9). The equation of continuity can be recast in frequency domain as

$$\nabla \cdot \tilde{\mathbf{j}} = -i\omega q_e. \quad (2.11)$$

2.4 Boundary Value Problem

The geomagnetic field variations can be studied by solving Maxwell's equations (2.9) and (2.10). The solution can be achieved in terms of field vectors $\tilde{\mathbf{e}}$ or $\tilde{\mathbf{b}}$, by transforming these two equations into a well posed EM boundary value problem. For this, Cartesian coordinate system is being used. The plane $z = 0$ is considered as air-earth interface and z is taken to be +ve downward into the earth. Along with assumption of plane wave propagating vertically downward, few more assumptions, given below, are made about physical nature of earth,

- 1) Earth is considered to be source free and a passive medium,
- 2) Since the frequencies used are less than 10^5 Hz and the resistivities commonly encountered in earth are less than 10^4 Ω -m, the free charge decays almost instantaneously.

Therefore, equations (2.1) and (2.11) can be simplified as

$$\nabla \cdot \tilde{\mathbf{d}} = 0, \quad (2.12)$$

$$\nabla \cdot \tilde{\mathbf{j}} = 0. \quad (2.13)$$

Equations (2.12) and (2.13) imply that for an isotropic medium the decay of charge is faster than the propagation of EM wave and that the charge density will reach equilibrium in negligible time. The surface charge may accumulate at the interface of two homogeneous regions.

Since the frequencies employed are less than 10^5 Hz (Ward and Hohmann, 1988), the displacement current term is negligible in comparison to the conduction current term and therefore can be neglected. Using ohm's law the equation (2.10) becomes,

$$\nabla \times \tilde{\mathbf{b}} = \mu_0 \sigma \tilde{\mathbf{e}} \quad (2.14)$$

and equation (2.9) remains unchanged,

$$\nabla \times \tilde{\mathbf{e}} = -i\omega \tilde{\mathbf{b}}. \quad (2.15)$$

The complete statement of boundary value problem requires statement of the requisite boundary conditions on electric field vector ($\tilde{\mathbf{e}}$) or magnetic field vector ($\tilde{\mathbf{b}}$).

There are two types of boundary conditions first one, termed as 'Interface Boundary Condition', is at the interface where conductivity discontinuity occurs within the domain of study and the second one, known as 'Domain Boundary Condition', at the domain boundary.

2.4.1 Interface boundary conditions

It is imposed on an interface, separating two media, of different physical properties. This is used to derive smooth resistivity function at the interface of different properties. This may be obtained by simply replacing the operator ∇ by the unit normal vector \mathbf{n} and setting the time derivative or else $i\omega$ term to zero in the Maxwell's equation as,

- i) the normal components of $\tilde{\mathbf{d}}$ are discontinuous and it is equal to the surface free charge density q_f ,

$$\mathbf{n} \cdot (\tilde{\mathbf{d}}_2 - \tilde{\mathbf{d}}_1) = q_f. \quad (2.16)$$

- ii) the normal component of $\tilde{\mathbf{b}}$ are continuous,

$$\mathbf{n} \cdot (\tilde{\mathbf{b}}_2 - \tilde{\mathbf{b}}_1) = 0. \quad (2.17)$$

iii) the tangential components of $\tilde{\mathbf{e}}$ are continuous,

$$n \times (\tilde{\mathbf{e}}_2 - \tilde{\mathbf{e}}_1) = 0. \quad (2.18)$$

iv) the tangential components of $\tilde{\mathbf{h}}$ are discontinuous and it is equal to the surface current density,

$$n \times (\tilde{\mathbf{h}}_2 - \tilde{\mathbf{h}}_1) = \tilde{\mathbf{j}}. \quad (2.19)$$

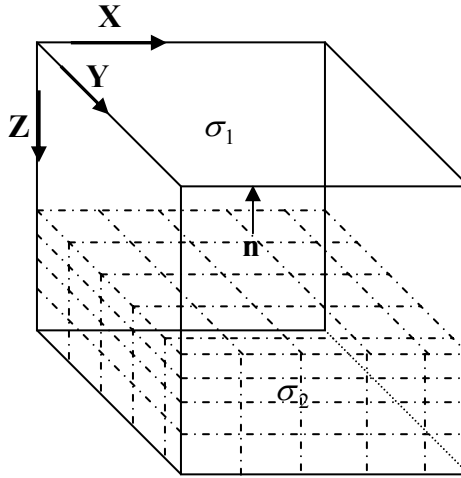


Figure 2.1: Presentation of interface boundary condition.

2.4.2 Domain boundary conditions

These are imposed on the bounding surfaces of the domain. One can impose either Dirichlet or Neumann or mixed boundary conditions (BCs). Dirichlet BC means that the EM field variable values are known at the boundary, while Neumann BC means that the normal derivative of fields is known at the boundary. The mixed BC means that a linear superposition of the field variable and its normal derivative is known.

We would apply mixed boundary conditions, as used by Weaver (1994), at the four vertical side surfaces of the solution domain. The bottom boundary surface is assumed to be underlain by a perfectly conducting halfspace. Finally, at the top surface an integral boundary condition (Appendix A1) that transfers the effect of air halfspace to the air-earth interface, is imposed.

2.5 Eigenmode Formulation of EM Problem

Since in magnetotellurics, there is no active source term within the domain of study, we consider the effect of external sources in terms of boundary conditions imposed on the air-earth interface. After imposing all the domain boundary conditions, let the known right hand side vector term be represented as the vector \mathbf{s}_0 . Under the assumption of negligible displacement current, after eliminating \mathbf{B} field in equation (2.3) and using equations (2.4) and (2.6), the MT equation in time domain can be written as,

$$\nabla \times \nabla \times \mathbf{E}(r, t) + \mu_0 \sigma \frac{\partial \mathbf{E}(r, t)}{\partial t} = \mathbf{s}_0 . \quad (2.20)$$

The corresponding homogeneous equation will then be

$$\nabla \times \nabla \times \mathbf{E}(r, t) + \mu_0 \sigma \frac{\partial \mathbf{E}(r, t)}{\partial t} = 0 . \quad (2.21)$$

Now, for eigenmode computation in real arithmetic, let us assume the time dependence as

$$\mathbf{E}(r, t) = \mathbf{e}(r) \exp(-\lambda t) . \quad (2.22)$$

Here λ is the decay constant for EM fields.

This relation transforms equation (2.21) as

$$\nabla \times \nabla \times \mathbf{e}(r) = \lambda \mu_0 \sigma(r) \mathbf{e}(r) , \quad (2.23)$$

where λ is the eigenvalue and $\mathbf{e}(r)$ is eigenfunction. Equation 2.23 states the EM eigenproblem. Here, it may be emphasized that equation 2.23 states a generalized eigenproblem and as a result the eigenfunctions will not be simple orthonormal rather these will be sigma-orthonormal. The sigma-orthonormality condition is defined as

$$\int_V \sigma \mathbf{e}_n(r) \cdot \mathbf{e}_m(r) d^3r = \delta_{mn}, \quad (2.24)$$

where δ_{mn} is kronecker symbol.

As the general MT equation with harmonic time dependence of $\exp(i\omega t)$, the equation (2.20) can be recast as the vector Helmholtz equation as,

$$\nabla \times \nabla \times \tilde{\mathbf{e}} + i\omega\mu_0\sigma\tilde{\mathbf{e}} = \tilde{\mathbf{s}}_0. \quad (2.25)$$

Since any vector can be expanded as a sum of orthonormal vectors, we expand $\tilde{\mathbf{e}}$ as

$$\tilde{\mathbf{e}}(r, \omega) = \sum a_n(\omega)\mathbf{e}_n(r). \quad (2.26)$$

Substituting equation (2.26) in equation (2.25) and using equation (2.23), we get

$$\mu_0 \sum_n a_n(\lambda_n + i\omega)\sigma\mathbf{e}_n = \tilde{\mathbf{s}}_0. \quad (2.27)$$

Multiplying by \mathbf{e}_n on both sides, integrating over the whole domain and taking sigma orthogonality into account, we get

$$a_n(\omega) = \frac{1}{\mu_0(\lambda_n + i\omega)} \int_V \tilde{\mathbf{s}}_0 \cdot \mathbf{e}_n dV. \quad (2.28)$$

This coefficient relation is valid when we are solving the total field problem. Using these coefficients and equation (2.26) one obtains the total electric field.

The electric field is not continuous at boundaries between media with different resistivities. This condition gives errors in numerical modeling using Differential Equation Methods (DEM). To overcome this, secondary field formulation comes in use resulting

from anomalies (Mogi, 1996). To avoid unnecessary calculation one prefers to work in secondary fields. In secondary field formulation total field is described as

$$\tilde{\mathbf{e}}_T = \tilde{\mathbf{e}}_P + \tilde{\mathbf{e}}_S. \quad (2.29)$$

Where subscript T denotes total field, P corresponds to primary and S corresponds to secondary field.

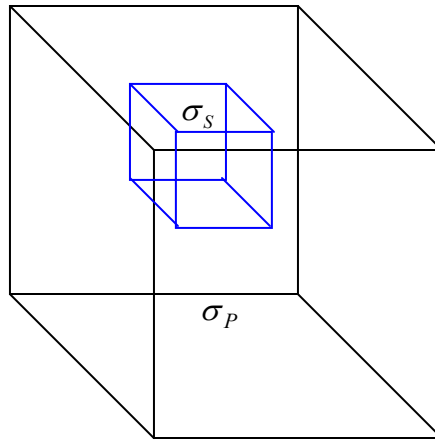


Figure 2.2: Anomalous conductive block in a half space

Primary field is the response of layered 1D model, while secondary field is the response due to inhomogeneity present in the layered earth or half space. Figure 2.2 shows 3D inhomogeneity present in the half space. σ_P and σ_S respectively are the conductivities of half space and anomalous region present in it. Thus, the total conductivity is defined as sum,

$$\sigma_T = \sigma_P + \sigma_S. \quad (2.30)$$

So in wave number domain one can define k_T^2 as

$$k_T^2 = k_P^2 + k_S^2, \quad (2.31)$$

where $k^2 = i\omega\mu_0\sigma$.

Substituting equations (2.29), (2.30) and (2.31) into (2.25), we get

$$(\nabla^2 + k_T^2)\tilde{\mathbf{e}}_s = -k_s^2\tilde{\mathbf{e}}_p, \quad (2.32)$$

with the identity $\nabla \times \nabla \times \tilde{\mathbf{e}} = \nabla(\nabla \cdot \tilde{\mathbf{e}}) - \nabla^2 \tilde{\mathbf{e}}$.

Using equation (2.27) the coefficient relation is modified as,

$$a_n(\omega) = -\frac{i\omega}{\lambda_n + i\omega} \int_V \sigma_s \tilde{\mathbf{e}}_p \cdot \mathbf{e}_n dV. \quad (2.33)$$

These coefficients are substituted in equation (2.26) to obtain the secondary field values, $\tilde{\mathbf{e}}_s$. These secondary field values are added with primary field to get the total electric field values using equation (2.29). Equation (2.14) is used to solve for the magnetic induction vector $\tilde{\mathbf{b}}$ and then equation (2.8) is used to obtain the magnetic field intensity vector $\tilde{\mathbf{h}}$. However, these field component values do not directly reflect effect of changes in the subsurface resistivity in a perceptible manner. So, more representative response functions, derived from these field values are discussed in the following.

2.6 MT Response Function

Although the response functions derived from the fields values also do not present a direct functional relationship with the subsurface resistivity yet these reflect the bulk information about the resistivity distribution.

The appropriate choice of response function is governed by the objective of the study, whether lateral or vertical variation in resistivity is desired. The spatial variation can

be studied in two modes, (i) profiling mode, for a given frequency, the observations are taken at points along a profile, and (ii) sounding mode, the observations are taken at a single point for different frequencies. Profiling delineates the lateral variations while sounding helps in deciphering the vertical variation of resistivity.

2.6.1 MT apparent resistivity and phase

The magnetotelluric method was first described by Tikhonov (1950) and Cagniard (1953) independently. Using the assumption of a plane wave source, the ratio of observed horizontal electric field ($\tilde{\mathbf{e}}_x$ or $\tilde{\mathbf{e}}_y$) and the orthogonal magnetic field component ($\tilde{\mathbf{h}}_x$ or $\tilde{\mathbf{h}}_y$), is called the impedance;

$$\mathbf{Z} = \frac{\tilde{\mathbf{e}}_x}{\tilde{\mathbf{h}}_y} = -\frac{\tilde{\mathbf{e}}_y}{\tilde{\mathbf{h}}_x}. \quad (2.34)$$

The impedance values are used to define the commonly used MT response function as apparent resistivity, which may be defined as the resistivity of equivalent fictitious half space. The apparent resistivity, ρ_a , and the impedance phase, ϕ , are respectively given by the relation

$$\rho_a = \frac{1}{\omega\mu} |\mathbf{Z}|^2, \quad (2.35)$$

$$\text{and } \phi = \tan^{-1} \left(\frac{\text{Im}(\mathbf{Z})}{\text{Re}(\mathbf{Z})} \right), \quad (2.36)$$

where $0 \leq \phi \leq 90^\circ$.

For a homogeneous half space, phase will always be 45° . For a conductive body in half space phase varies from 45° to 90° , while for a resistive body it varies from 0° to 45° .

The variation of resistivity in the earth is rarely one-dimensional, therefore above definition of apparent resistivity and phase has only limited utility. To describe higher dimensionality or anisotropy, Cantwell (1960) introduced a rank 2 impedance tensor \mathbf{Z} .

$$\begin{bmatrix} \tilde{\mathbf{e}}_x \\ \tilde{\mathbf{e}}_y \end{bmatrix} = \begin{bmatrix} \mathbf{Z}_{xx} & \mathbf{Z}_{xy} \\ \mathbf{Z}_{yx} & \mathbf{Z}_{yy} \end{bmatrix} \begin{bmatrix} \tilde{\mathbf{h}}_x \\ \tilde{\mathbf{h}}_y \end{bmatrix} \quad (2.37)$$

or

$$\tilde{\mathbf{e}} = \mathbf{Z} \tilde{\mathbf{h}},$$

where Z_{xy}, Z_{yx} are principal impedances and Z_{xx}, Z_{yy} are additional impedances. For a 1D earth,

$$Z_{xy} = Z_{yx}$$

$$Z_{xx} = Z_{yy} = 0$$

In case of 3D one can find out the solution in any of the horizontal directions. If we fix one direction as strike direction then we can find the solution for both E-polarization and H-polarization analogous to 2D case. (This is case when we assume that our strike direction is Y) Different field components for both cases are defined as

$$\tilde{\mathbf{e}}_{\text{TM}} = (\tilde{\mathbf{e}}_x, 0, 0), \quad \tilde{\mathbf{h}}_{\text{TM}} = (0, \tilde{\mathbf{h}}_y, 0), \quad (2.38)$$

$$\tilde{\mathbf{e}}_{\text{TE}} = (0, \tilde{\mathbf{e}}_y, 0), \quad \tilde{\mathbf{h}}_{\text{TE}} = (\tilde{\mathbf{h}}_x, 0, 0). \quad (2.39)$$

For H_{pol} (2D TM), the impedance and apparent resistivity and phase are defined as

$$\mathbf{Z}_{xy} = \frac{\tilde{\mathbf{e}}_x}{\tilde{\mathbf{h}}_y}, \quad \rho_{xy} = \frac{1}{\omega\mu_0} |\mathbf{Z}_{xy}|^2, \quad \phi_{xy} = \tan^{-1} \left(\frac{\text{Im}(\mathbf{Z}_{xy})}{\text{Re}(\mathbf{Z}_{xy})} \right). \quad (2.40)$$

Similarly for E_{pol} (2D TM)

$$\mathbf{Z}_{yx} = -\frac{\tilde{\mathbf{e}}_y}{\tilde{\mathbf{h}}_x}, \rho_{yx} = \frac{1}{\omega\mu_0} |\mathbf{Z}_{yx}|^2, \phi_{yx} = \tan^{-1} \left(\frac{\text{Im}(\mathbf{Z}_{yx})}{\text{Re}(\mathbf{Z}_{yx})} \right). \quad (2.41)$$

The vector Helmholtz equation with requisite boundary conditions is posed as EM eigenvalue problem. The theory of EM problem using eigenmode is presented. Total field formulation, secondary field formulation, derivation of $\tilde{\mathbf{h}}$ field and the response functions such as impedance, apparent resistivity and phase are described here. The EM eigenvalue problem can not be solved analytically because the analytical solution does not exist for boundary value problems with arbitrary variation of resistivity. Therefore, the EM eigenvalue problem, in its generality, can only be solved using some numerical technique. In present work the numerical technique Finite Difference Method is used to transform the EM eigenvalue problem (2.23) to the corresponding matrix eigenvalue problem and Lanczos/Arnoldi methods are used to solve for the eigenvalue/eigenvectors of the matrix. These methods are discussed in the next chapter.

FINITE DIFFERENCE IMPLEMENTATION

3.1 Introduction

The EM data interpretation activity crucially depends upon the accuracy and efficiency of the forward modeling algorithm. The analytical solutions of the governing partial differential equation, derived from Maxwell's equations, exist only for models with simple geometry and resistivity variation such as layered earth, sphere, etc. Even these analytical solutions involve complex integral or infinite series. Hence, an exact solution of most EM problems is not computable. The only alternative is to opt for numerical solutions.

There are two broad classes of numerical methods; Integral Equation Method (IEM) and Differential Equation Method (DEM). Both of these classes of methods have merits and demerits in terms of their efficiency and versatility. Preference of one method over the other is governed by the complexity of the model and available computer resources. These methods translate the integro-differential operator equation into a matrix equation. In IEM, the integral operator equation is transformed to the matrix equation through quadrature formulae. In IEM only anomalous region is modeled, resulting in a small but full coefficient matrix. However, the popular use of IEM is restricted to only finite volume targets buried in a simple geometry host.

For arbitrary variation of conductivity, the DEMs, like Finite Difference Method (FDM) and Finite Element Method (FEM), are commonly used. In these methods the whole domain of study is discretized. This results in large but grossly sparse coefficient

matrix. Recent advances in iterative matrix solvers, has resulted in these methods becoming superior to IEM. In FEM, the differential operator is reduced to a matrix through functional minimization while in FDM, it is reduced through finite difference equations. The mathematics of FDM is easier to implement than that of FEM. In the present work, FDM is used for 3D MT modeling.

3.2 Finite Difference Implementation

In FDM, the derivatives are approximated by the appropriate difference formula obtained by the Taylor series expansion. For detailed description of FDM, one can refer to standard texts like Forsythe and Wasow (1964), Hildebrand (1974), Mitchell and Griffiths (1980), Taflove (1995). A brief account of FD formulation of EM problem follows.

The EM eigenproblem defined by equation (2.23) can be transformed using the vector identity given in equation (2.32), to the differential equation

$$-\nabla^2 \mathbf{e}(\mathbf{r}) = \lambda \mu_0 \sigma \mathbf{e}(\mathbf{r}) . \quad (3.1)$$

This eigenproblem can be rewritten as

$$\iiint_v \nabla^2 \varphi \, dv = - \iiint_v \lambda \mu_0 \sigma \varphi \, dv , \quad (3.2)$$

where, φ denotes the scalar quantity representing any one of the three electric field components. Using Gauss integral theorem, the left hand side of the equation (3.2) can be transformed into surface integral equation

$$\iiint_v \nabla \cdot (\nabla \varphi) \, dv = \iint_s \nabla \varphi \cdot \hat{n} \, ds , \quad (3.3)$$

This step transforms the second order partial differential equation into first order one which is then approximated using central difference formulae.

For implementation of FDM to solve equation (3.1), the 3D grid discretization of a block domain is presented in the Figure 3.1. It is discretized by straight lines parallel to the three- coordinate axes (x-, y-, z-) in cartesian coordinates.

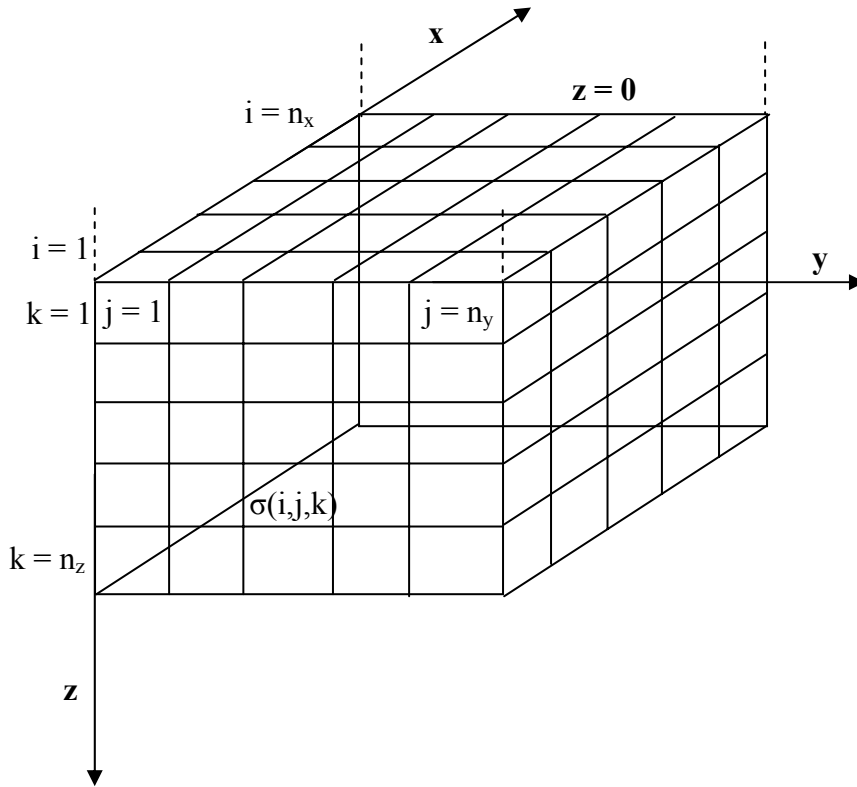


Figure 3.1: 3D Finite Difference grid.

3.2.1 Implementation of staggered grid

One can use either a normal grid or a staggered grid to implement FDM. In normal grid all the six electric and magnetic field components are assigned to one node while in staggered grid these are assigned to different points in a grid. As a result of numerical computations, $\nabla \cdot \mathbf{B}$ is not exactly zero in case of normal grid. However, in case of staggered grid, due to the arrangement of the electric and magnetic field values, $\nabla \cdot \mathbf{B}$ is implicitly zero. Thus, the field values, computed using staggered grid, are less erroneous

than those obtained using nodal grid. The staggered grid was introduced by Yee (1966) for electrical engineering problems but is now widely used to solve the EM problems in various disciplines.

Let the number of cells in the grid be n_x , n_y and n_z in x -, y - and z - directions respectively. Conductivity of the cell (i,j,k) is represented as $\sigma(i,j,k)$ and its volume as $v(i,j,k) = a(i).b(j).c(k)$, where $a(i)$, $b(j)$ and $c(k)$ are the distances between two adjacent nodes in x -, y - and z - directions respectively (Figure 3.2). The edges of the cube are $(x(i), x(i+1))$, $(y(j), y(j+1))$ and $(z(k), z(k+1))$. The cell edge centers are defined as $x_c(i)$, $y_c(j)$ and $z_c(k)$ with

$$x_c(i) = \frac{x(i) + x(i+1)}{2}, \quad y_c(j) = \frac{y(j) + y(j+1)}{2} \text{ and } z_c(k) = \frac{z(k) + z(k+1)}{2}.$$

The distance between two adjacent midpoints are defined by $a_h(i)$, $b_h(j)$ and $c_h(k)$ in x -, y - and z - directions respectively.

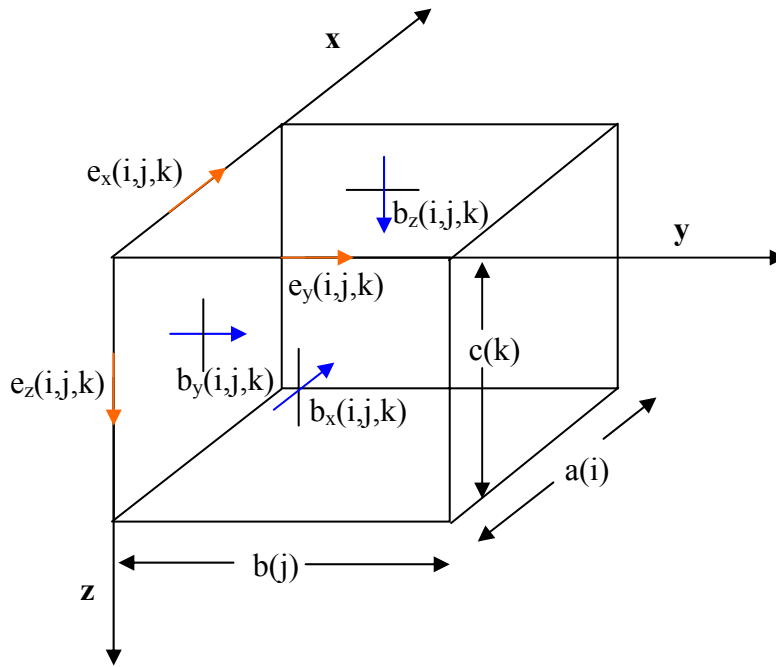


Figure 3.2: Arrangement of electric and magnetic field components on Yee's grid.

In Yee's staggered grid implementation, the six field components (three electric and three magnetic) are assigned to different points of each cell. In the current presentation (Figure 3.2) electric field components are assigned to the centre of cell edges while magnetic components are assigned to the centre of cell faces. In Figure 3.2, $e_x(i, j, k)$ is defined at $\{x_c(i), y(j), z(k)\}$ position, $e_y(i, j, k)$ at $\{x(i), y_c(j), z(k)\}$ and $e_z(i, j, k)$ at $\{x(i), y(j), z_c(k)\}$ respectively.

At the air-earth interface ($z = 0$), the grid is artificially extended to half cell height $c(1)/2$, into the air and the missing values are obtained by using field continuation algorithm given in Appendix A1 in detail. Rest of the five domain bounding surfaces are assumed to be perfectly conducting and the homogeneous Dirichlet boundary condition i.e. vanishing tangential component of electric eigenmodes at each surface, is imposed.

When employing FDM to solve the problem, it is better to take spatial average of conductivity at a node (Weaver, 1976). The integration is taken over a prism centered at the point where the electric component is evaluated to calculate the volume weighted average conductivity of the surrounding prism. The average conductivities, $\bar{\sigma}_x(i, j, k)$, $\bar{\sigma}_y(i, j, k)$ and $\bar{\sigma}_z(i, j, k)$, correspond to eigenmode components are $e_x(i, j, k)$, $e_y(i, j, k)$ and $e_z(i, j, k)$ respectively. The average conductivity $\bar{\sigma}_x(i, j, k)$, shown in Figure 3.3, is defined as

$$\bar{\sigma}_x(i, j, k) = \frac{1}{4V_x(i, j, k)} \left\{ b(j)c(k)\sigma(i, j, k) + b(j-1)c(k)\sigma(i, j-1, k) + \right. \\ \left. b(j-1)c(k-1)\sigma(i, j-1, k-1) + b(j)c(k-1)\sigma(i, j, k-1) \right\},$$

where $V_x(i, j, k) = a(i) \cdot b_h(j) \cdot c_h(k)$. (3.4)

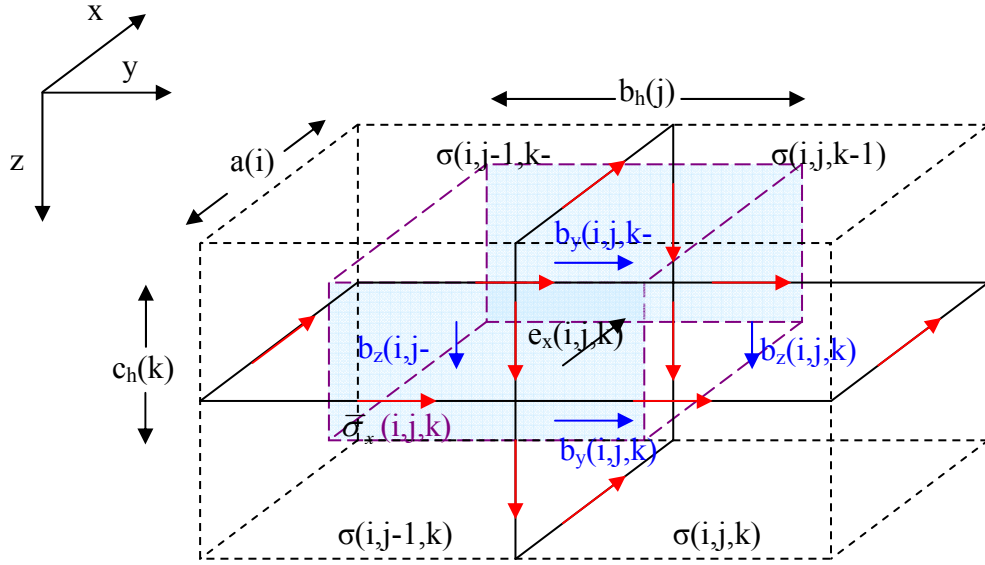


Figure 3.3: The grid cells and associated electric (red colour) and magnetic (blue colour) components required for the FD equation of $e_x(i,j,k)$. The shaded prism is of averaged conductivity $\bar{\sigma}_x(i, j, k)$.

The Finite Difference (FD) approximation of eigenvalue equation for e_x component is obtained from equation (3.3),

$$\frac{b_z(i, j, k) - b_z(i, j - 1, k)}{b_h(j)} - \frac{b_y(i, j, k) - b_y(i, j, k - 1)}{c_h(k)} = \mu_0 \bar{\sigma}_x(i, j, k) e_x(i, j, k). \quad (3.5)$$

Here, b_y and b_z are magnetic field components in y and z directions and these are further FD approximated, when applying equation (2.22) into equation (2.3) as

$$\frac{e_y(i + 1, j, k) - e_y(i, j, k)}{a(i)} - \frac{e_x(i, j + 1, k) - e_x(i, j, k)}{b(j)} = \lambda b_z(i, j, k). \quad (3.6)$$

From the two equations (3.5) and (3.6), it is clear that each electric component is connected with only surrounding twelve electric components. Therefore, the resulting

coefficient matrix will be 13 diagonal matrix. The symmetry of this matrix is conserved by the transformation;

$$\bar{e}_x(i, j, k) = d_x(i, j, k) e_x(i, j, k), \quad (3.7)$$

where the transformation factor $d_x(i, j, k)$ is

$$d_x(i, j, k) = \sqrt{\mu_0 \bar{\sigma}_x(i, j, k) V_x(i, j, k)},$$

with $V_x(i, j, k)$ being volume of the prism surrounding the point (i, j, k) where field is evaluated.

The resulting final equation for all electric field components in all the three directions is described in Appendix A2.

3.3 Description of System Matrix

After employing finite differences representation, the algebraic equations are assembled to form a matrix equation;

$$A \bar{e} = \lambda \bar{e}. \quad (3.8)$$

The electric field components can be arranged in different ways. Using different arrangements the eigenvalues and eigenvectors are not changed but the computational efficiency may be affected. The matrix A is real, symmetric, semi-positive definite and grossly sparse. The size of the matrix depends upon the total number of electric field components. The numbers of three electric field components are,

$$\text{number of } e_x \text{ components} = n_x (n_y - 1) n_z,$$

$$\text{number of } e_y \text{ components} = (n_x - 1) n_y n_z,$$

$$\text{number of } e_z \text{ components} = (n_x - 1) (n_y - 1) n_z.$$

Thus, the size of the matrix is

$$N_A = N_h n_z + (n_x - 1) (n_y - 1) n_z. \quad (3.9)$$

with $N_h = n_x (n_y - 1) n_z + (n_x - 1) n_y$.

The system matrix has a maximum 13 non-zero elements in each row or column besides the full block, due to field continuation, corresponding to the horizontal field components at air-earth interface. This full block is of dimension $N_h \times N_h$.

Firstly, the matrix eigenvalue problem is solved using the direct method of Singular Value Decomposition (SVD). This method does not take into account symmetry and sparsity and hence is not suitable for large size problems because of the explicit storage requirement of the matrix. To check the working of eigenmode formulation, the method was tested for half space model having resistivity $10 \Omega\text{-m}$, discretized using a uniform grid having $6 \times 6 \times 5$ cells in x-, y- and z-directions respectively. The resulting eigenvalues are plotted vs. eigenvalue number in Figure 3.4.

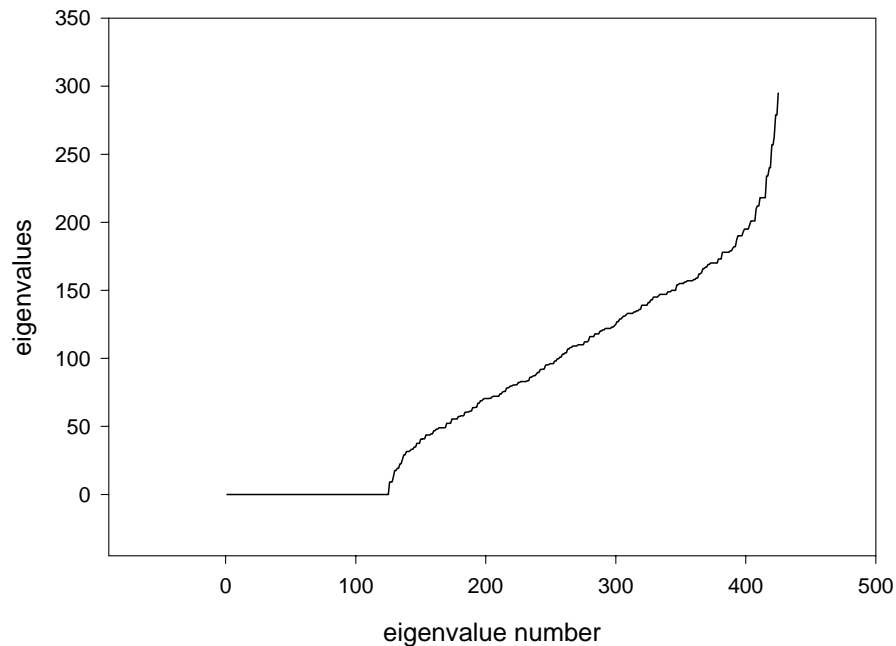


Figure 3.4: The eigenvalue plot for uniformly discretized half space.

Striking feature of the full spectrum of eigenvalues, shown in Figure 3.4, is that about one third of the total eigenvalues are equal to zero. In fact, the number of these zero eigenvalues is exactly equal to the number of internal nodes of the grid which is also equal to the number of e_z components, i.e. $\{(nx-1)(ny-1)nz\}$. These zero eigenvalues are termed as spurious eigenvalues and corresponding eigenvectors are also termed as spurious eigenvectors as these do not contribute to the field synthesis. Only the positive eigenvalues contributes to the solution. The positive eigenvalues are generally simple but may be multiple for degenerate case like, half space model. These positive eigenvalues are bounded in a region $(\lambda_{\max} - \lambda_{\min})$ as given below,

The min value of eigenvalue λ_{\min} is defined as,

$$\lambda_{\min} \approx \frac{1}{\mu_0 \sigma_{\max}} \left(\frac{\pi^2}{L_{\max}^2} + \frac{\alpha^2}{L_z^2} \right), \quad \pi/2 < \alpha < \pi. \quad (3.10)$$

The maximum value λ_{\max} is defined by,

$$\lambda_{\max} \approx \frac{1}{\mu_0 \sigma_{\min}} \left(\frac{1}{(\Delta x)^2} + \frac{1}{(\Delta y)^2} + \frac{\gamma}{(\Delta z)^2} \right), \quad \gamma > 1. \quad (3.11)$$

Here, lower bound depends on the overall dimension of the model while the upper bound depends upon grid discretization (Weidelt, 2009). Next section describes how these spurious eigenvalues are eliminated.

3.4 Elimination of Spurious Eigenmodes

The spurious eigenvalues suggest that the system has less degree of freedom than envisaged from the geometry. To study how these spurious modes can be eliminated, take the divergence of the eigenvalue equation (2.23),

$$\nabla \cdot (\nabla \times \nabla \times \mathbf{e}(r) - \lambda \mu_0 \sigma \mathbf{e}(r)) = 0, \quad (3.12)$$

$$\nabla \cdot (\lambda \mu_0 \sigma \mathbf{e}(r)) = 0. \quad (3.13)$$

There are only two possibilities;

- i) either $\lambda \neq 0$ then $\nabla \cdot (\sigma(r)\mathbf{e}(r)) = \nabla \cdot \mathbf{j} = 0$
- ii) or $\lambda = 0$ then $\nabla \cdot \mathbf{j} \neq 0$.

In the second case, the divergence free current density condition is not satisfied. Thus, to avoid spurious eigenmodes, the divergence free condition is enforced explicitly.

$$\nabla \cdot \mathbf{j} = 0, \quad (3.14)$$

$$\frac{\partial j_x}{\partial x} + \frac{\partial j_y}{\partial y} + \frac{\partial j_z}{\partial z} = 0. \quad (3.15)$$

Now, applying FD to this divergence equation we get,

$$\frac{j_x(i, j, k) - j_x(i-1, j, k)}{a_h(i)} + \frac{j_y(i, j, k) - j_y(i, j-1, k)}{b_h(j)} + \frac{j_z(i, j, k) - j_z(i, j, k-1)}{c_h(k)} = 0. \quad (3.16)$$

The definition of j_x , j_y and j_z are,

$$\begin{aligned} j_x(i, j, k) &= \bar{\sigma}_x(i, j, k) e_x(i, j, k), \\ j_y(i, j, k) &= \bar{\sigma}_y(i, j, k) e_y(i, j, k), \\ j_z(i, j, k) &= \bar{\sigma}_z(i, j, k) e_z(i, j, k). \end{aligned} \quad (3.17)$$

The number of spurious eigenmodes is equal to the number of e_z components, solving above equation for e_z component,

$$e_z(i, j, k) = \frac{\bar{\sigma}_z(i, j, k-1)}{\bar{\sigma}_z(i, j, k)} e_z(i, j, k-1) - \frac{c_h(k)}{\bar{\sigma}_z(i, j, k)} \left[\frac{j_x(i, j, k) - j_x(i-1, j, k)}{a_h(i)} + \frac{j_y(i, j, k) - j_y(i, j-1, k)}{b_h(j)} \right]. \quad (3.18)$$

Using Ohm's law to express j_x and j_y in terms of e_x and e_y respectively we get,

$$\bar{e}_z(i, j, k) = \frac{\bar{\sigma}_z(i, j, k-1)d_z(i, j, k-1)}{\bar{\sigma}_z(i, j, k)d_z(i, j, k)} \bar{e}_z(i, j, k-1) - \frac{c_h(k)}{\bar{\sigma}_z(i, j, k)d_z(i, j, k)} \quad 3.19)$$

$$\left[\begin{array}{l} \frac{\bar{\sigma}_x(i, j, k)d_x(i, j, k)}{a_h(i)} \bar{e}_x(i, j, k) - \frac{\bar{\sigma}_x(i-1, j, k)d_x(i-1, j, k)}{a_h(i)} \bar{e}_x(i-1, j, k) + \\ \frac{\bar{\sigma}_y(i, j, k)d_y(i, j, k)}{b_h(i)} \bar{e}_y(i, j, k) - \frac{\bar{\sigma}_y(i, j-1, k)d_y(i, j-1, k)}{b_h(i)} \bar{e}_y(i, j-1, k) \end{array} \right]$$

For first layer corresponding to $k = 1$, the first term in above equation is zero because $\bar{\sigma}_z(i, j, k-1) = 0$. Thus, each vertical component can be represented by four horizontal components of the same layer and four components of the layer just above it. Thus, for each vertical component a total of $4 \cdot k$ components are added to each row. This equation is applied to all \bar{e}_z components, reducing the matrix dimension to $N_R = N_A - N_V$, N_V being the number of e_z components. In the reduced matrix, the number of non-zero elements from the direct FD coefficient matrix reduces to 9 from 13 because of replacement of four \bar{e}_z vertical components with horizontal components. This suggests a maximum of $16 \cdot k$ replacements in general, and it leads to $6 \cdot (2k - 1)$ non-zero elements in a row of layer k .

This increase of additional elements in a row leads to loss of symmetry. Each layer components are related to all the components of above overlying layers.

3.5 Reduced System Matrix

The reduced coefficient matrix structure is shown in Figure 3.5. The eigenvectors have only the horizontal components. The dimension of reduced system matrix is $N_R = (n_x(n_y - 1) + (n_x - 1)n_y)n_z$. The matrix is real, non-symmetric, positive definite, and smaller in size by a factor of approximately 1/3. It is less sparse in comparison with the original symmetric matrix. The matrix elements are stored in compressed sparse row (CSR)

format (Saad, 1994) because of its efficient performance for some of the standard matrix operations.

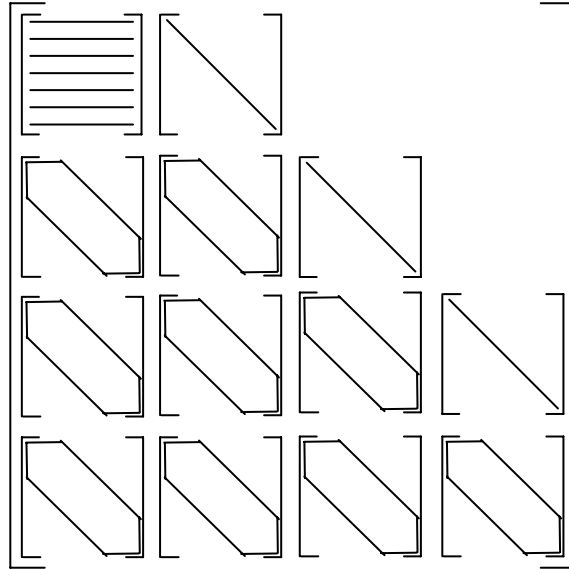


Figure 3.5: Representation of reduced matrix structure.

After implementing the divergence correction, the final reduced matrix is obtained. Now, the eigenmodes of this matrix are to be found using some efficient eigenmode solver.

3.6 Eigensolver for the Matrix

A variety of matrix eigensolvers such as direct, iterative and semi iterative are used in EM problems (Sarkar et al., 1981). Direct solvers, where the complete matrix banded or full matrix is stored, provide the solution in finite but large number of steps. In iterative methods, on the other hand, where an initial guess is improved in a series of iterations, the procedure can be stopped whenever the approximate solution with prescribed accuracy is obtained. Iterative methods exploit sparsity structure of the matrix to the maximum (Jacobs, 1981) and are therefore preferred for sparse systems. Though iterative solvers

score on sparsity ground, yet their use is not recommended when diagonal dominance is not guaranteed or when the matrix is indefinite. Semi-iterative methods based on Conjugate Gradient (CG) method are commonly used even for indefinite matrices.

When the coefficient matrix is real, positive definite and large in size, iterative methods are widely used to obtain the eigenvalues and eigenvectors. The oldest method to find eigenvalue iteratively is the power method. This method was first used to find the largest eigenvalue of the system matrix. Krylov subspace projection methods are based upon the intricate structure of the sequence of vectors naturally produced by the power method. In Krylov methods, only product of the matrix with a vector is needed. Arnoldi and Lanczos are popular Krylov subspace methods. Lanczos is used for symmetric matrices while Arnoldi is used for non-symmetric matrices. Since in our eigenmode solution of EM field problem, only a small subset of smallest eigenvalues is needed, we have adapted the ‘ARPACK software’ subprograms based on Arnoldi method, in the development of our eigenmode solver to find the eigenvalues.

ARPACK (Arnoldi Package) (Lehoucq et al., 1997) is a collection of FORTRAN subroutines used to solve large eigenvalue problems. This is based on implicit restart scheme, known as Implicit Restarted Lanczos/Arnoldi Method (IRAM/IRAM), which is very efficient in finding a small subset of desired (either smallest or largest) number of eigenvalues and eigenvectors of a matrix. Storage requirement are of the order of $N \cdot (O(k) + O(k^2))$. This software is capable to determine the desired pre-specified number of eigenvalues for largest magnitude (LM), smallest magnitude (SM), largest algebraic part (LA) and smallest algebraic part (SA). To obtain the desired subset the implicit restarted scheme is presented in the next section.

3.6.1 Implicitly restarted Lanczos/Arnoldi method

Lanczos/Arnoldi method is a Krylov subspace based method. A basis of Krylov subspace can be obtained from any arbitrary starting vector (V_1) and its repeated product with the system matrix A . The Krylov basis vectors not being orthogonal, are orthogonalized and the orthogonalized basis vectors serve as Lanczos/Arnoldi vectors. Lanczos/Arnoldi method was used to solve for all eigenvalues and eigenvectors of a symmetric/nonsymmetric matrix using the relation

$$AV = VH + r, \quad (3.20)$$

where A is the coefficient matrix, V is the matrix of Lanczos/Arnoldi vectors of dimension N column-wise, H is a symmetric tri-diagonal/upper Heisenberg matrix and r is the residual vector. The Matrix A is of $N \times N$ and the vector r is an N dimensional vector.

Complete eigenanalysis of the tridiagonal/upper Hessenberg matrix H need be performed. This, in turn, leads to eigenvectors of matrix A . Theoretically, r should be zero but in finite precision arithmetic it has a prescribed very small value.

Presently, Lanczos/Arnoldi Method is widely used to find a desired subset of eigenvalues as described by Sorensen (1992). In the present case, the interest is in M smallest eigenvalues and corresponding eigenvectors. After the generation of M Lanczos/Arnoldi vectors, the residual vector has a finite value. To find M smallest eigenvalues and corresponding eigenvectors, we have to generate a subspace with $M+P$ Lanczos/Arnoldi vectors as given below

$$AV_{M+P} = V_{M+P}H_{M+P} + r_{M+P}e_{M+P}^T. \quad (3.21)$$

In this case V matrix is of the order of $N \times (M+P)$ and H matrix is of the order of $(M+P) \times (M+P)$. Eigenanalysis of this smaller dimensional matrix H is performed rather

than full $N \times N$ matrix. The eigenvalues obtained from this $M+P$ factorization reflects characteristics of full spectrum of N eigenvalues. We arrange $M+P$ eigenvalues in increasing order so that last P largest eigenvalues becomes unwanted ones. These P values are used as shifts to update the first M values via QR iterations. In this updating process Lanczos/Arnoldi vectors are forced to belong to the subspace corresponding to smallest eigenvalues and the residual vector r_{M+P} becomes very small iteratively. This technique is known as Implicit Restart Techinque. It is recommended that P be greater than M . There are two modes to find the subset of eigenvalues defined as ‘regular mode’ and ‘shift and invert mode’ as discussed below.

3.6.1.1 Regular mode

In regular mode, one deals with the problem

$$Ax = \lambda x. \quad (3.22)$$

In this mode only product of the matrix with a vector is needed. Arnoldi method converges faster for larger magnitude eigenvalues; therefore to calculate smallest eigenvalues with SM or SA it takes longer time.

3.6.1.2 Shift and invert mode

In shift and invert mode, the dealing equation is

$$(A - \xi I)^{-1} x = x \nu, \quad \nu = \frac{1}{\lambda - \xi}. \quad (3.23)$$

The eigenvalues converges near to applied shift ‘ ξ ’. This method converges faster when determining the smallest eigenvalues. The main disadvantage of implementing this mode is that one must provide a matrix solver, either direct or iterative, to obtain the term $(A - \xi I)^{-1} x$.

Any one of the conjugate gradient based methods can be used to solve for the product $(A-\xi I)^{-1}x$. There are different variants of conjugate gradient methods such as Conjugate Gradient (CG), Bi-Conjugate Gradient (BiCG) and Bi-Conjugate Gradient Stabilized (BiCGStab) methods. To increase efficiency of these methods, different preconditioners such as Jacobi or incomplete factorization methods are also used. Incomplete factorization method ILU (0) means that during LU factorization there is zero fill in. Van der Vorst (2003) suggested that BiCGStab with ILU(0) gives better results. The number of iterations needed to solve a matrix equation by various methods using the preconditioner ILU (0), are given in Table 3.1. The matrix was of order 50×50 .

Table 3.1: Comparison of different methods with preconditioners for best invert matrix solver.

Method	Number of iterations
CG	30
BiCG	20
BiCGStab	15
CG + ILU(0)	12
BiCGStab + ILU(0)	9

3.7 Synthesis of Full Eigenvector

The eigenvectors of the reduced matrix obtained using IRAM are orthogonal to each other. As the reduced eigenvectors comprise only the horizontal components, these have dimension N_R . The eigenvectors must be transformed into full eigenvectors for use in

field synthesis. The remaining components of the eigenvectors are obtained by using spurious eigenvector relation (3.19). The e_z components are appended to the reduced eigenvector components. A good feature is that these full eigenvectors are also numerically orthogonal. Hence, there is no need to orthogonalize these full eigenvectors again explicitly. However, these eigenvectors should follow the sigma orthogonality relation,

$$\sum_{m=1}^{N_A} \sigma(m) \hat{\mathbf{e}}_1(m) \hat{\mathbf{e}}_n(m) V(m) = \delta_{ln}. \quad (3.24)$$

This condition yields a scaling factor η_n , given in Appendix A2, which provides the final sigma orthogonalized eigenvectors as,

$$\hat{\mathbf{e}}_n = \eta_n \cdot \mathbf{e}_n, \quad (3.23)$$

where \mathbf{e}_n are back transformed from $\bar{\mathbf{e}}_n$ using the transformation relation (3.13).

This completes the discussion of implementation of Finite Difference for the solution of eigenmodes. These eigenmodes are used to solve for the superposition coefficients using equation (2.33). Secondary field values are then solved using equation (2.26) and finally equation (2.29) gives the total field values, $\tilde{\mathbf{e}}_T$. These field values are next used to derive the magnetic field $\tilde{\mathbf{h}}$ and the response functions: impedance, apparent resistivity and phase. In next chapter, developmental details of the algorithms MT_2D_EA and MT_3D_EA are discussed.

DEVELOPMEENT AND DETAILS OF ALGORITHM

4.1 Introduction

We started with the development of 2D algorithm MT_2D_EA and finally developed the 3D algorithm MT_3D_EA. In both these algorithms Finite Difference Method (FDM) is used to obtain the discretized EM eigenvalue problem. The eigenmodes of the corresponding coefficient matrix, obtained using Lanczos/Arnoldi method, are then used to synthesize the electric field vector which, in turn, was used to obtain the magnetic field vector and the derived MT response functions impedance, apparent resistivity and phase. The sequence of development, highlighting the difficulties faced and the manner in which these were overcome, is presented below.

4.2 Sequence of Development

The present study was spanned over a period of about five years. In this period 1D, 2D and 3D modeling algorithms for magnetotelluric data were developed. In this section, the different versions of algorithm are presented. It may be stressed here that MT_2D_EA development took only 10% of the time spent on the development of MT_3D_EA. This was so because in the 3D case, bulk of the time was spent in overcoming the problems resulting from coarseness of the grid used. Use of a coarse grid became necessary because of the limitation on size of the problem imposed by the available PC or work station. As a byproduct, this study has led to a better understanding of the effect of coarseness of the grid on MT response.

4.2.1 *Development of MT_2D_EA algorithm*

Initially, the 2D algorithm was developed using the same methodology as was to be used in 3D case i.e. eigenmode analysis using FDM. In the first development, the Dirichlet boundary condition was applied on all the four domain boundaries i.e. the two horizontal and the two vertical sides. The problem was solved only for internal nodes using total field formulation. The results were satisfactory at the centre of the model but these were somewhat anomalous near the vertical domain boundaries. The problem was circumvented by using autogrid and more appropriate boundary conditions. We replaced the manual grid with an autogrid generated scheme employing the skin-depth EM field decay criterion. Further, the application of integral boundary condition at the air earth interface and of asymptotic boundary condition at the vertical sides provided the accurate results even at the vertical boundaries of the domain. Since in MT formulation, the derived observables: impedance, apparent resistivity and phase, depend on the ratio of the components of \mathbf{E} and \mathbf{H} field values, we verified that for both E and H field boundary conditions the results are same. Prior to this conclusion achieved, all the eigenmodes were computed and then used to synthesize the electric field.

Sufficiently large time and memory is required for the solution of all eigenmodes. In the expression of the superposition coefficient, in equation (2.27) or (2.32), the eigenvalue appears in the denominator and thus smallest eigenvalues dominate in the field synthesis. This observation suggested that use of only a small subset of smallest eigenvalues and corresponding eigenvectors may accurately synthesize the electric field values and thereby significantly reduce the computational time. For implementation of this step, the Implicitly Restarted Lanczos Method (IRLM) is used. This implementation

produces numerically accurate field values for 5% of eigenmodes in one fourth of the computational time needed for all eigenmodes.

4.2.2 *Development of MT_3D_EA algorithm*

In the case of 3D, taking cue from the experience of 2D algorithm, right from the beginning we implemented the integral boundary condition (IBC) at air earth interface.

Following the formulation given in chapter 3, first the coefficient matrix (equation (3.8)) was generated for all electric field components. The resulting matrix was a 13-diagonal symmetric matrix. We used Singular Value Decomposition (SVD) to solve for the eigenvalues and eigenvectors of this matrix. About one third (exactly equal to no. of vertical electric field components) of the total eigenvalues of this symmetric matrix was found to be zero. These zero eigenvalues and corresponding eigenvectors are termed as ‘spurious’ and these are not used for field synthesis. The secondary field values are obtained without these spurious eigenmodes. Finally, the derived magnetic field and response functions are calculated using the electric field values.

The zero eigenvalues create difficulty in getting the smallest non-zero eigenvalues. This problem was resolved by using the current divergence equation (3.18) to eliminate the vertical electric field components by expressing these in terms of the horizontal components. However, in this process, the structure of resulting coefficient matrix is changed from symmetric to non-symmetric. Due to this we were unable to use the IRLM which is applicable only to symmetric matrices. Implicitly Restarted Arnoldi Method (IRAM) is used for non-symmetric matrices. In IRAM to obtain smallest eigenmodes Bi-CGStab (Bi- Conjugate Gradient Stabilizer) with preconditioner ILU(0) is used. Using the IRAM, we observed that the convergence is achieved after two iterations itself. This

process did result in the convergence of eigenvalues. However, inspite of the fact that the remainder vector becomes null, the eigenvectors did not converge. This problem gets resolved, if in the next updating of eigenmodes, a non null vector (that is orthogonal to the previous eigenvectors) is used. These eigenmodes are finally used for field synthesis and response computations.

4.3 Salient Features of MT_3D_EA Algorithm

Besides the eigensolvers, various other steps are taken to enhance the efficiency and versatility of the algorithm MT_3D_EA. Since the algorithm has a compact modular structure, a subroutine can be plugged in or taken out easily without affecting the remaining program. The features to enhance versatility or efficiency are discussed below.

4.3.1 Response functions

The algorithm is presently developed to get the responses for magnetotelluric profiling. The responses are computed at the surface for a single frequency. The algorithm can compute response functions like impedance, apparent resistivity and phase, for both the modes, 2D-TE and 2D-TM given by equations (2.41) and (2.40) respectively. The choice of response modes is controlled by the counter *mode_type*. The response functions impedance and apparent resistivity and phase are computed in subroutine *output_3D*.

4.3.2 Source term

The program is so structured that the computations are carried out in terms of secondary fields. Later on, for total field computations, the primary fields are added to these secondary fields. Thus, in order to incorporate the source effect, only a subroutine computing the responses of primary layered earth model in the presence of given source, is

added in lieu of the existing subroutines *eigenmode_1D* and *output_1D* which compute the 1D field due to a plane wave source.

4.3.3 *BiCGStab method*

Arnoldi method converges better in invert mode when evaluating the smallest eigenvalue. In invert mode, the matrix solver Bi Conjugate Gradient Stabilized (BiCGStab) is used because with appropriate preconditioner it provides the solution in optimal time.

4.3.4 *Multi-frequency response*

In the proposed approach, eigenmodes are independent of source or frequency and these depends only on the model characteristics. In conventional FDM algorithms, the program has to be re-run to generate the response for each frequency, while in our approach, once the eigenmodes are evaluated, the responses for different frequencies can be easily computed in negligible computer time.

4.4 Description of MT_3D_EA Algorithm

The algorithm, MT_3D_EA, employs FDM for solving the EM eigenproblem to compute the 3D MT responses. The algorithm comprises 11005 lines and 60 subroutines. It employs 4 complex arrays, 75 real arrays, 14 real variables and 24 integer variables. It works in double precision arithmetic. In order to control dimension overflows, various checks with error and stop messages are inserted in the program. The arrays are initialized and reused to optimize the memory requirement. The description and salient features are highlighted in the Figure 4.1.

Total seven I/O units are opened in the program. The parameters and data controls are read from the input file. Two scratch files are used for buffer storage. The remaining

four output files are used for different outputs helpful in analyzing the results. Sample input/output files are given in the Appendix A4.

Basic Algorithm Statistics	
MT_3DEA	- 11005 Lines
Main program	- 158 Lines
Subroutines	- 10847 Lines
	60 (40+20*)
* Adapted from other program	
Methodology	
Finite Difference Method to transform the EM eigenproblem to matrix eigenproblem	
Eigenmode Formulation to express the electric field components as a linear superposition of eigenvectors of the EM eigenproblem	
Bi-CGStab with ILU(0) Preconditioner to implement the shift and invert mode of IRAM efficiently	
Salient Features	
Integral boundary condition at the air-earth interface	
IRLM/IRAM for eigenproblem solution	
Very fast Multi-frequency response computation using eigenmodes	

Figure 4.1: Algorithm in nutshell.

4.5 Structure of MT_3D_EA Algorithm

The main module of the algorithm MT_3D_EA provides the infrastructure and runs the controls. In the main program the control parameters are defined, input and output files are opened and the subprograms are called as shown in Figure 4.2. Input data and other

parameters are read in the subroutine *input*. A list of various subprograms highlighting their purpose and other details is given in Table A3.3 of Appendix A3.

The grid data can be read in two ways either as a manually generated grid or as a logarithmically generated grid. The control parameters *irx*, *iry* and *irz* respectively control the grid choice in x-, y- and z-directions. The logarithmic grids are computed in subroutine *grid*. The resistivity or conductivity is read for the half space and for the anomalous prisms and finally stored in 3D arrays *sx*, *sy* and *sz*. Calculations of the elements of coefficient matrix, for all electric field components, are carried out in subroutine *weight*. Subroutine *weight_ez* is used for calculations for updating the elements corresponding to the horizontal components of coefficient matrix in the reduced matrix case where the e_z components are replaced in terms of horizontal components e_x and e_y (equation (3.18)). Integral boundary condition is implemented in subroutines *conti1*, *conti2*, *conti3* and *conti4* depending upon the uniformity and non-uniformity of grids in horizontal directions. The starting vector is initialized in subroutine *init*.

The subroutine *eigenmode_1D* is used for 1D layered model coefficient matrix and eigenmode computations and the subroutine *output_1D* generates primary field values for given frequency. 3D eigenmodes are computed in subroutine *eigenmode_3D*. These eigenmodes are used in subroutine *output_3D* for response function computations. The responses are obtained, in subroutine *output_3D*, by computing (i) the superposition coefficients using equation (2.33), (ii) the secondary field values using equation (2.26), (iii) the total field values using equation (2.29), and (iv) the response functions impedance and apparent resistivity and phase using equations (2.40) and (2.41) respectively.

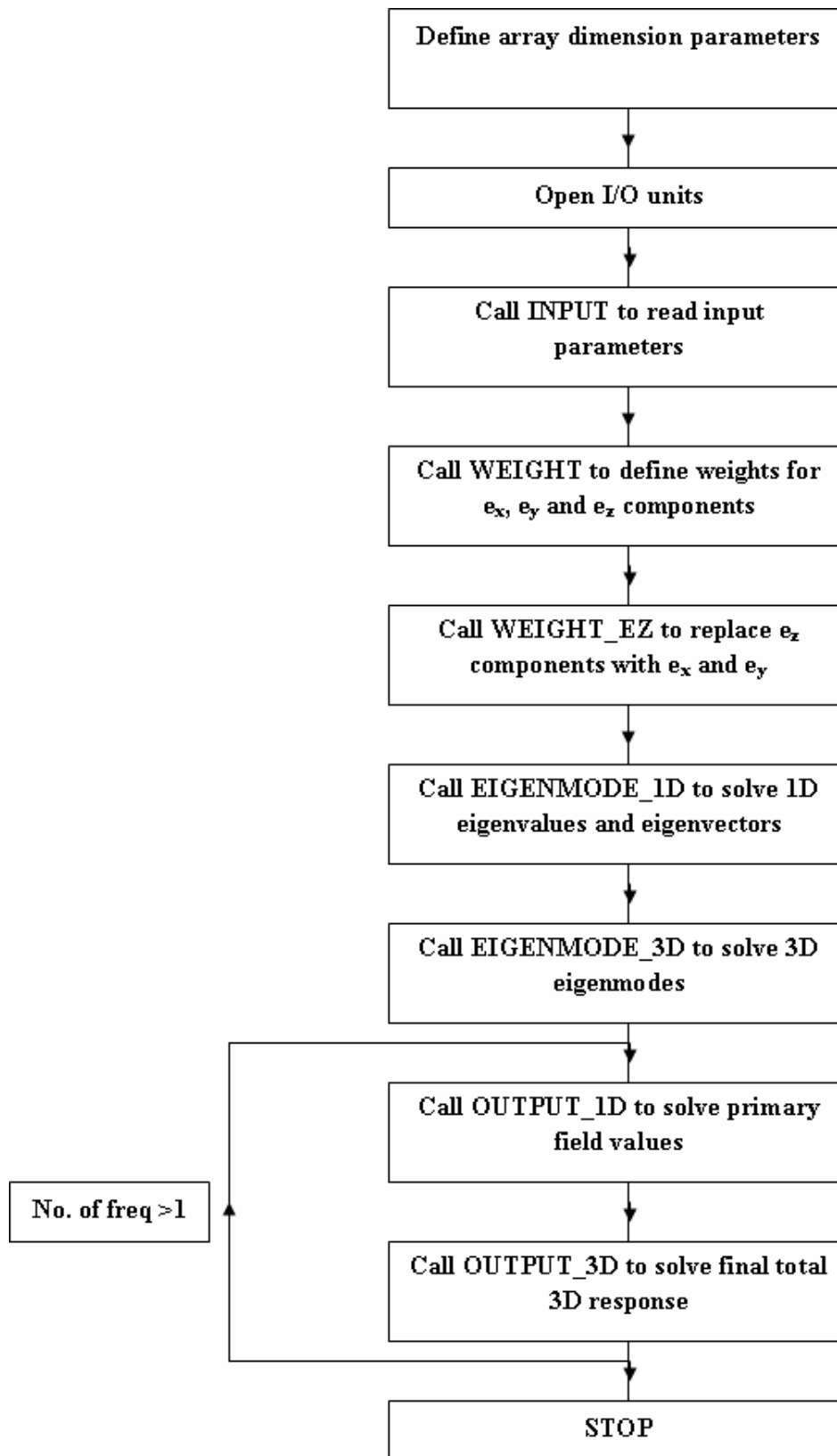


Figure 4.2: Flow chart of main program.

The subroutines *output_1D* and *output_3D* are recalled when the responses for multi-frequencies are to be computed.

Bulk of the computer time is consumed in eigenmode computations carried out in the subroutine *eigenmode_3D* whose flow chart is shown in Figure 4.3. It calls subroutine *eigenstep* to generate the Hessenberg matrix of Arnoldi formulation element and new Lanczos/Arnoldi vector (equation (3.20)). *eigenstep* implements the updating of eigenmodes using equation (3.21). This subroutine *eigenstep* is called twice if a subset 'k' of eigenmodes is needed, first for computing k components and secondly for computing p components ($p > k$). Eigenvalues and eigenvectors are solved in subroutine *dlahqr*. The eigenvalues of the computed Hessenberg matrix are ordered increasingly and last p eigenvalues are applied as shift to update first k eigenvalues in subroutine *dnapps*, adapted from ARPACK. During the iterative process last p values are discarded after *dnapps* and *eigenstep* is recalled for p component computation. This iterative process stops after reaching a threshold value *lanc_tolr*. The outcome eigenvectors contains only e_x and e_y components and remaining e_z components are calculated in subroutine *get_ez* to constitute full eigenvector.

Subroutine *bicgstab* is used in invert mode of IRAM (equation (3.23)) to solve a subset of eigenmodes as desired in *eigenstep* for subset of eigenmodes computation as shown in Figure 4.4. Subroutine *ael* is used for all eigenmode computation. In this subprogram Arnoldi steps are applied twice to get numerically orthogonal eigenvectors. Finally Hessenberg matrix is the outcome of this subprogram.

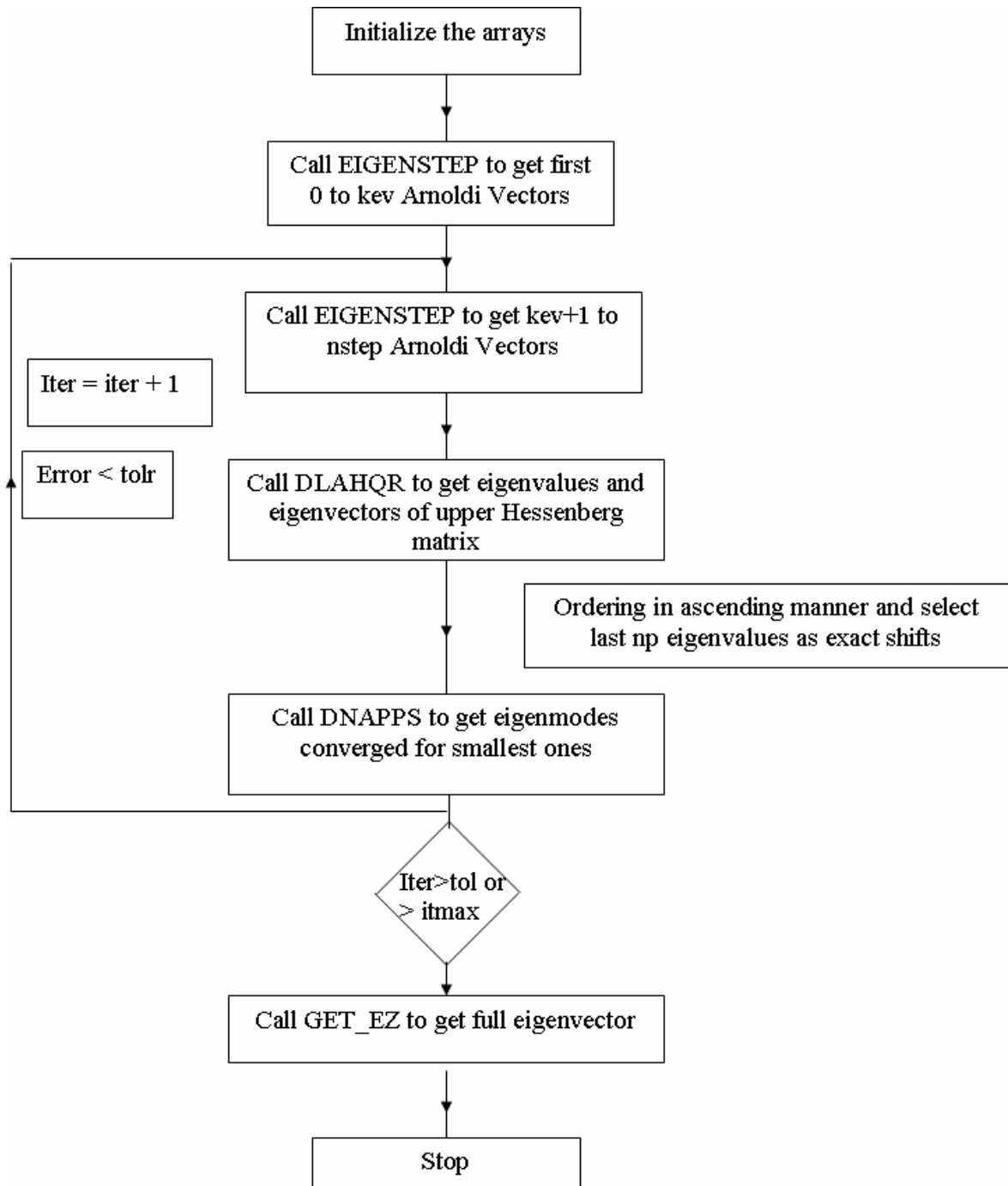


Figure 4.3: Flow chart of EIGENMODE_3D subprogram.

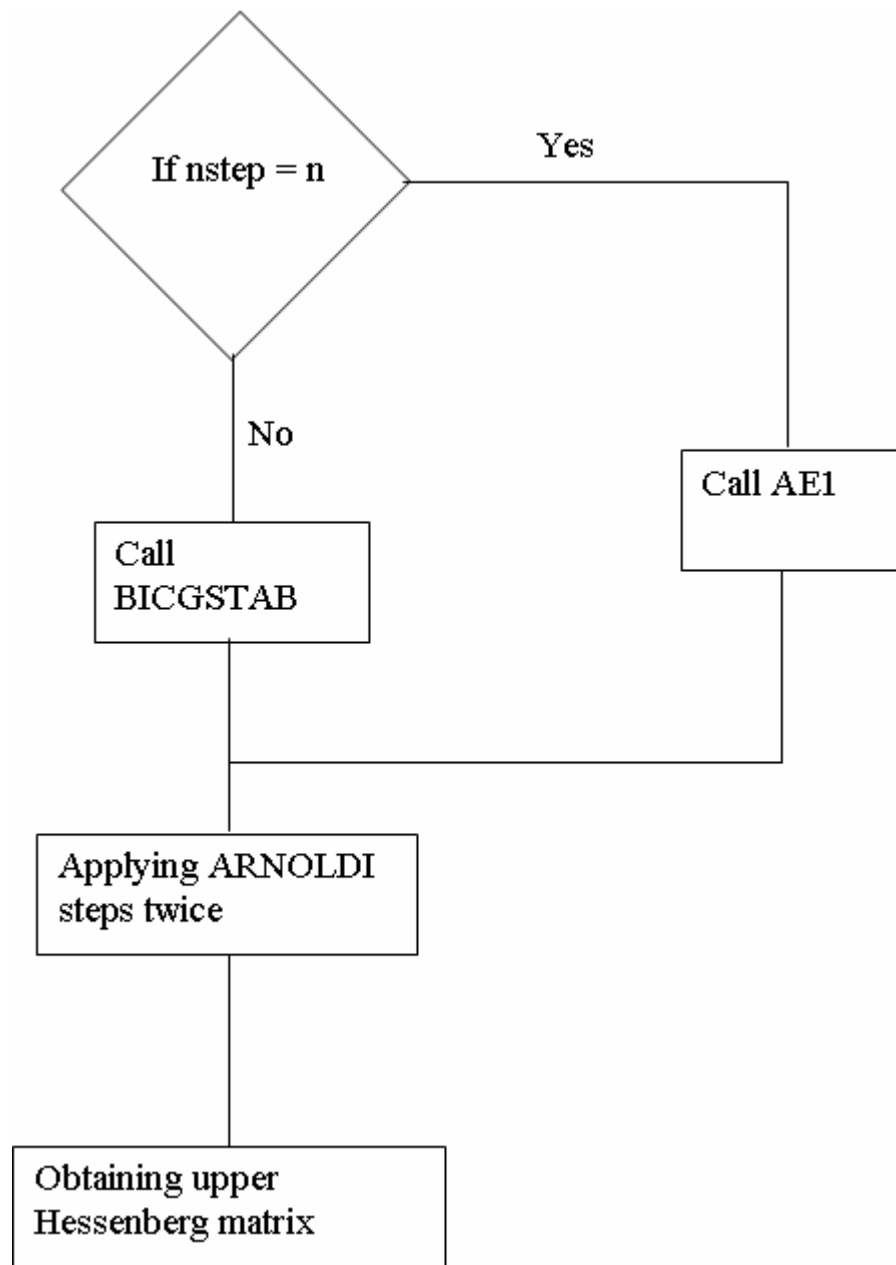


Figure 4.4: Flow chart of EIGENSTEP subprogram.

The control parameters and their purpose and numerical value for different options are listed in Table A3.1 of Appendix A3. The grid parameters and other run environment parameters used in different subprograms are described in Table A3.2 of Appendix A3. The description of development of algorithm is completed. The results of experiments performed for checking and validation of MT_2D_EA and MT_3D_EA are presented in the following chapter.

RESULTS AND DISCUSSION

After developing the requisite software it is natural to establish its efficiency and accuracy. The accuracy is established by performing various consistency design experiments and by reproducing the analytical results and the numerical results published in literature. The development of 3D algorithm was preceded by the developments of 1D and 2D codes. Therefore, first the 1D and 2D versions were tested and there after the 3D version. However, only the comparison for the responses of 2D and 3D models is discussed.

5.1 2D Experiments

The best check of any algorithm is the reproduction of established published results. Two 2D models were taken from COMMEMI (Comparison Of Modeling Methods for Electro-Magnetic Induction) paper (Zhdanov et al., 1997), one simple and other complex one. In COMMEMI paper authors describe the results of different algorithms based on Finite Difference, Finite Element and Integral Equation Methods for the same models for confidence. The comparison is presented here for electric field and apparent resistivity values only.

5.1.1 *Simple model*

The simple model, (2D-1) in the COMMEMI paper, is reproduced in Figure 5.1(a). It comprises a symmetrical rectangular insert embedded in homogeneous half space. The resistivity of the inserted block is 0.5 Ω -m while that of the half space is 100 Ω -m.

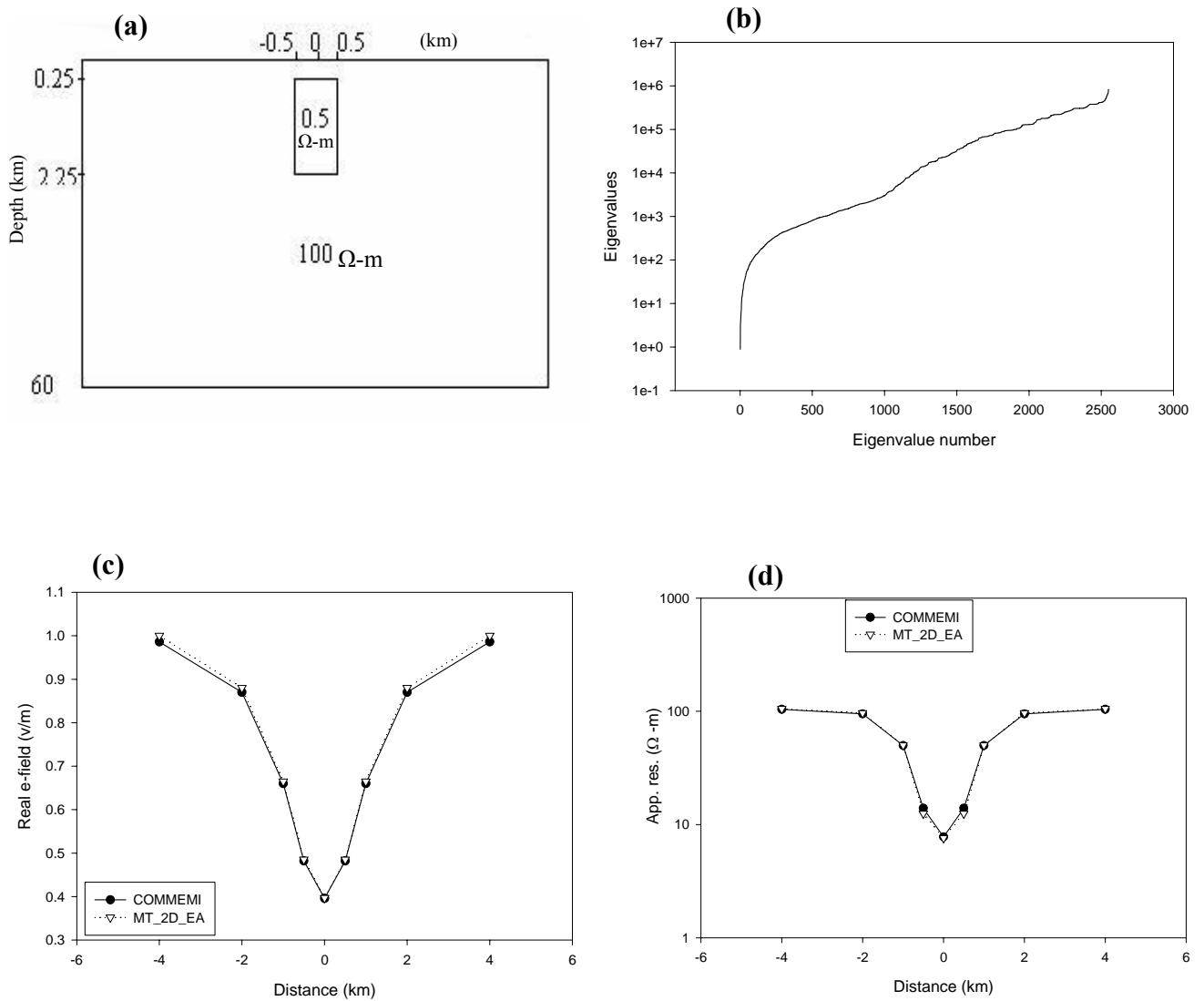


Figure 5.1: (a) Simple model (Model 2D-1 of COMMEMI, distance in km and resistivity in $\Omega\text{-m}$), (b) eigenvalue plot; Comparison of COMMEMI (Zhdanov et al., 1997) and MT_2D_EA at 0.1s (c) electric field and (d) apparent resistivities.

The block, placed at a depth of 250 m from the earth surface, has a width of 1 km and thickness 2 km. The response is computed at a period 0.1s. In Figure 5.1(b) the eigenvalue plot for the model is presented and in Figure 5.1(c) and 5.1(d) respectively electric field and apparent resistivity responses are compared with the average values given in the COMMEMI paper. The RMS error between the two responses is 0.01.

5.1.2 *Complex model*

The complex model, (2D-4) of Zhdanov's paper, is given in Figure 5.2(a). It consists of different blocks with resistivities varying from 2.5 Ω -m to 1000 Ω -m and with different widths and thicknesses. In the paper, they observed that the error is minimum at 1s. They also stated that due to the secondary field calculations, the error in apparent resistivities varies in the range 5-10%. We are also using secondary field formulation, so we compared the responses at the same period. The eigenvalue plot for the complex model is given in Figure 5.2(b). The response of this model is compared in Figure 5.2(c). Again comparison is with the average values published in the paper. The RMS error in apparent resistivity is 0.06 or 6%, which is in the acceptance limits. We have observed that our results are closer to the Integral Equation Method results.

After having a good response from the 2D modeling algorithm, we moved on to study the performance of 3D algorithm. In case of 3D, due to limited computer facility, a severe limitation on the number of grid points was imposed and we were able to run models with very coarse grids. The effects of coarse grid led us to overcome several spurious numerical problems. To test the algorithm, several tests are performed as described below.

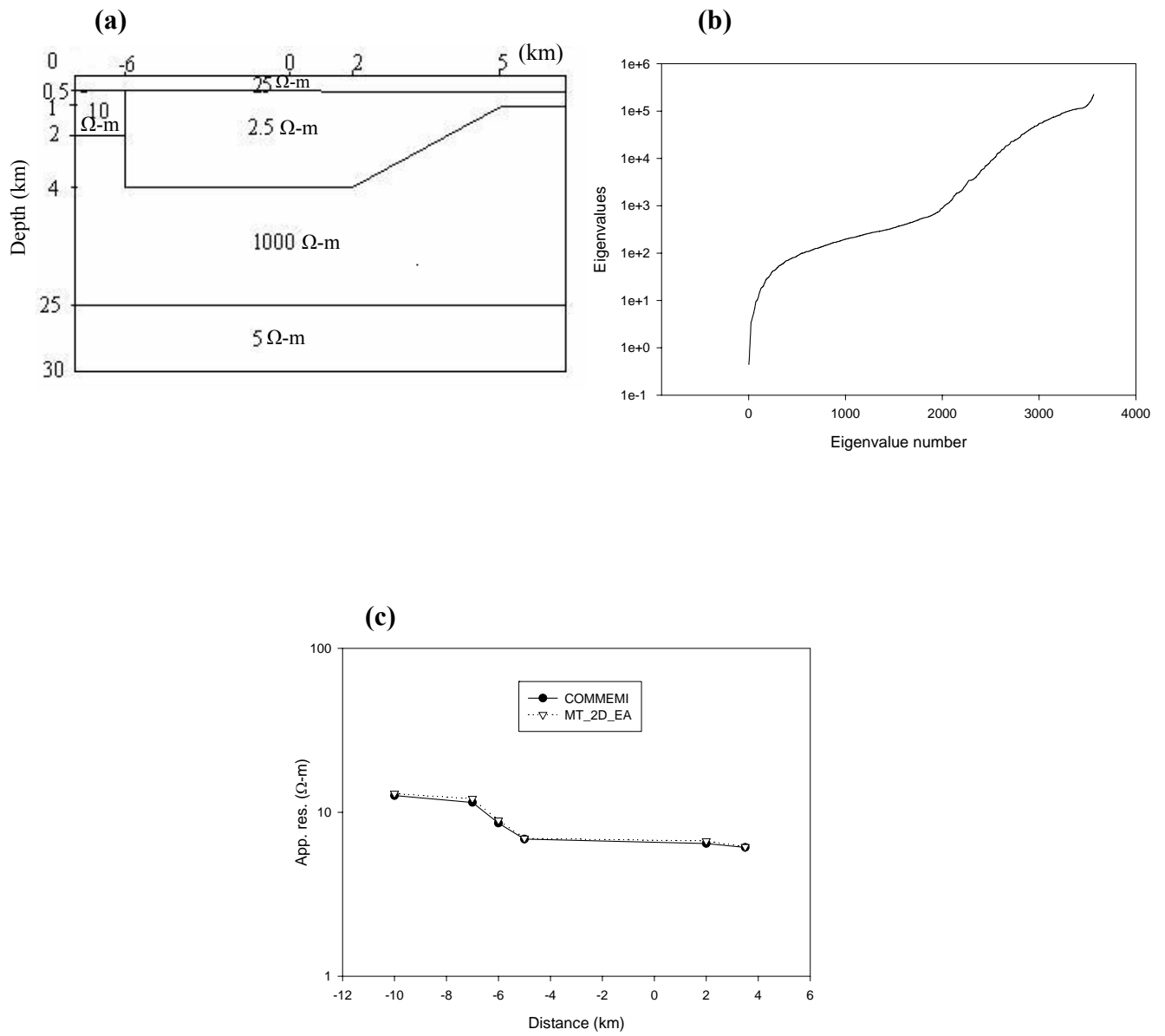


Figure 5.2: (a) Complex model (Model 2D-4 of COMMEMI, distances in km and resistivity in $\Omega\text{-m}$), (b) eigenvalue plot and (c) comparison between apparent resistivities of COMMEMI and MT_2D_EA at 1s.

5.2 3D Experiments and Results

For 3D modeling experiments, we designed a simple model, shown in Figure 5.3(a), comprising a cube buried in a homogeneous half space. The dimensions of the cube are 500m x 500m x 500m, its resistivity is 0.1 Ω -m while the resistivity of half space is 1.0 Ω -m. We term it as 3D test model.

The list of consistency and accuracy experiments conducted for 3D case is given below:.

1. Comparison with analytical solution
2. Convergence of electric field with the refinement of grid
3. No contrast study
4. Electrically same model
5. Reduced and full version responses
6. Effect of working with different percentages of eigenmodes
7. Multi-frequency response computation
8. Convergence of responses with Extending strike length to corresponding 2D response
9. Comparison of our response of 3D-2 model of COMMEMI paper with their response.

5.2.1 Comparison with analytical solution

In the first exercise, we compared the eigenvalues and eigenvectors for a half space, discretized with uniform grid spacing in all three directions, with corresponding analytical results. The code for obtaining the analytical eigenvalues-eigenvectors was provided by Weidelt (2009). The eigenvalues and eigenvectors of full and reduced versions of the code matched exactly with the analytical ones.

5.2.2 *Convergence of electric field with the refinement of grid*

To check the grid convergence, we chose three range of grids viz. coarse, medium and fine. In the coarse grid, the number of nodes were 10, 10 and 7 with (minimum, maximum) grid spacings being (250, 1000 m), (250, 1000 m) and (100, 1000 m) in X-, Y- and Z- directions respectively. In the medium grid, the number of nodes were 14, 14 and 9 with (minimum, maximum) grid spacings being (125, 920 m), (125, 920 m) and (100, 1000 m). Finally, in the fine grid, the number of nodes were 16, 16 and 12 and the (minimum, maximum) grid spacings were (80, 920 m), (80, 920 m) and (50, 1000 m) in X-, Y- and Z- direction respectively.

The graphical presentations of eigenvalues for coarse, medium and fine grid cases are shown in Figures 5.3(b), 5.3(c) and 5.3(d) respectively. In Figure 5.3(e) and 5.3(f) the behavior of convergence of electric field and apparent resistivity is depicted for time period 1s. In the coarse grid case, the spread in electric field response curve in both horizontal and vertical directions are maximum. In this case one can sense the presence of the conducting body but its location can not be exactly marked. In the medium and fine grid cases, the response curves are approximately same. So, one infer that as the grid is refined the response values converge to limiting true values. In the medium and fine grid cases, the horizontal position of the block can be clearly identified. In apparent resistivity curves the coarse grid one shows minimum deviation at the position of the block. The convergence of apparent resistivity response curves with refinement of grid is evident.

It may be mentioned that in all three cases, the refinement of the grid was primarily carried out inside the cube and only one or two nodes were added outside the body. The

RMS errors of coarse and medium grid with respect to fine grid are 0.045 and 0.006 respectively.

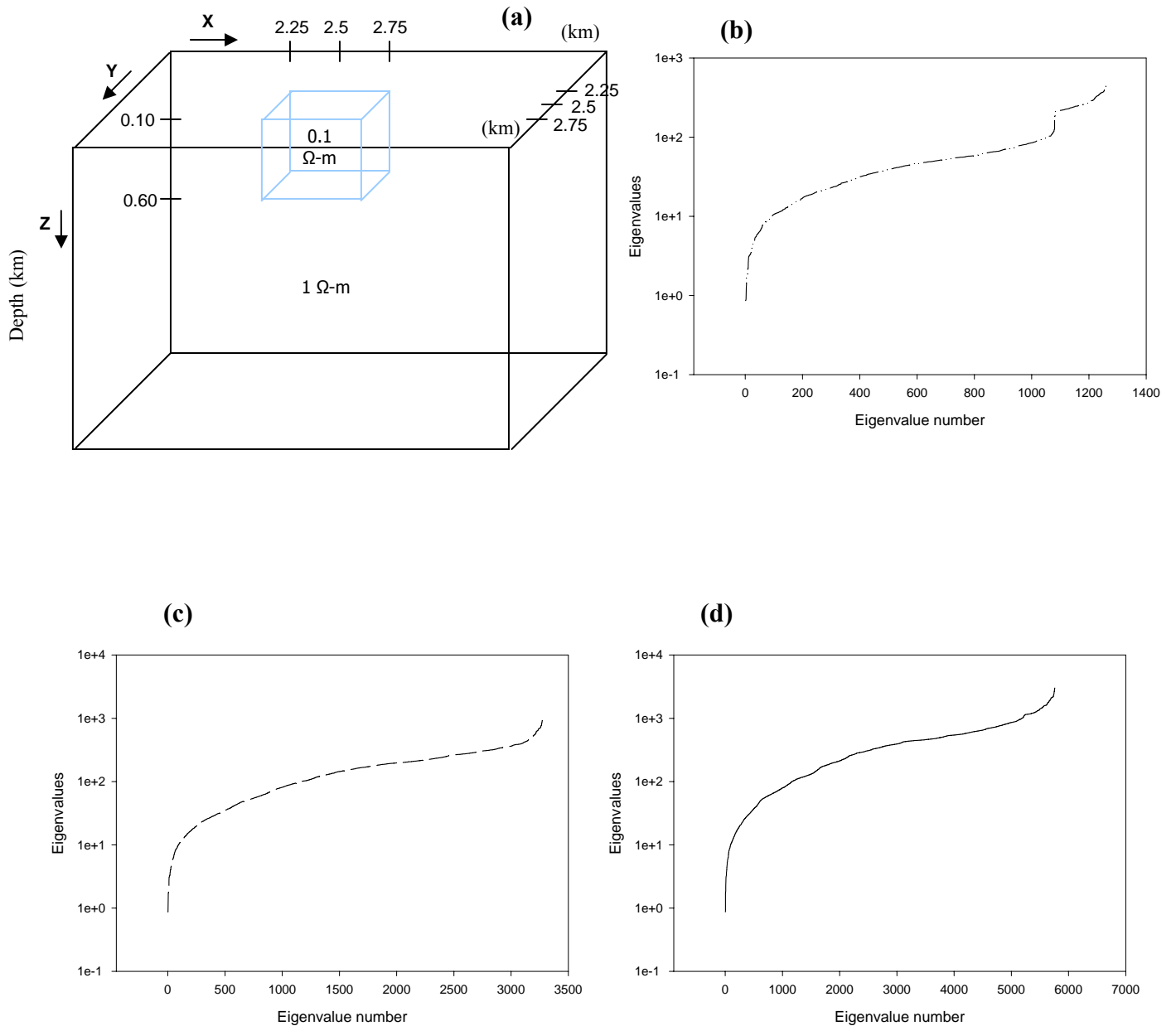


Figure 5.3: (a) 3D Test model (distances in km); Eigenvalue plot (b) coarse grid, (c) medium grid, (d) fine grid,

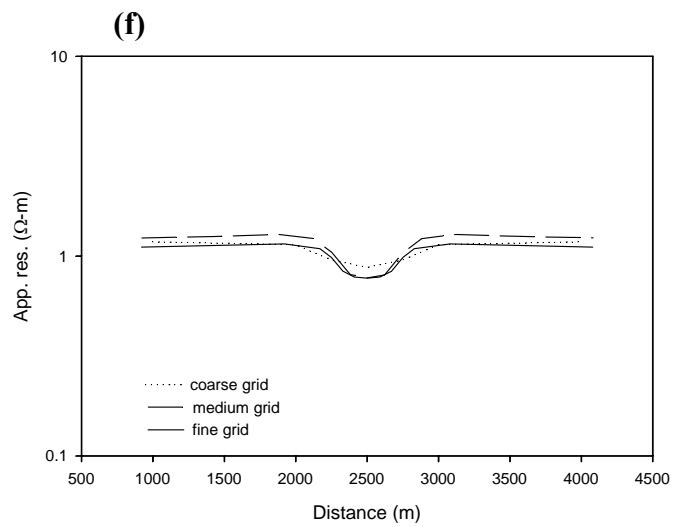
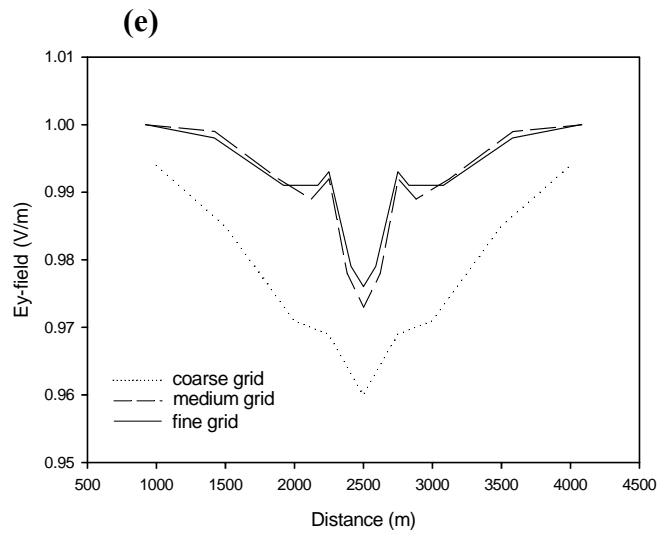


Figure 5.3 continued: Plots for different grids at 1s (e) electric field and (f) apparent resistivities.

5.2.3 No contrast study

Another test conducted on the algorithm is to verify the convergence of a buried target response to that of half space when the resistivity of block is taken approximately equal to that of half space. The resistivity of block is modified to $0.9 \Omega\text{-m}$ for this experiment. The electric field and impedances are computed and found to be almost identical to that of half space.

5.2.4 Electrically similar models

Next experiment is performed on electrically similar models to check the consistency. The electrically similar model of 3D test model is $0.05 \Omega\text{-m}$ insert in a $0.5 \Omega\text{-m}$ half space with same dimensions at time period 2.0s. Theoretically both models should produce the same results. The behavior of electric field and apparent resistivity corresponding to 2D TE and 2D TM are shown in Figures 5.4(a), 5.4(b) and Figures 5.4(c), 5.4(d) respectively. These responses also match with each other exactly. Thus it can be concluded that the algorithm is producing consistent results.

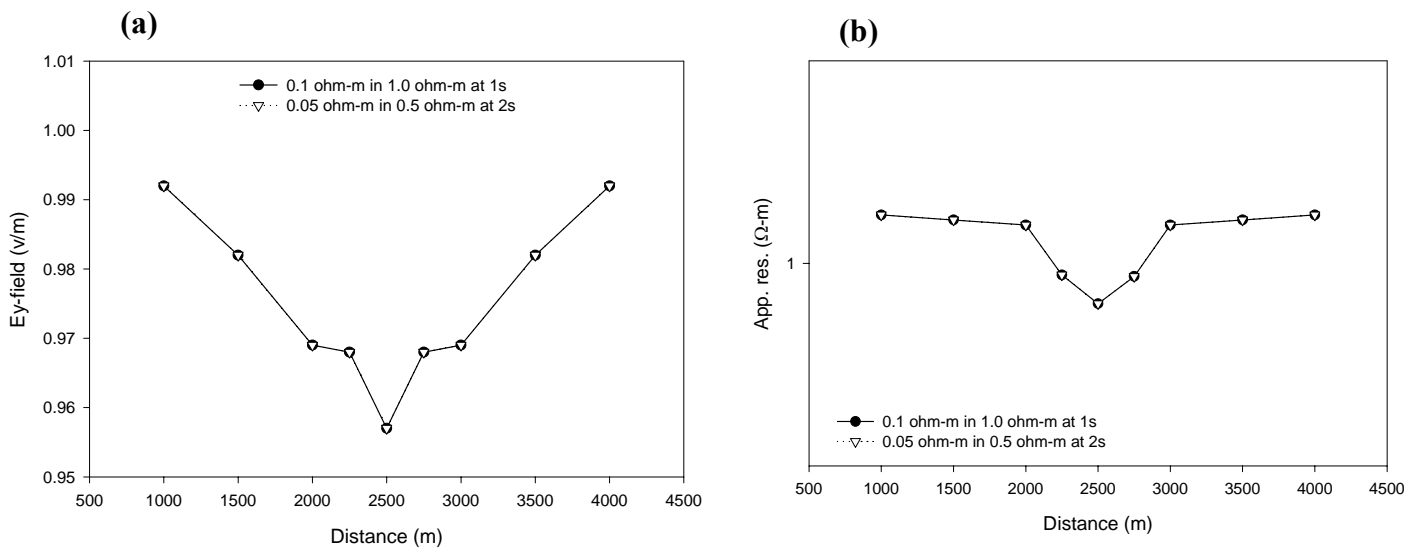


Figure 5.4: Plots corresponding to 2D TE mode for electrically similar models (a) real Ey field, (b) apparent resistivities,

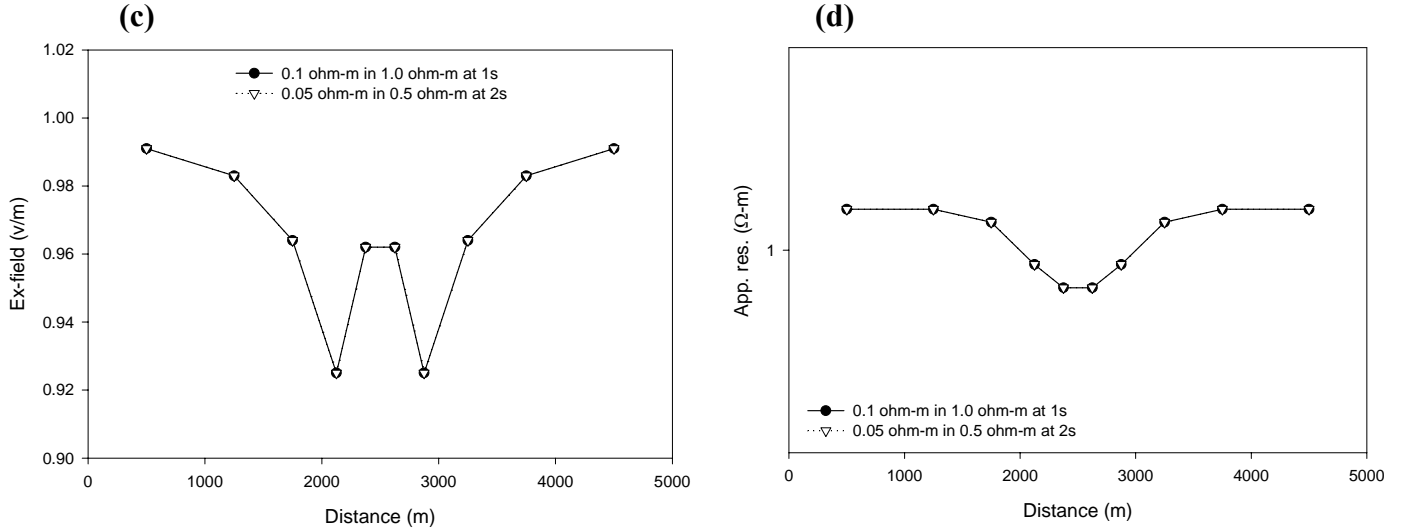


Figure 5.4 continued: Plots corresponding to 2D TM mode for electrically similar models (c) Re Ex field and (d) apparent resistivities.

5.2.5 Reduced and full version

Eventually in the final algorithm, we are using the reduced version and generating full eigenvectors from the reduced eigenvectors. To check the effect of numerical errors in the full eigenvectors obtained from reduced eigenvectors, we compared the response of reduced version with the response computed using the full version. The response is compared for both the modes; one is corresponding to 2D TE as shown in Figures 5.5(a), 5.5(b) and another corresponding to 2D TM as shown in Figures 5.5(c), 5.5(d). The comparison is given here for electric field and apparent resistivity values. These curves match exactly with each other. This means the reduced version is working accurately.

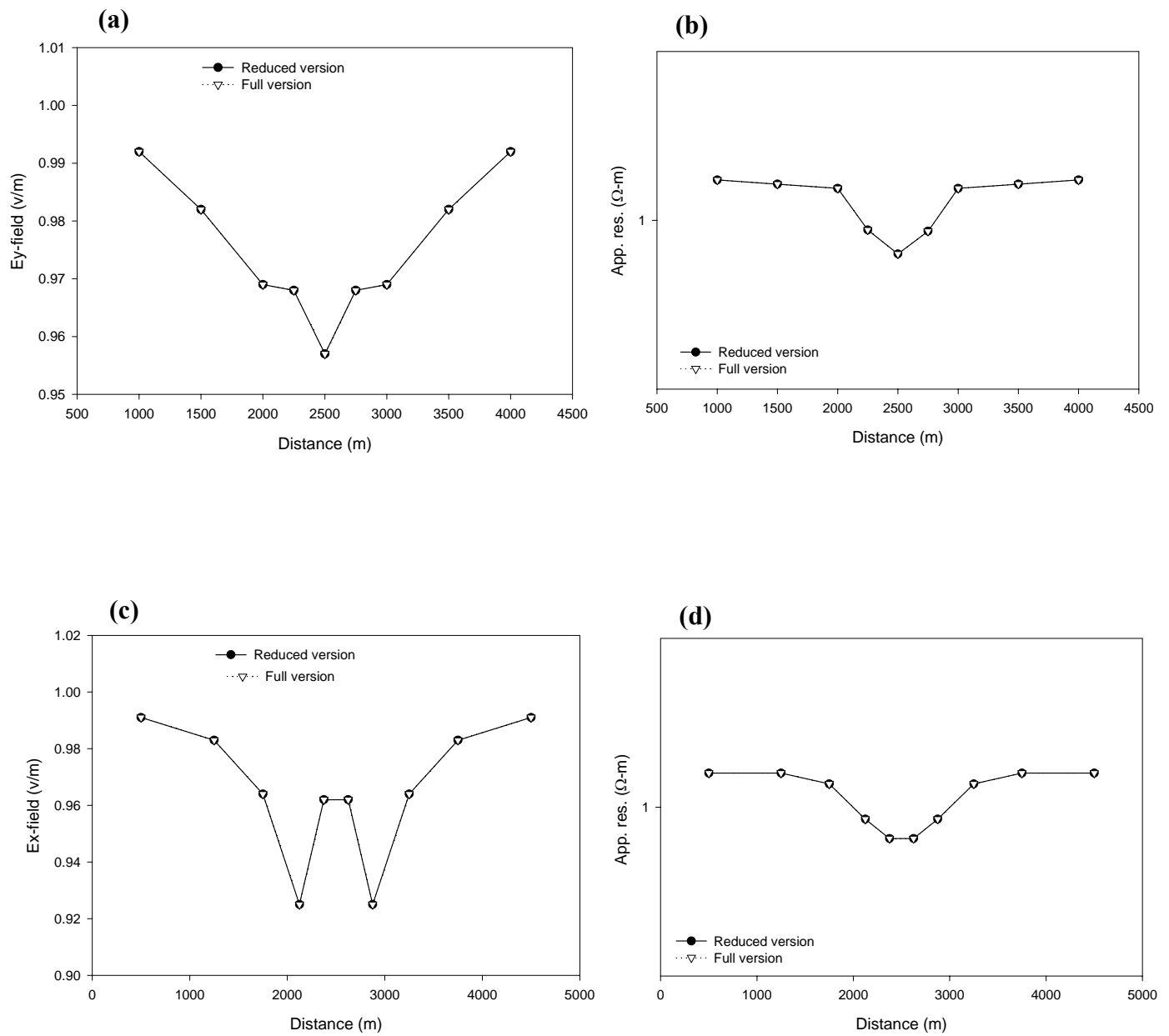


Figure 5.5: Plots for reduced and full versions corresponding to 2D TE mode (a) Ey field, (b) apparent resistivities; and Plots corresponding to 2D TM mode (c) Re Ex field, (d) apparent resistivities.

5.2.6 Effect of working with different percentage of eigenmodes

As discussed in the chapter 2, the eigenvalues appear in the denominator of the expression of superposition coefficient (equation (2.32)). So, in field synthesis, maximum contribution comes from the smallest eigenvalues. The present experiment is designed to know how many eigenvalues and corresponding eigenvectors are sufficient for numerically accurate response. In view of limited computer resources, we chose the coarse grid model so that we can also understand the effect of coarseness on the responses with different percentages of eigenmodes. In this experiment the percentage of eigenmodes taken are 5, 10, 15 and 20. For these four percentage cases, the real and imaginary parts of electric field are compared with all eigenmode response in Figures 5.6(a) and 5.6(b) respectively.

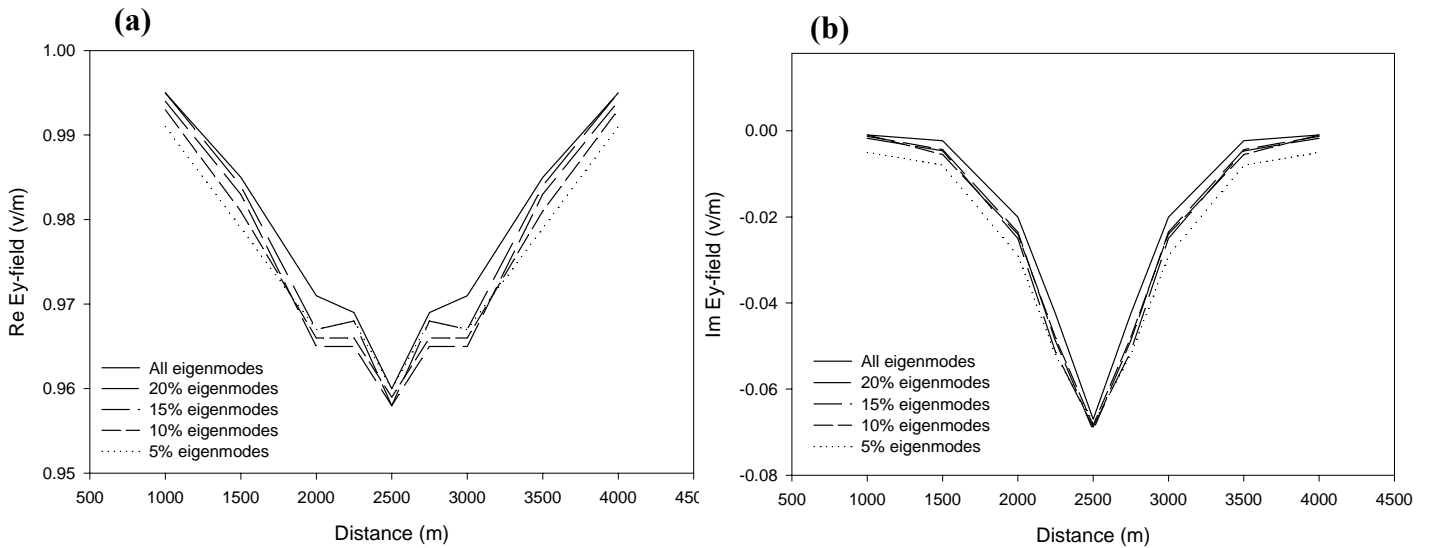


Figure 5.6: Electric field plots for different percentages of eigenmodes (a) real part and (b) imaginary part.

In both the plots, the maximum spread is observed for 5% and the responses converge towards all eigenmodes response as percentage of eigenmodes increases from 5% to 20%. The RMS errors for different percentage of eigenmodes with respect to all eigenmodes are described in Table 5.1. This spread behavior is not expected, so we conducted the same experiment on 2D version of this 3D test model termed as 2D test model.

Table 5.1: RMS errors for different percentage of eigenmodes in case of 3D.

Percentage of eigenmodes	Real e-field	Imag e-field
5	0.0823	0.0851
10	0.0811	0.082
15	0.0798	0.08
20	0.0565	0.0583

In case of 2D, two grids are chosen to check the effect of coarseness with different percentage, (i) the same coarse grid as used in 3D test model and (ii) the grid generated by the auto grid generator, based on skin depth criterion. Figure 5.7(a) shows the 2D test Model. Figures 5.7(b) and 5.7(c) show the eigenvalue curves for auto and coarse grids. In auto grid the curve rises steeply while in the case of coarse grid the steepness is much less. Figures 5.7(d) and 5.7(e) present the electric field and apparent resistivity responses for auto grid while Figures 5.7(f) and 5.7(g) present the same responses for coarse grid.

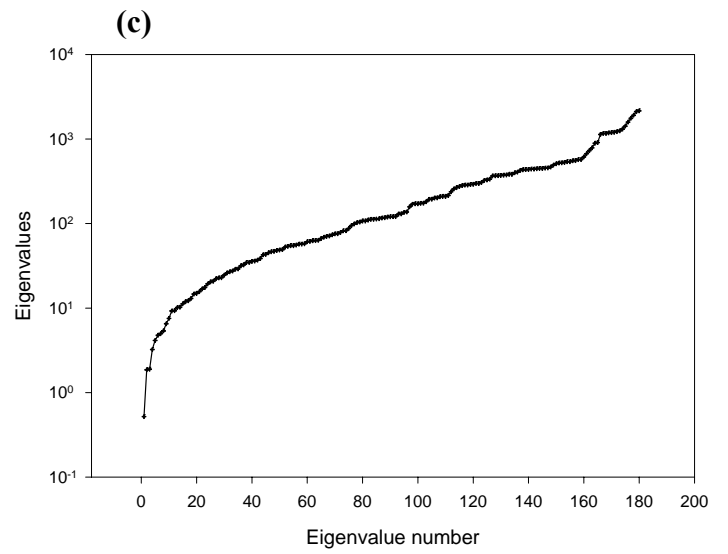
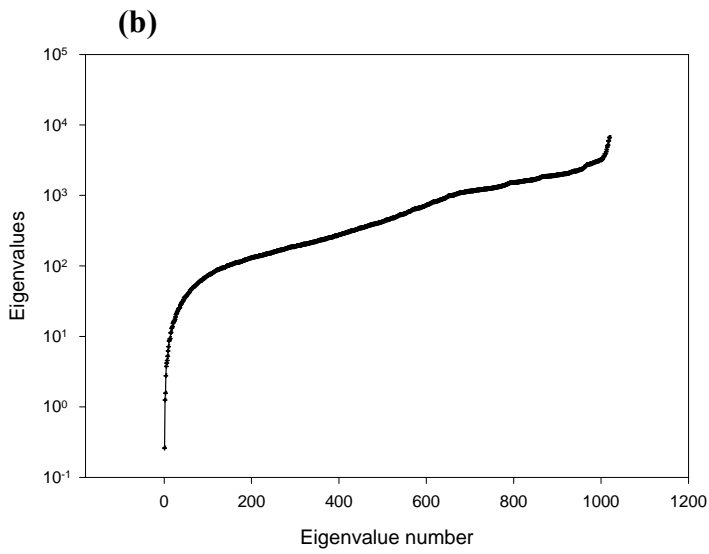
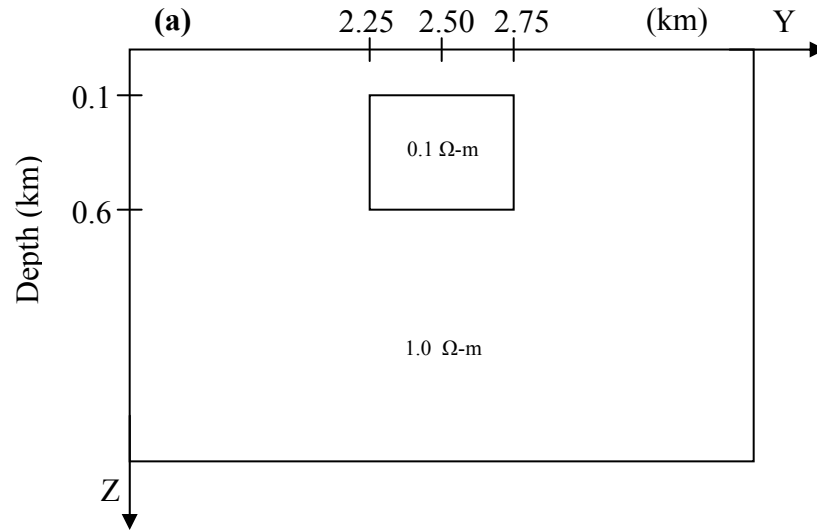


Figure 5.7: (a) 2D Test model (distances in km); Eigenvalue plot (b) skin-depth based grid, (c) coarse grid,

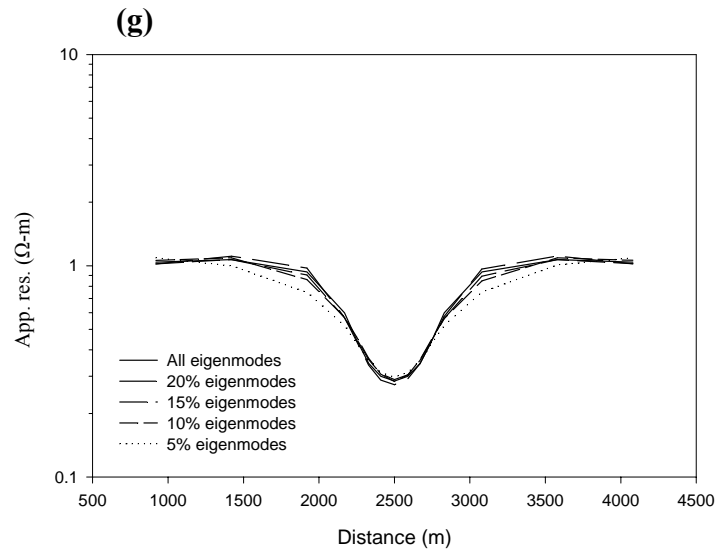
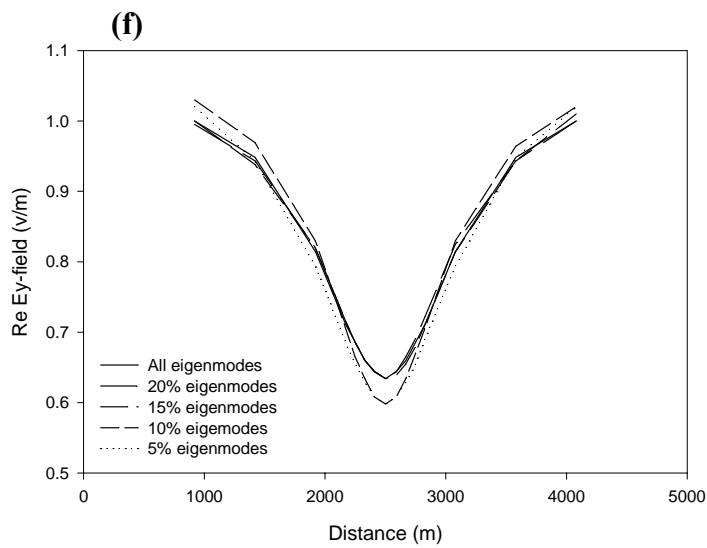
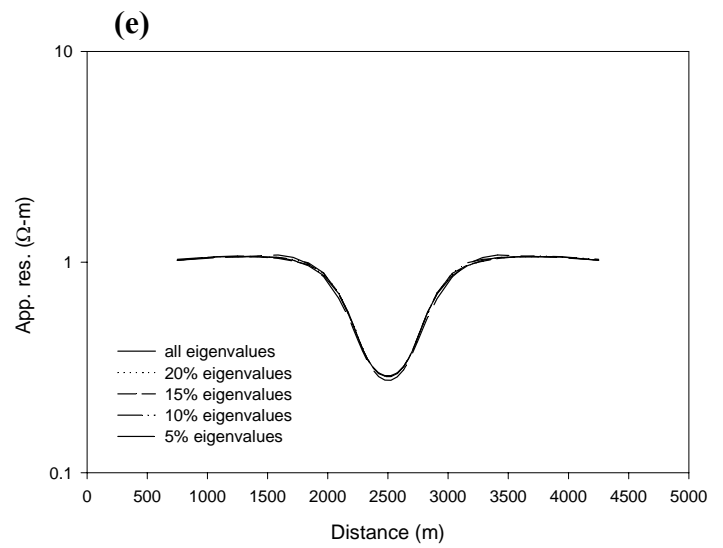
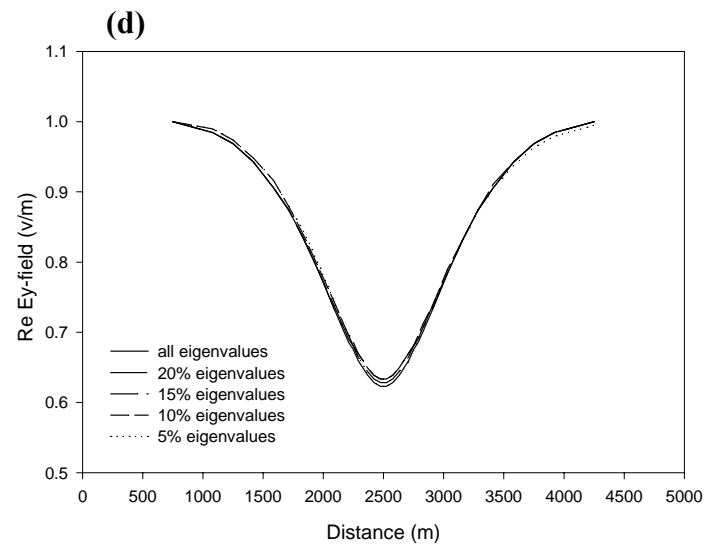


Figure 5.7 continued: Plots for different percentage of eigenmodes; For skin depth based grid (d) Re-electric field and (e) apparent resistivities and for coarse grid (f) Re-electric field, (g) apparent resistivity.

In auto grid case, the response curves for the four percentage cases match well with the all eigenmode case, even 5% of eigenmodes are sufficient for accurate field synthesis. For the coarse 2D grid, a spread behavior similar to that in 3D case is observed. However, with increasing percentage values, the responses do converge to that for all eigenmodes. From this exercise we conclude that auto grids provide accurate field values even for small percentage of eigenmodes.

We also conducted the experiment to observe the effect of different percentages of eigenmodes on the response of a resistive block model. For this purpose the model described as 2D-3 in COMMEMI report is considered. In this model the resistive and conductive blocks are placed at the surface. The model is shown in Figure 5.8(a) and the corresponding eigenvalue plot is presented in Figure 5.8(b).

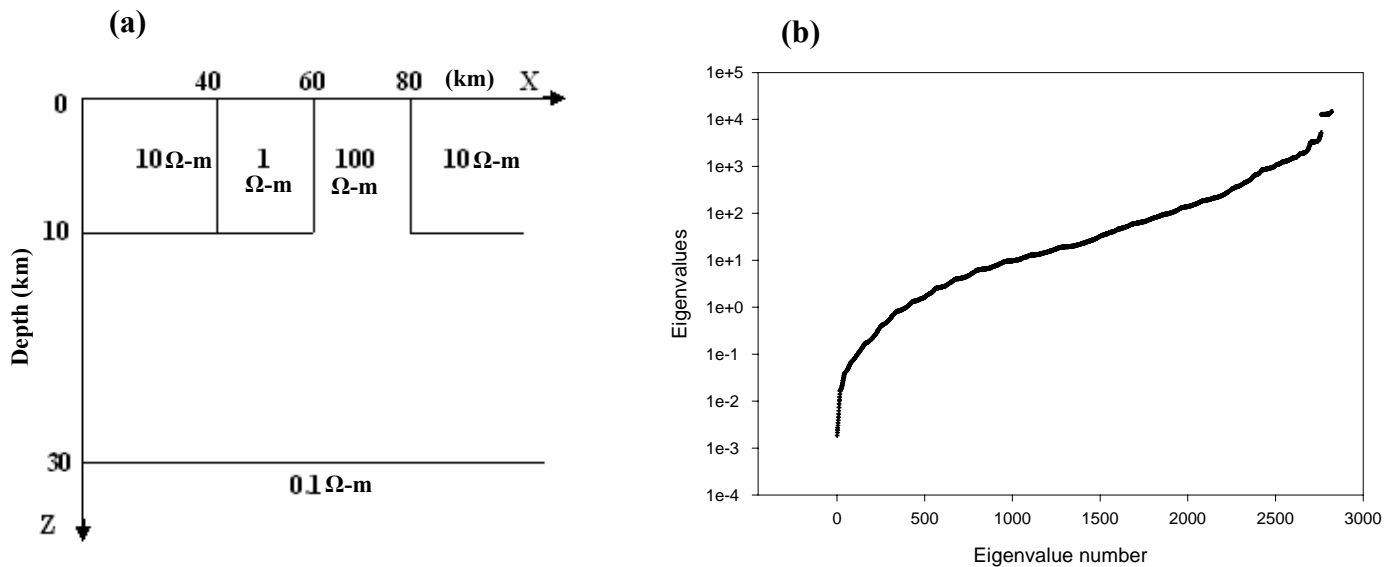


Figure 5.8: (a) 2D-3 model of COMMEMI, (b) eigenvalue plot,

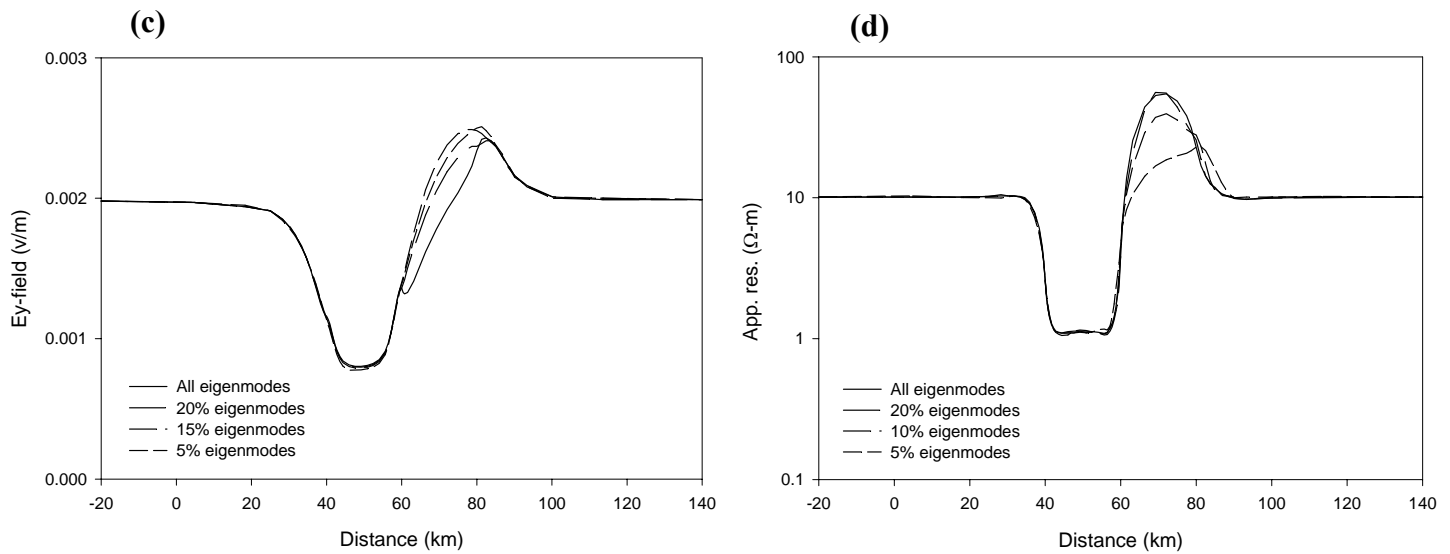


Figure 5.8 continued: Plot for different percentage of eigenmodes at 10s (c) Real e-field (d) apparent resistivity.

The response curves for 10s period are presented for 5, 10, 15 and 20% of eigenmodes. Electric field and apparent resistivity curves for different percentages are presented in Figures 5.8(c) and 5.8(d). In conductive block even 5% eigenmodes are sufficient but in resistive block only 20% eigenmodes gives satisfactory results. Thus for conductive block smaller number of eigenmodes are sufficient while for resistive block a larger number of eigenmodes are required. The RMS errors for 5, 10 and 20% eigenmodes with respect to all eigenmodes are 0.055, 0.122 and 0.255 respectively.

Tables (5.2) and (5.3) present RMS (Relative Root Mean Square) error values with respect to all eigenmode response for both grids.

Table 5.2: RMS errors for different percentages using skin depth based grid.

% of Eigenmodes	RMS Error
20	0.011
15	0.020
10	0.023
5	0.025

Table 5.3: RMS errors for different percentages using coarse grid.

% of Eigenmodes	RMS Error
20	0.014
15	0.012
10	0.066
5	0.075

5.2.7 Multi-frequency response computation

In the proposed approach, eigenmodes are independent of source characteristics, rather these depend only on the model characteristics. Once the eigenmodes are computed for a grid, responses for any given set of frequencies can be obtained within insignificant amount of time while for other traditional algorithms it takes same amount of computational time for each frequency. We tested it on 3D test model for time periods

ranging from 0.001s to 50.0s. The electric field curves are shown in Figure 5.9(a). The 0.001s curve senses only the upper half space and as time period increases the curves start sensing the conducting block. Upto time period values 0.5s, the central dip in the curve becomes more and more prominent as time period increases. However, for time periods greater than 0.5s this dip in curve decreases to the extent that it becomes a horizontal straight at 50s period.

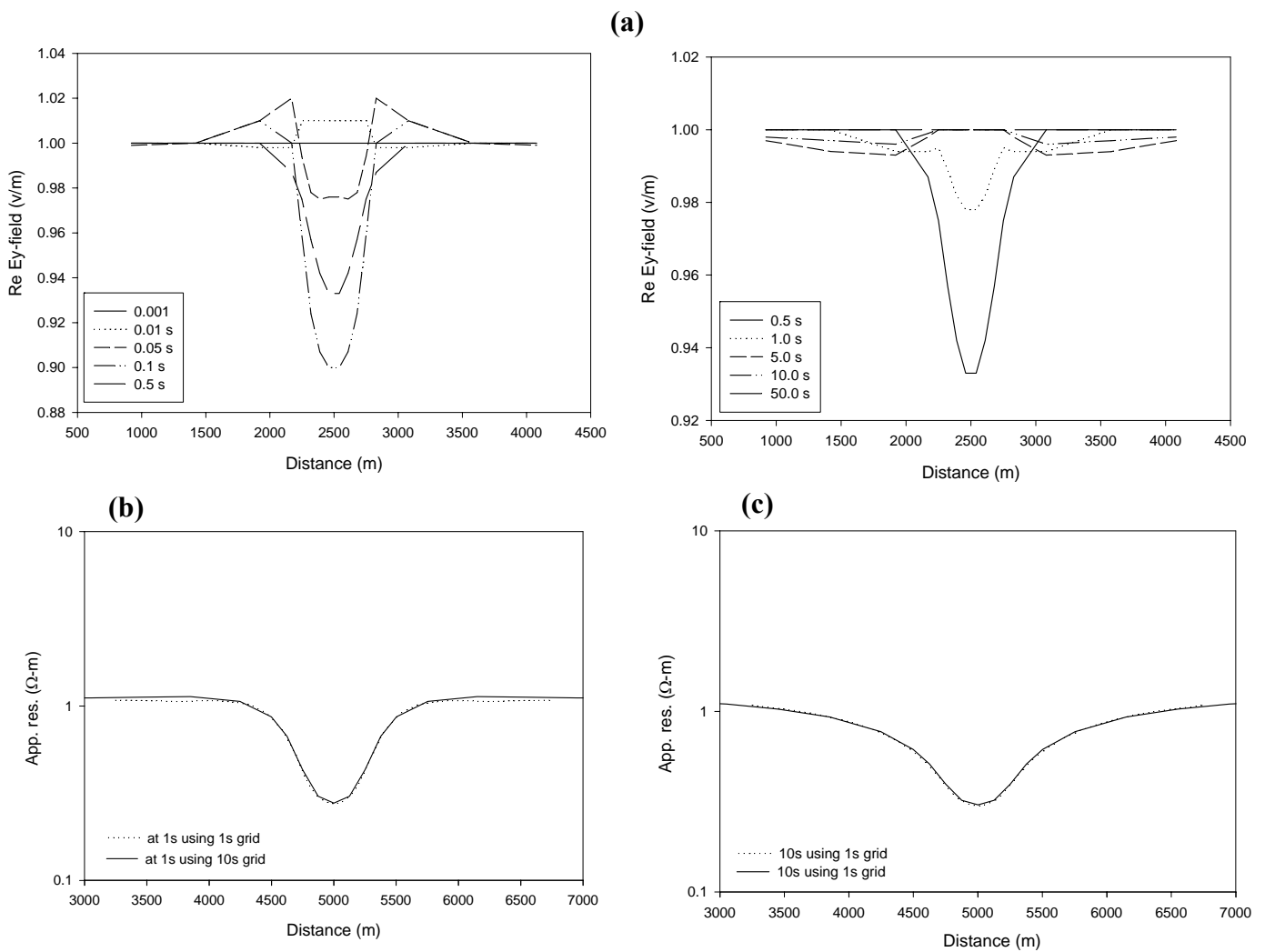


Figure 5.9: (a) Electric field plots for different frequencies in 3D; 2D apparent resistivity curves using 1s and 10s grid eigenmodes (b) at 1s, (c) at 10s.

In order to study accuracy of the multi frequency response computations using eigenmodes, we again considered the 2D model. We generated autogrids corresponding to two time periods 1s and 10s and computed the responses for the two time periods using each one of these grids. The comparison of the response values for 1s and 10s time periods obtained using both the grids are respectively shown in Figures 5.9(b) and 5.9(c). The RMS error with respect to true response for 1s response is 0.014 and for 10s is 0.008. Hence, the multi-frequency responses computed using eigenmodes are quite accurate.

5.2.8 *Extension of strike length*

We have observed that the all eigenmodes response of a 2D model lies in the same range whether computed using a coarse grid or using a fine grid. Keeping this in mind, we chose a model (Brewitt-Taylor and Weaver, 1976) with same resistivities as of the test model but dimensions 1.0 km x 1.0 km x 0.65 km. In this experiment, the strike length of the block is extended in Y-direction as 1.0 km, 2.0 km, 5.0 km and 10.0 km, keeping the X and Z dimensions fixed. Figure 5.10(a) shows the model and Figure 5.10(b) shows the eigenvalue plots for different strike lengths. In the eigenvalue plots, the smallest and largest eigenvalues are same because the dimension of the body is fixed and smallest discretization and maximum and minimum values of resistivities are same.

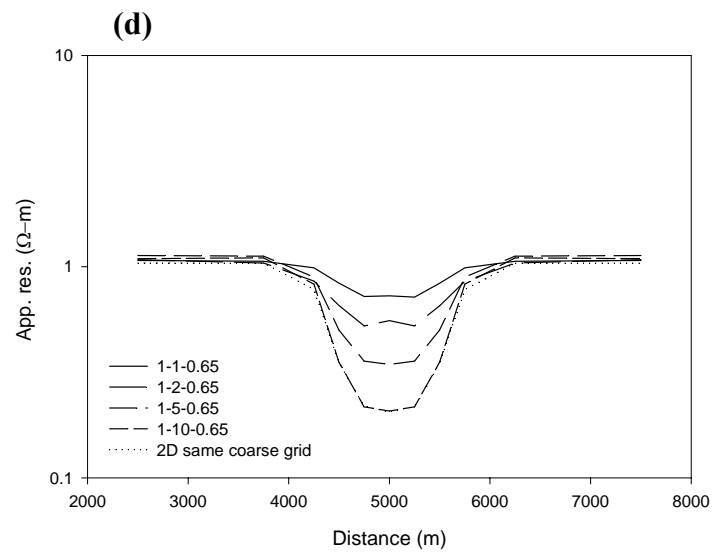
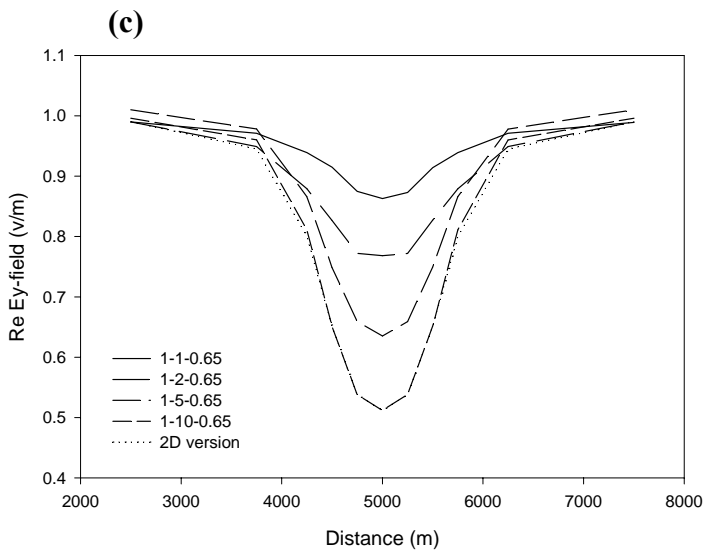
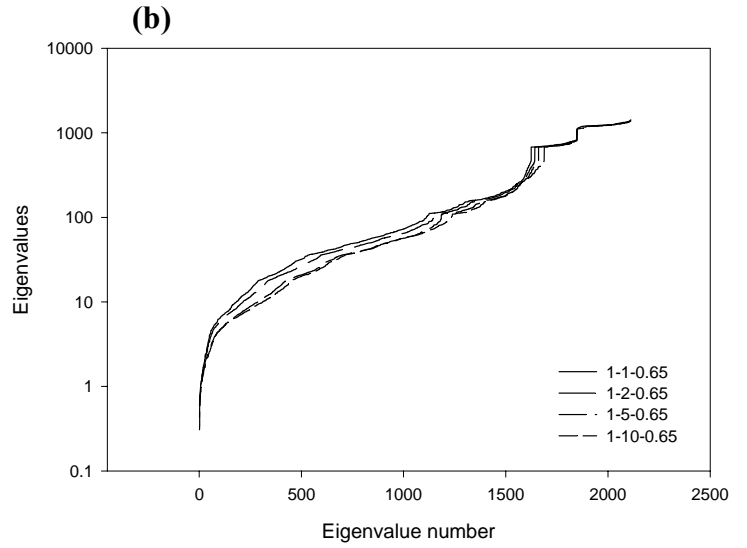
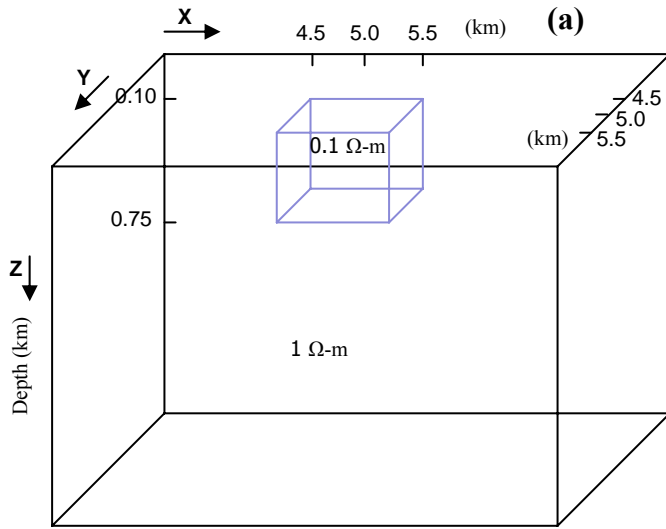


Figure 5.10: (a) Test model (distances are in km); Plots for different strike lengths (b) eigenvalues, (c) Re electric fields, and (d) apparent resistivities.

The differences in the middle segments of the eigenvalue curves are due to the change in the conductivities values as strike length increases. In Figures 5.10(c) and 5.10(d), the real part of electric field and the apparent resistivity plots for different strike lengths are respectively presented. In both response curves, as strike increases the response approaches towards the corresponding 2D response and for the 10 km strike length case the 3D curves are analogous to the corresponding 2D curves. The RMS errors for 1, 2, 5 and 10 km strike lengths are 0.386, 0.268, 0.142 and 0.009 respectively with respect to 2D result.

5.2.9 Comparison with 3D-2 model of COMMEMI report

Finally, to establish accuracy of the algorithm, a comparison with published result is presented. In case of 3D, the model is again taken from COMMEMI report, described as 3D-2 in the paper and presented here in Figure 5.11(a). In this model a conductive block of $1 \Omega\text{-m}$ and a resistive block of $100 \Omega\text{-m}$ is embedded in a $10 \Omega\text{-m}$ surface layer, the two bottom layers are of 100 and $0.1 \Omega\text{-m}$ respectively.

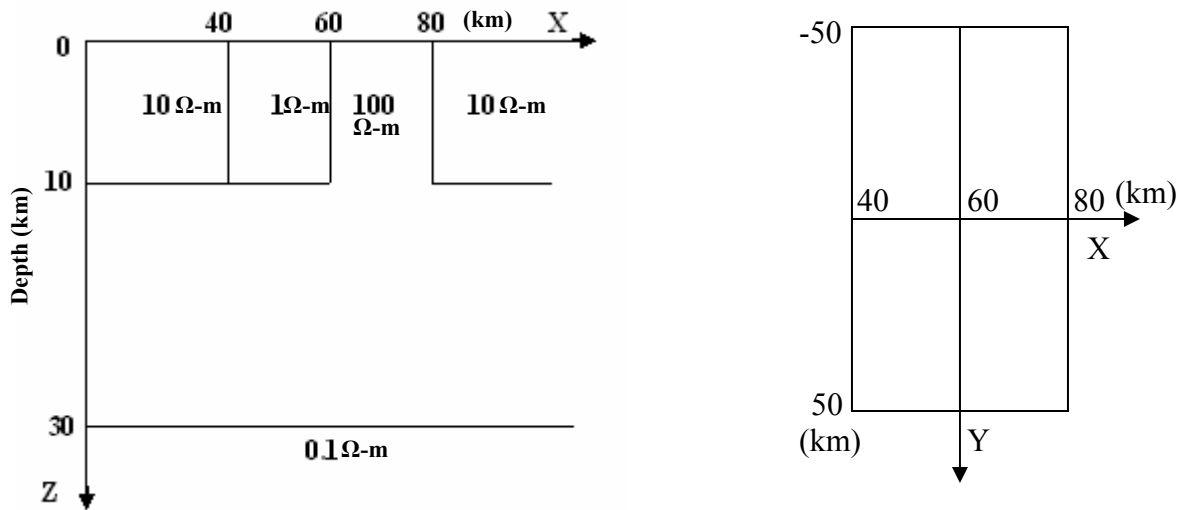


Figure 5.11: (a) 3D-2 model of COMMEMI,

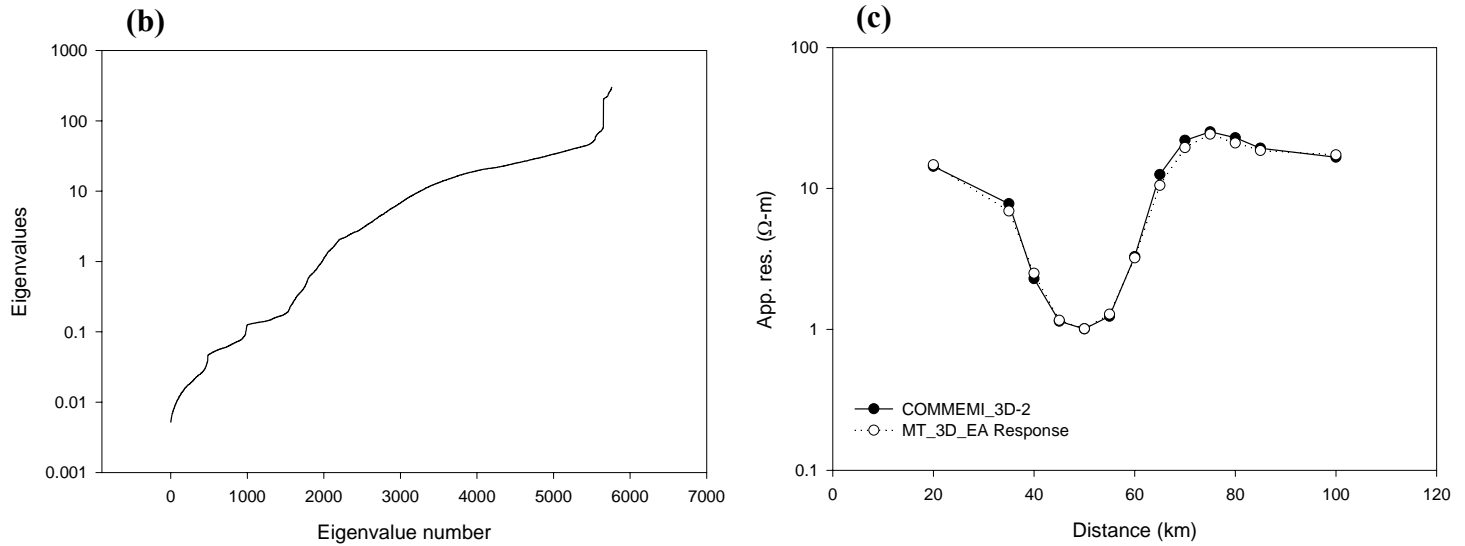


Figure 5.11 continued: (b) eigenvalue plot and (c) plots of apparent resistivity for COMMEMI and MT_3D_EA at 100s.

The comparison is given for 100 km strike length and for 100s time period. Figure 5.11(b) shows the eigenvalue pattern while Figure 5.11(c) presents the comparison between the apparent resistivity values of our algorithm and those of COMMEMI report. The RMS error between the two responses is 0.026.

Once the accuracy and efficiency checks have been performed satisfactorily, we applied the algorithm, MT_3D_EA, on the MT field data obtained from Garhwal Himalaya for a DST (Department of Science and Technology, New Delhi, India) sponsored research project with the Department of Earth Sciences, IIT Roorkee. This exercise is described in the following.

EXPERIMENT WITH FIELD DATA

6.1 General

After testing the algorithm on synthetic models, we conducted an exercise to generate 3D models for updating the 2D interpretation of the MT field data available with the Department of Earth Sciences, IIT Roorkee. During the period 2004-2006, a Broad Band Magnetotelluric (BBMT) survey was carried out by Israil et al. (2008) to infer geo-electrical structure of Garhwal Himalaya. The MT data was recorded in Garhwal Himalaya on a profile from Roorkee to Gangotri. The location map of the region of study in Himalaya is presented in Figure 6.1. The designed profile line, comprising 44 sites, is shown in Figure 6.2. It crosses through major Himalayan Thrusts as, Himalayan Frontal Thrust (HFT), Main Boundary Thrust (MBT) and Main Central Thrust (MCT). Himalaya being a complex and inaccessible terrain, to minimize noise, the site interval was not uniform over the profile and varied from 2 km to 10 km. The observed data was processed using the technique of Shalivahan et al. (2006) for error minimization. They applied hybrid processing technique along with remote reference, coherence weighted estimation and Robust M estimation to reduce the errors in electric and magnetic field data. Tyagi (2007) obtained impedances using this processing technique. He also used strike code of (Groom and Bailey, 1989; McNeice and Jones, 2001) to get the regional strike and regional 2D impedances. The data was rotated along and perpendicular to the geoelectric strike to get TE- (Transverse Electric) and TM- (Transverse Magnetic) mode responses. He also

considered the effect of topography and found that the effect of topography was below noise level.

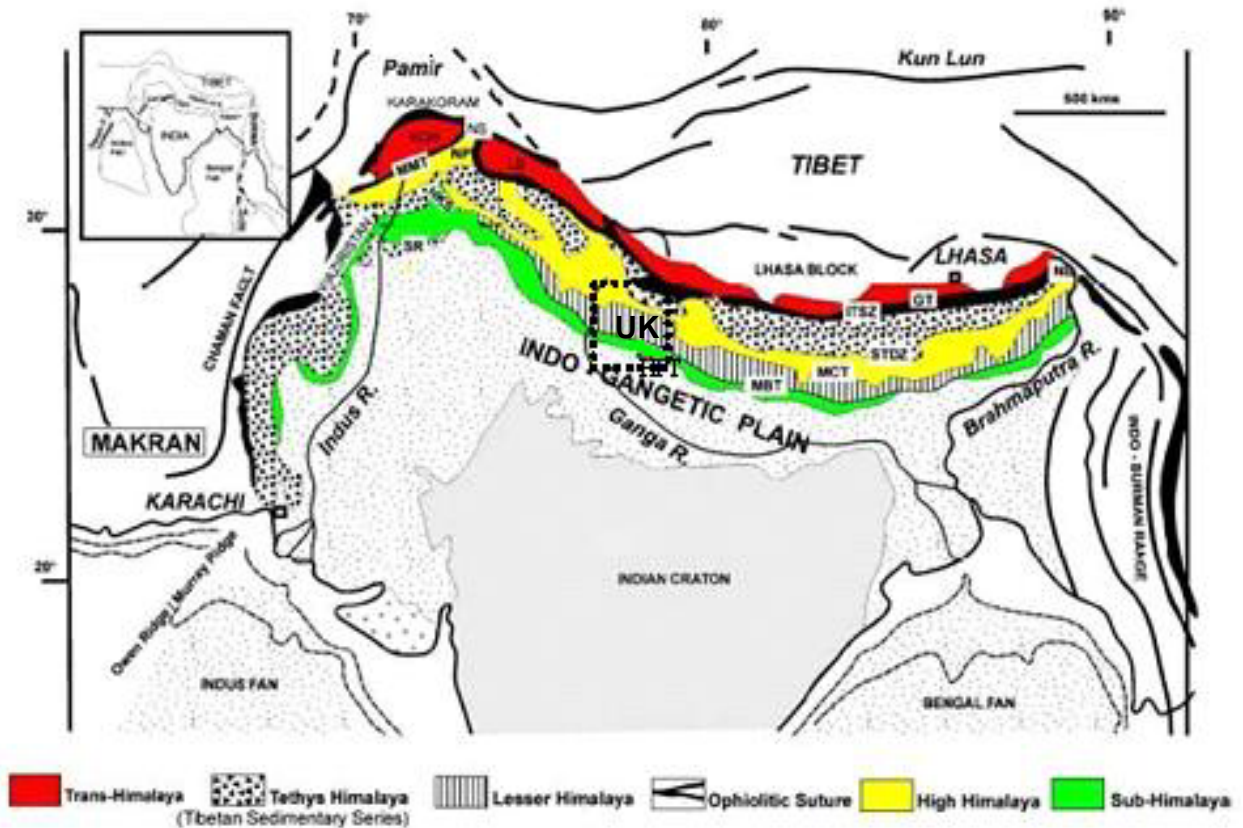


Figure 6.1: Location map of Himalayan region. NB: Namche Barwa; GT: Gangdese Thrust; HKS: Hazara-Kashmir Syntaxis; ITSZ: Indus Tsangpo Suture Zone; KOH: Kohistan Island arc; LB: Ladakh Batholith; MBT: Main Boundary Thrust; MCT: Main Central Thrust; HFT: Himalayan Frontal Thrust; MMT: Main Mantle Thrust; NP: Nanga Parbat; NS: Northern Suture; SR: Salt Range; SDTZ: South Tibetan Detachment Zone; UK: Uttarakhand (Najman, 2006) (after Tyagi, 2007).

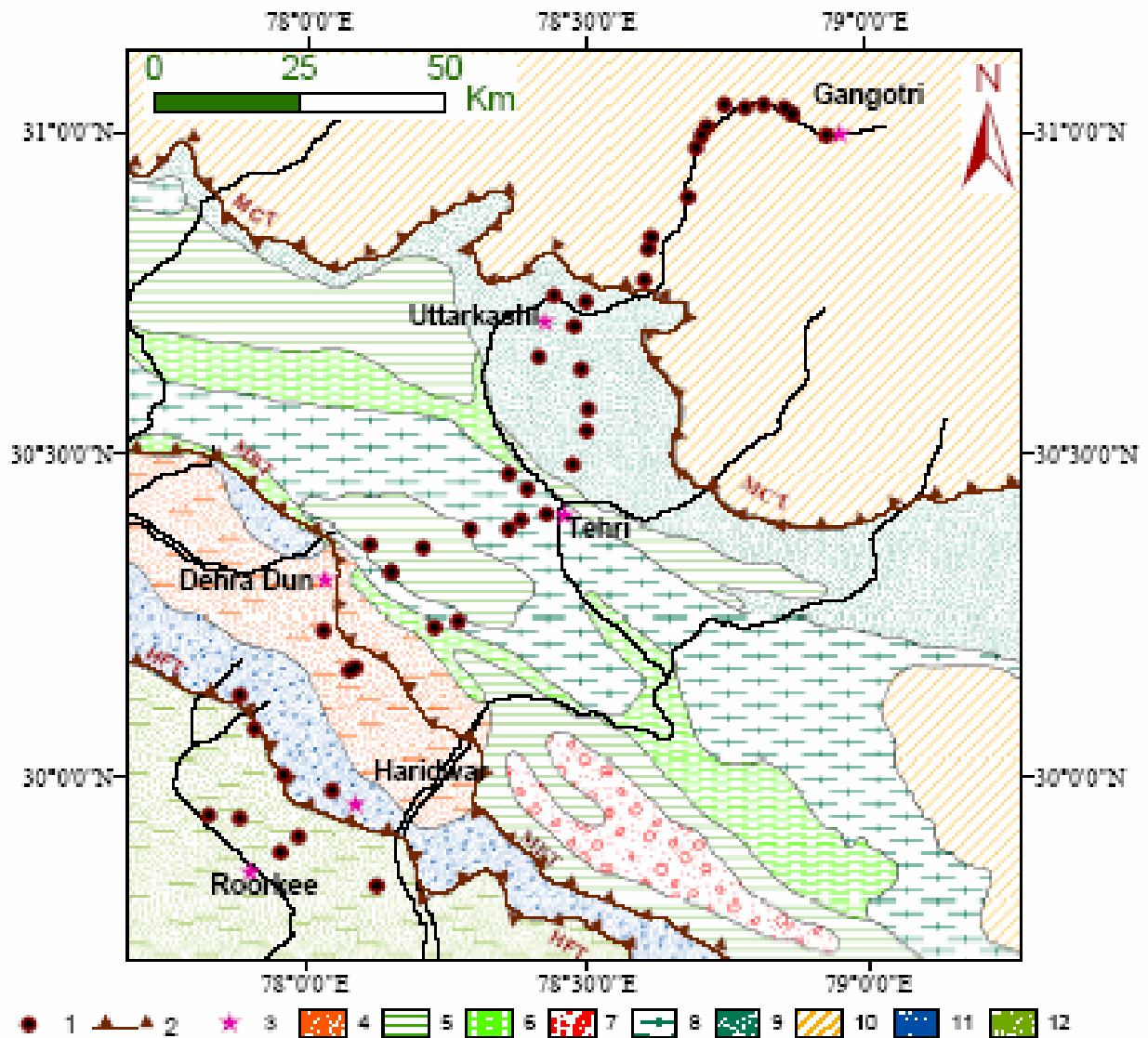


Figure 6.2: Geological map of the study area (compiled from Viridi, 1988; Sorkhabi et al., 1999; Kumar et al., 2002). 1- MT Sites; 2- Thrust; 3- Cities; 4- Dehra Dun Reentrant; 5- Blaini-Infrakrol-Krol; 6- DaMTha; 7- Garwhal Nappe; 8- Jaunsar-Simla (Undifferentiated); 9- Sunder Nagar-Berinag Groups; 10- Undifferentiated Metamorphics; 11- Undifferentiated Tertiaries; 12- Piedmont zone. MT data collected in the Indo-Gangetic Plains, Siwalik, Lesser and Higher Himalayan region in Garhwal Himalaya. (after Tyagi, 2007).

Tyagi (2007) used WinGLink software to obtain the 2D inverted models from data. The Final 2D models were obtained for TE-, TM- and joint TE-TM modes. We have considered the joint TE-TM model, given in Figure 6.4, as the base model for our study. The location of the earthquakes coincides with the conducting feature near MCT in the model proposed by Tyagi (Figure 6.4). This is interesting in the light of work of Khattri (1992) presenting a distribution of local earthquakes in Garhwal-Kumaon Himalaya as shown in Figure 6.3. From this, it is clear that majority of earthquakes occur near MCT. The association of the conductive feature with the local earthquakes motivated us to further study the characteristics of this feature in detail and try to decipher its 3D geometry.

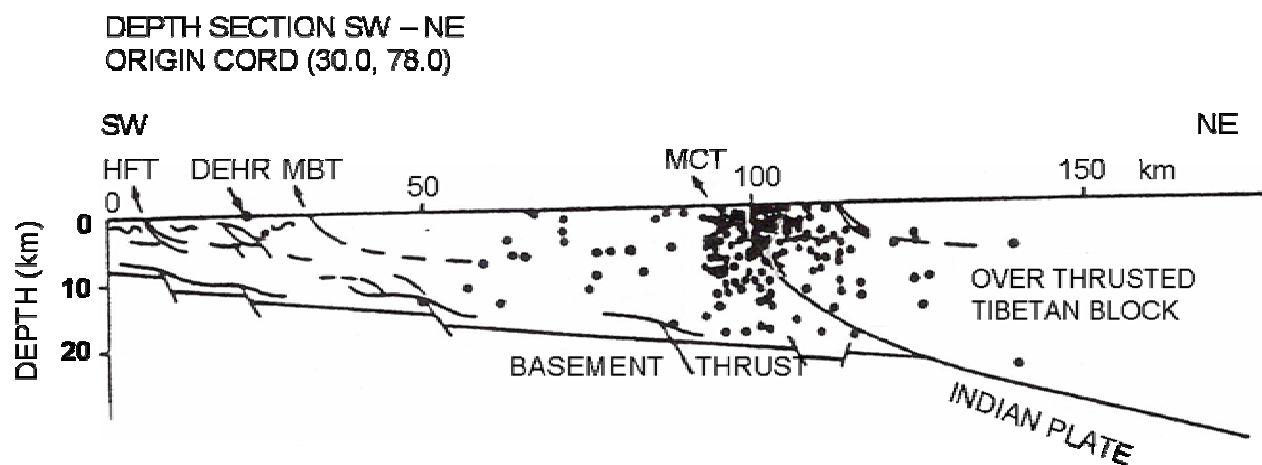


Figure 6.3: Depth section showing local earthquakes recorded in Garhwal-Kumaon Himalaya (Khattri, 1992) (after Tyagi, 2007).

Our exercise was aimed at generating 3D models whose response will match the data. To start the exercise, first we experimented with 2D models to decide upon a simple 3D model.

6.2 2D Experiment

The designed simple model from the complex 2D model proposed by Tyagi (2007) is shown in Figure 6.5. To match the computed 2D responses with the field data and with the inverted model response, we varied the model parameters. Multi frequency responses were compared with corresponding field data. From the time period list of MAPROS processing software, we chose two time periods 11.61s and 90.45s so that we can compare our response values with actual data values. Of these two time periods 3D study was carried out at 90.45s. This choice was made to meet the constraint on number of nodes in 3D grid necessitated by the existing limited computational facility.

Different experiments designed for 2D case are;

- 1) Study with different basement depths
- 2) Study with different block resistivities
- 3) Multi-frequency responses
- 4) Comparison with and without salient features

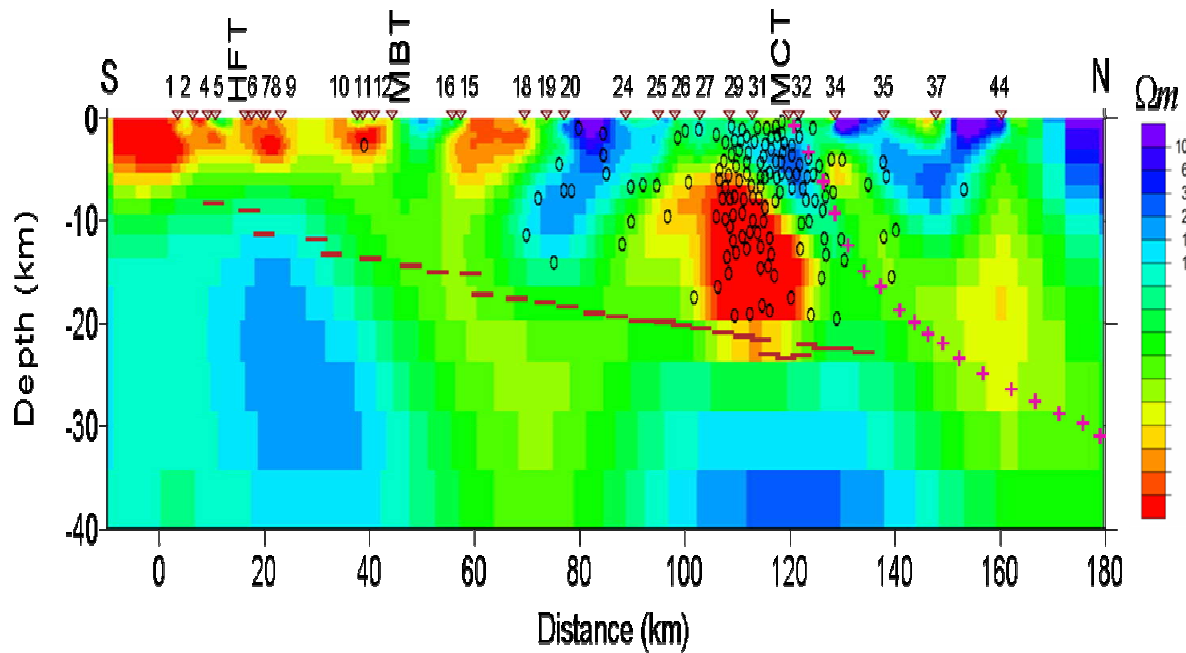


Figure 6.4: 2D resistivity models of the crust derived from inversion of joint TE-TM mode MT data (Tyagi, 2007).

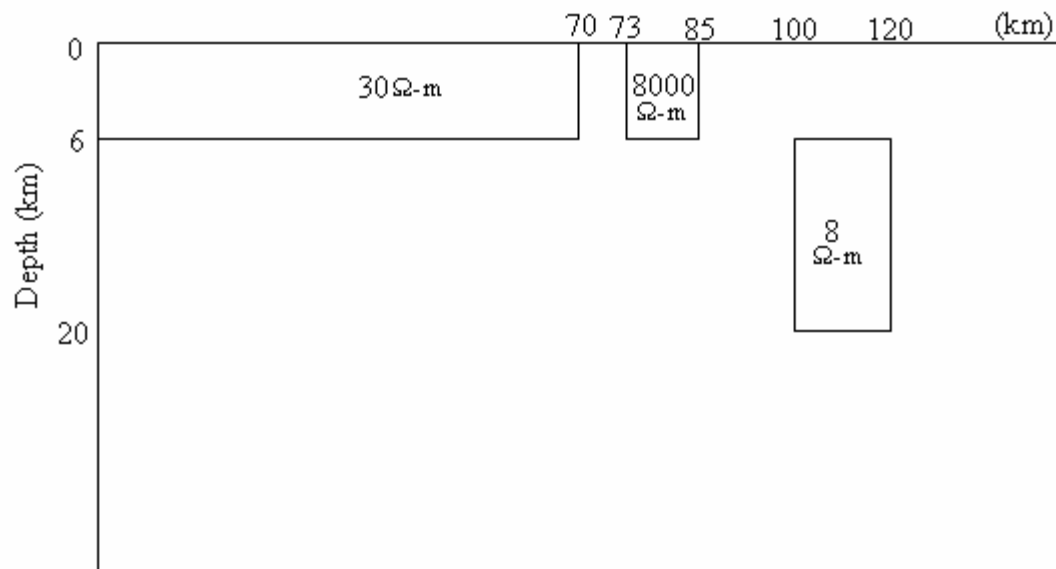


Figure 6.5: Gangotri simplified model.

6.2.1 Study with different basement depths

In our code we have employed perfectly conducting basement. To study the effect of this conductive basement, we experimented with two basement depth values, 50 km and 200 km. At 11.61s, there is no effect of basement depth as shown in Figure 6.6(a) where the 50 km and 200 km curves overlap. However, at 90.45s period the effect of basement depth is clearly visible as shown in Figure 6.6(b) where the two curves are separated. Since we are using 90.45s period for 3D case, the depth of the basement is finalized as 200 km.

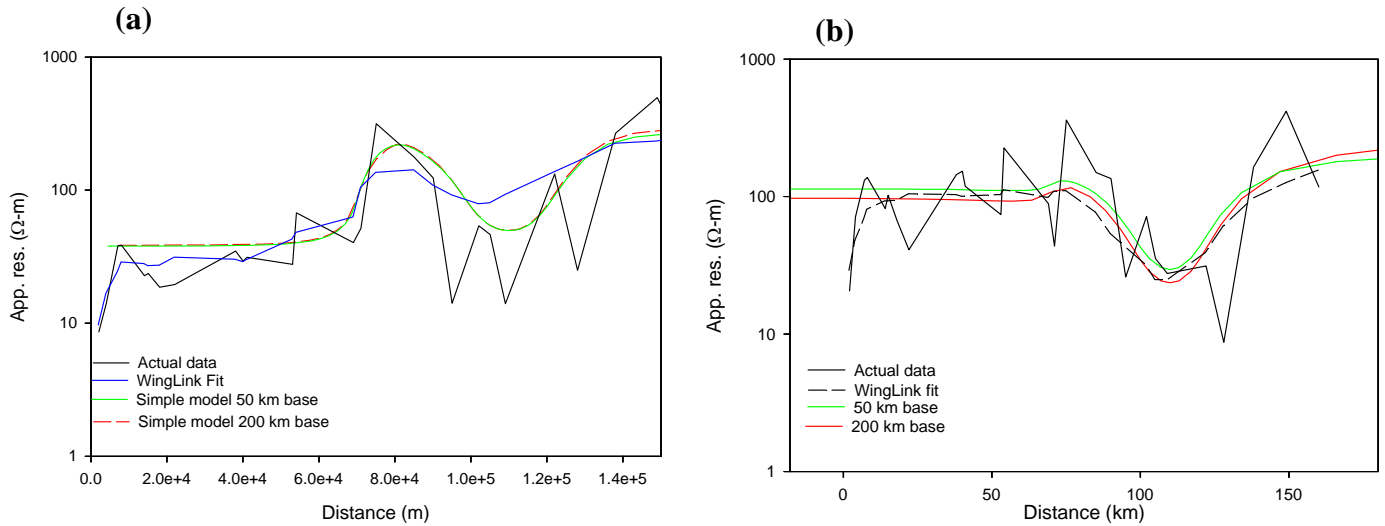


Figure 6.6: 2D plot with different basement (a) at 11.61s, (b) at 90.45s.

6.2.2 Study with different block resistivities

Next, we varied the resistivity of conductive block to find the appropriate resistivity of blocks. The responses are compared in Figure 6.7(a) and Figure 6.7(b) at 11.61s and 90.45s periods respectively. Our main emphasis is on the study of the conductive feature near MCT. We carried out the experiment with resistivity value of this block as 5 and 8 Ω -m keeping other parameters unchanged. It is clear that the 8 Ω -m response matches well with the data. So, we finally used 8 Ω -m resistivity of the conductivity block for further studies.

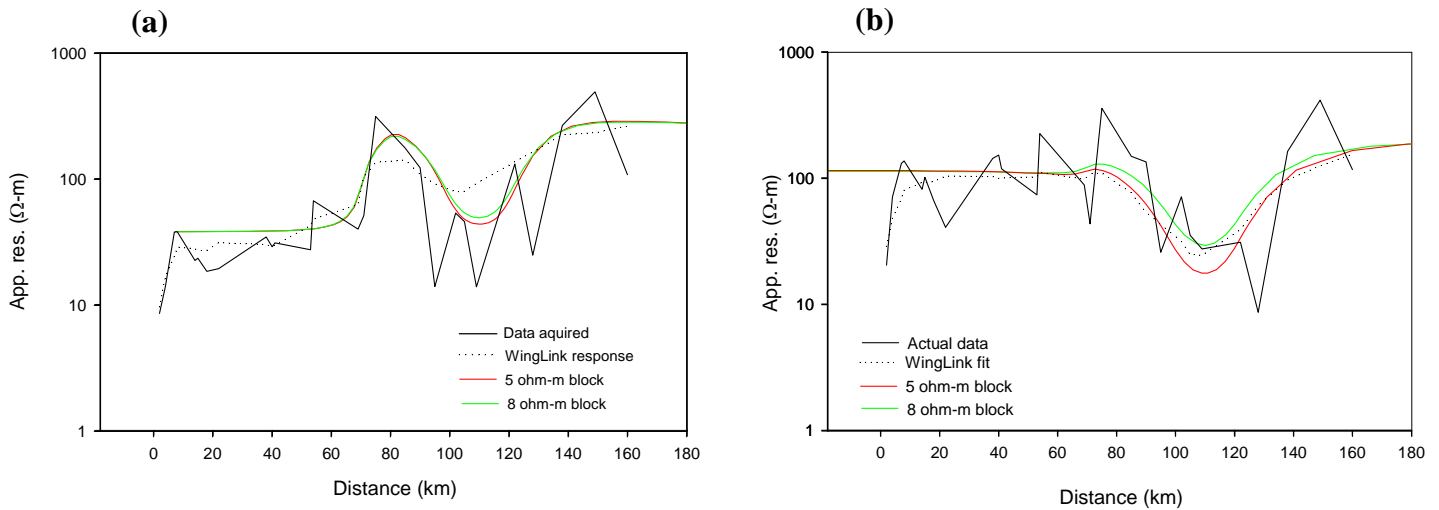


Figure 6.7: 2D plot with resistivity variation of conductive block (a) at 11.61s, (b) 90.45s.

6.2.3 Multi-frequency responses

Next we checked the multi-frequency response computed using present algorithm and compared these with the field data. Two autogrids for periods 11.61s and 90.45s were generated for this study. The responses at 11.61s using the 11.61s autogrid and the 90.45s autogrid are compared with each other and with the field data and WinGLink response in Figure 6.8(a). The responses for both grids matches well with each other. In Figure 6.8(b), the 90.45s responses obtained using the 11.61s autogrid and the 90.45s autogrid are compared and these also match well with each other and with the data values. This experiment gives us confidence that the multi-frequency solution is not only accurate for simple geometry models but also for complex models.

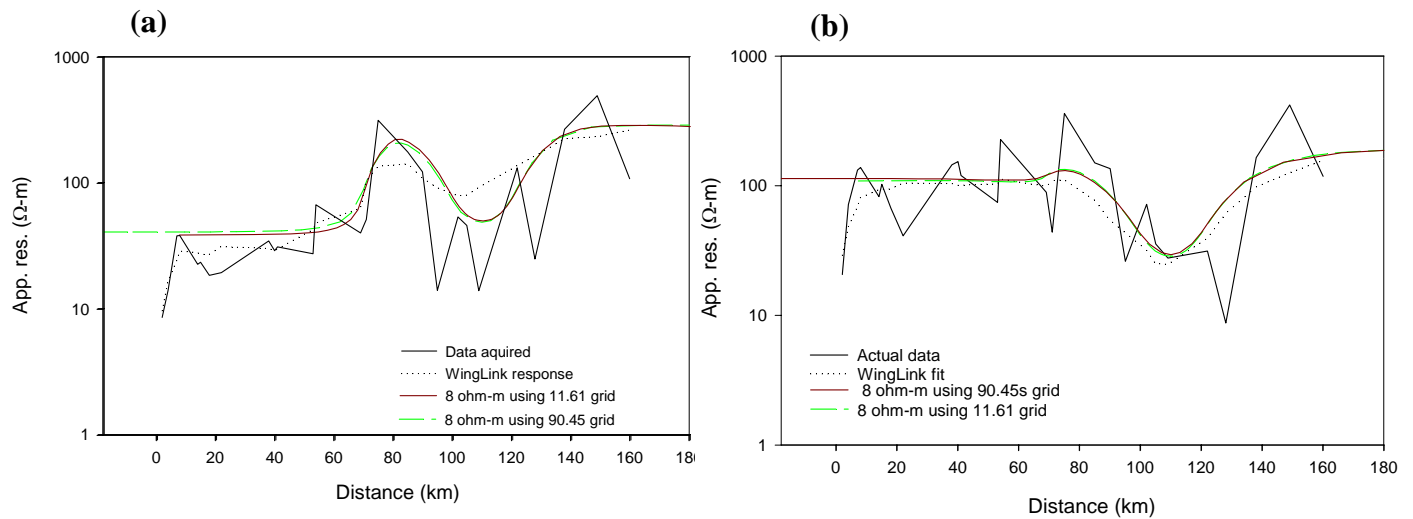


Figure 6.8: Response curves for multifrequency using eigenmodes of 11.61s and 90.45s grid (a) at 11.61s (b) at 90.45s.

6.2.4 Comparison with and without salient features

Since we are interested in the conductive feature near MCT and we used 90.45s period in 3D modeling, we tested the effect of other features, such as conductive layer and resistive block, on the response at this period only. We removed these features one by one and compared the responses with the response of model having only the conductive block near MCT. The response curves plotted in the Figure 6.9 reveal that the curve segment over the conductive block is not affected by other features. Thus the 2D experiments reveal that study of single 8 Ω -m block with basement at 200 km for time period 90.45s is good enough for designing 3D models. The 3D nature of this conductive block can be studied as if other features are not there.

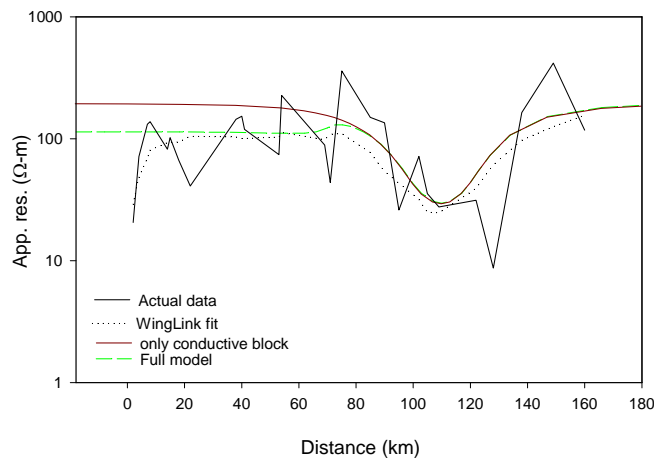


Figure 6.9: Curves with and without the features other than conductor.

6.3 3D Experiment

From 2D experimentation it is clear that the conductive block near MCT is main feature and its implication is presented in Figure 6.3 as many earthquakes occur near this zone and different 3D experiments performed on this conductive block are

- 1) Effect of varying strike length
- 2) Effect of changing depth to top of the conductive block
- 3) Effect of varying the thickness and width of the block

6.3.1 *Effect of varying the strike length*

The first question that comes to mind in a 3D study is regarding the strike length of the body. In this experiment, strike length is varied from 20 km to 100 km. The length of the block in strike direction is taken as 20, 50, 70 and 100 km keeping other parameters fixed. Figures 6.10(a) and 6.10(b) show the effect of strike length variation respectively for 2 km and 4 km depth to top of the block. In Figure 6.10(b), 70 km strike response lies closest to the 2D response. From Figure 6.10(c) it is clear that the 3D response curves approach the corresponding 2D response curve as the strike length increases.

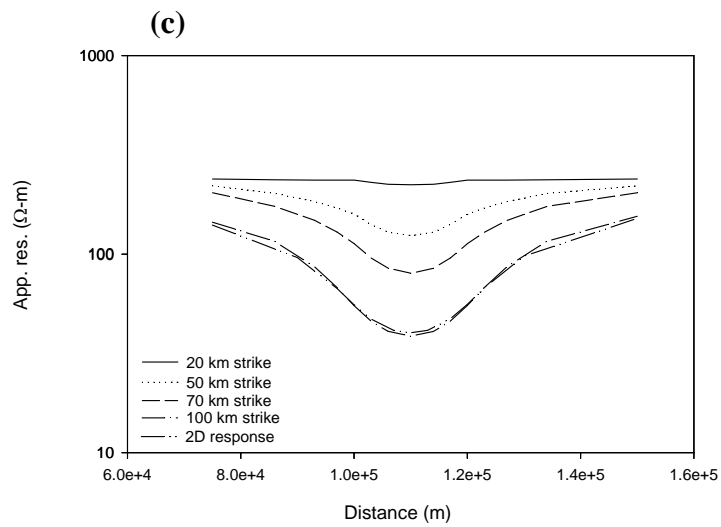
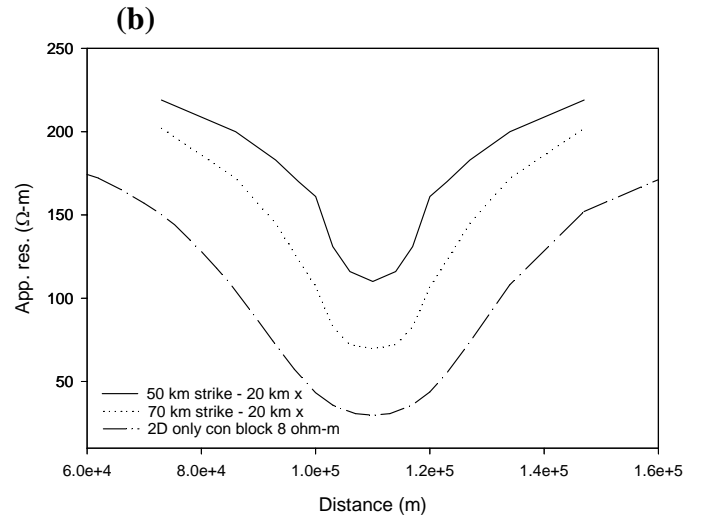
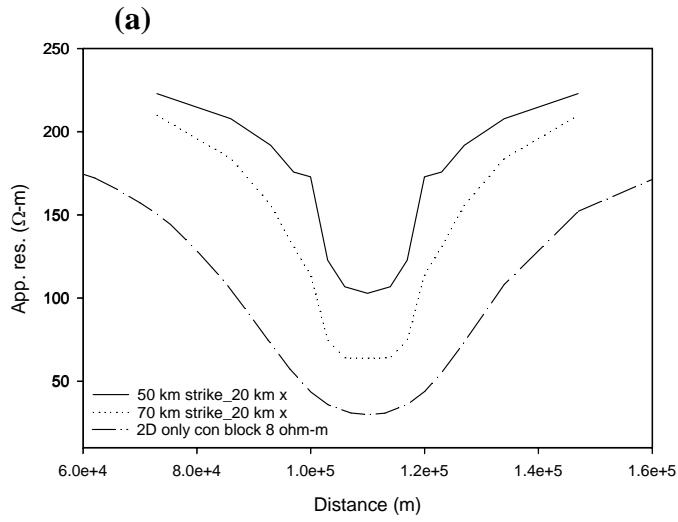


Figure 6.10: Strike variation curves for different depth to the top (a) at 2 km, (b) 4 km and (c) 6 km.

6.3.2 Effect of changing depth to top of the conductive block

Next we experimented with different depths to the top as 2, 4 and 6 km. At 2 km depth, curve did not follow the expected behavior outside the body as shown in Figure 6.11. In this figure the edges of the block are clearly identifiable but did not follow the 2D response. At 4 km depth, response curve is smoother at the edges and finally it approaches the behavior of 2D response at 70 km strike. At 6 km depth (as suggested by Tyagi (2007) model), the response curve lies above the response curve of 4 km depth. Thus response curve for 70 km strike and 4 km depth is the most suitable one.

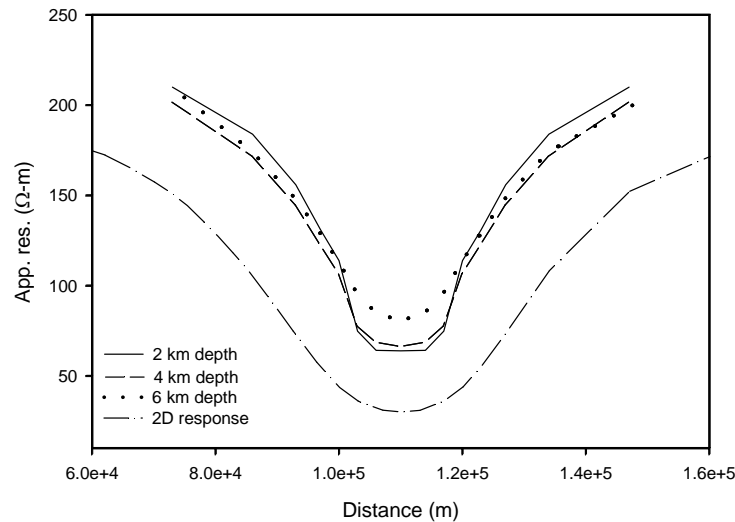


Figure 6.11: Plot for depth to the top of block.

In the next experiment, the depth and strike are kept fixed to these values and only the width of the block in other horizontal direction is varied.

6.3.3 Effect of varying the thickness and width of the block

We observed that at 70 km strike the curve suitably lies in the best range. Then we experimented by varying the dimension of block in orthogonal horizontal direction keeping the depth of burial and strike fixed. The depth to the top is taken 4 km and strike is fixed at 70 km. The width of block in other horizontal direction varies as 20, 26, 40 and 50 km and the computed responses are shown in Figure 6.12. We can observe that as width increases the curves started flattening while bottom of the curve is approximately the same. At 50 km width the curve seems roughly flat. Thus 20 or 26 km width may be the best for comparison with 2D behavior.

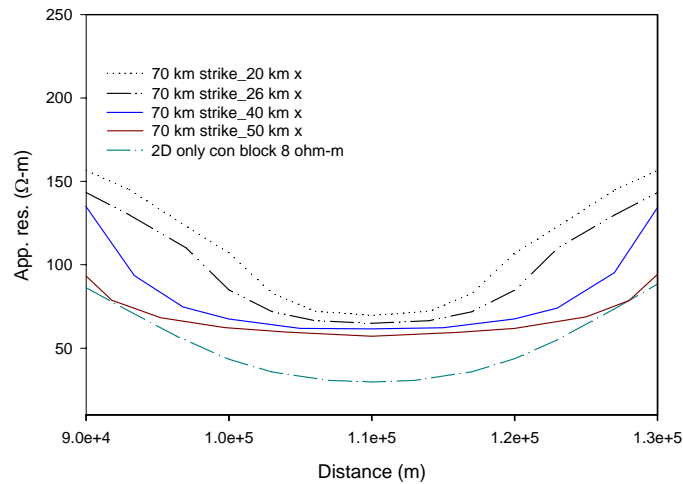


Figure 6.12: Variation in the block in other horizontal direction.

6.4 Conclusion

From these experiments we conclude that the conductive block geometry can be taken as 70 km strike, 20-26 km width and 4 km depth and its resistivity is 8 Ω -m. This 3D study suggests that the conductive block is practically 2D in nature.

SUMMARY AND CONCLUSION

The work on this thesis started with an objective of inversion of 3D magnetotelluric data. It is well known that an efficient modeling algorithm is a prerequisite for developing a competent inversion algorithm for data interpretation. The work presented herein is description and discussion related with the development of an efficient 3D modeling algorithm based on eigenmodes for magnetotelluric data.

The existing algorithms require re-run of the algorithm for each frequency. Thus, it requires same amount of computational time for each frequency. However, using eigenmode analysis, the multi-frequency responses are generated in negligible time once the eigenmodes, independent of frequency, are evaluated. In this approach, the eigenmodes depend only on the model characteristics. This efficiency is achieved by broadening the scope of the approach given in Stuntebeck (2003). She developed the technique for limited use of air-borne electromagnetics for which theory is provided in her thesis. Based on that theory we developed the algorithm for magnetotelluric data. In order to build up the sound methodology of the algorithm, we started with 1D modeling where closed form solution of forward problem is available. After obtaining satisfactory results in 1D case, we developed the 2D algorithm named as MT_2D_EA and finally developed the 3D modeling algorithm MT_3D_EA. For these algorithms, bulk of the computational time is taken for the computation of eigenmodes. MT_2D_EA and MT_3D_EA were tested for its accuracy and efficiency using number of 2D and 3D models, presented in the paper (Zhdanov et al., 1997), that are numerically solved using different algorithms based on matrix solver. We found that numerical responses obtained from the two approaches are same within

numerical errors. We observed that when responses for only few frequencies are computed, the computer time consumed by MT_3D_EA is more than the matrix solver based algorithms. However, when responses for large number of frequencies are required, a need for MT sounding, the total computer time requirement is less in case of eigenmode based technique than the matrix solver techniques. This is important to note here that the computed eigenmodes in forward modeling will be used as it is in computation of sensitivity matrix while developing the inversion software for 3D MT data.

The algorithm is employed to generate 3D models for the field data, acquired by Israil et al. (2008) in Garhwal Himalaya. On the basis of 2D interpretation of this data set, Israil et al. (2008) proposed a 2D electrical model of the region. The key feature of this 2D model is a conductor near MCT. We studied the 3D nature of this conductor and found that the 2D approximation of the conductor was justified.

The present algorithm is based on solving the secondary field EM eigenvalue problem using Finite Difference Method (FDM). The electric field values for any source are evaluated as superposition of the eigenvectors. The staggered grid, as proposed by Yee (1966), is used for accurate EM field computations. The FDM is used to transformed the EM eigenproblem to a symmetric matrix eigenproblem. It is found that one third of the eigenvalues of the 13-diagonal symmetric matrix becomes zero. As per concept of physics the zero eigenvalues and corresponding eigenvectors are not part of any physical system and we termed these as spurious eigenmodes. These eigenvalues are taken out of the study. by eliminating, using current divergence relation, the \mathbf{e}_z components from the system of equations. Now the system of equations deals only with the horizontal components \mathbf{e}_x and \mathbf{e}_y . This step reduces size of the resulting matrix to two third of the symmetric matrix.

However, the outcome of this reduction converts the symmetric matrix to non-symmetric. The eigenvalues and eigenvectors of the reduced non-symmetric matrix are computed. The electric field is continued analytically into the air through integral boundary condition. This step results in making nonzero all elements of the submatrix block corresponding to air-earth interface nodes.

Lanczos/Arnoldi method is used for evaluating the eigenmodes of symmetric/non-symmetric matrix. From the eigenmode formulation it is clear that, during superposition, only a subset of the smallest eigenvalues contributes significantly to the synthesis of field values. To get this subset of eigenmodes, Implicitly Restarted Lanczos/Arnoldi Method (IRLM/IRAM) is used in invert mode where product of inverse of the matrix with a vector is used. BiCGStab (Bi-Conjugate Gradient Stabilized) with preconditioner ILU(0) is used to efficiently obtain this product.. During the iterations of Arnoldi method, the eigenvectors loose their orthogonality. To reinstate orthogonality, the Arnoldi steps are applied twice. Only the non-zero elements of the coefficient matrix are stored to reduce the memory requirement. IRAM provides the eigenvalues and reduced eigenvectors, containing only the horizontal components \mathbf{e}_x and \mathbf{e}_y . For each eigenvector, the \mathbf{e}_z components are then obtained by using the current divergence relation. These full eigenvectors are made sigma-orthogonal. The eigenvalues and sigma-orthogonalized eigenvectors are next used to obtain the secondary electric field values. The primary electric field is already computed using layered earth model response. The total electric field values are obtained from primary and secondary electric field values. The total electric field values are used to derive the magnetic field. The electric field and magnetic field values are then used to compute impedance, apparent resistivity and phase values.

7.1 Conclusion

The algorithms, MT_2D_EA and MT_3D_EA developed in this thesis, are efficient and reliable softwares respectively for 2D and 3D magnetotelluric modeling. The algorithms have been rigorously and comprehensively tested within the limited time frame of this study and under the severe constraint on size of the 3D problem imposed by capacity of the available computer facility. This limitation, however, led us to perform detailed study of the effect of coarse grid on the EM response. Numerous experiments were performed to test the consistency and accuracy of the algorithms. These tests justified a qualified faith in the algorithms MT_2D_EA and MT_3D_EA. The results of various design exercises and comparison of the computed responses of different models with published ones, lead us to following conclusions

- The algorithm is able to model a complex structure.
- The eigenmode computations consume bulk of the computer resources and time. However, these are to be performed only once, even when responses for numerous frequencies are to be computed.
- Given the eigenmodes, the algorithm is capable of generating multi-frequency responses at a marginal cost.
- For conductive target use of only 5% eigenmodes is sufficient while for resistive target one must use 20% eigenmodes. So, this algorithm, in its present form, works better for conductive targets.
- In Garhwal Himalaya, the 3D geometry of the conductive block, buried under the Roorkee-Gangotri profile near MCT, can be taken as 70 km strike, 20-26 km width and 4 km depth and its resistivity is estimated as 8 Ω -m. However, the

detailed 3D study suggests that the conductive block can be approximated as a 2D one.

7.2 Limitations of the Algorithm

The limitations of the algorithm identified during testing are as follows.

- Presently, the manually generated grid is used in the algorithm.
- The algorithm takes major time in eigenmode computation.
- At the bottom of the modeling domain, perfectly conducting boundary condition is employed in the algorithm. This constraint forces one to take bottom at sufficient distance so that the tangential electric field will be zero at the domain boundary.
- Presently the algorithm can be used only for the plane wave source.
- The isotropic medium can be modeled using the algorithm.

7.3 Suggestions for Future Work

The present thesis has turned out to be an exploratory effort during which the computer programs MT_2D_EA and MT_3D_EA have been developed with an aim to enable quantitative interpretation of 3D MT data. The limitations listed above suggest that there exists a significant scope for further development. The limitations mentioned can be minimized by taking following steps.

- Implementation of auto grid generator which employs the skin depth criterion.
- Significant improvement can be made in the eigenmode evaluation, especially by using customized preconditioner in BiCGSTAB subprogram.

- Implementation of integral boundary condition at the bottom boundary of the domain.
- The algorithm can be modified for the computation of responses in case of controlled source EM methods simply by replacing the present primary field response computation subprogram with one corresponding to the given EM source.
- Inclusion of anisotropy.
- Adaptation of the MT_3D_EA code for parallel programming.

Finally, it may be stressed that after the code is adapted for parallel programming, the use of clusters of computers and supercomputers will significantly reduce the computational time and make it possible to undertake development of 3D MT data inversion algorithm.

INTERGRAL BOUNDARY CONDITION

The electric field is not constant at the air earth interface. It is decaying in the air also. This effect is taken into account by applying, at the air-earth interface, the integral boundary condition which models the continuation of electric field up to large distances in air. The integral boundary condition is described below.

A1.1 Integral Boundary Condition at the Air-Earth Interface

We are taking z +ve in downward direction. So, in the air, z is negative ($z < 0$). In the air ($\sigma = 0$) Maxwell's vector equations are reduced to

$$\nabla \times \mathbf{E} = -\dot{\mathbf{B}}, \quad (\text{A1.1})$$

$$\nabla \times \mathbf{B} = 0. \quad (\text{A1.2})$$

Taking divergence of equation (A1.1) we get

$$\nabla \cdot \dot{\mathbf{B}} = 0. \quad (\text{A1.3})$$

Further, equation (A1.2) permits the substitution

$$\mathbf{B} = \nabla \phi. \quad (\text{A1.4})$$

Equations (A1.3) and (A1.4) together yield

$$\nabla^2 \phi = 0. \quad (\text{A1.5})$$

The equation (A1.5) can be recast as

$$\phi''(z) = \frac{\partial^2 \phi}{\partial z^2} = -\frac{\partial^2 \phi}{\partial x^2} - \frac{\partial^2 \phi}{\partial y^2}, \quad (\text{A1.6})$$

Assuming exponential z -dependence of $\phi(x, y, z)$, it can be expressed as

$$\phi(x, y, z) = u(x, y) \exp(\chi z). \quad (\text{A1.7})$$

Substituting this relation into equation (A1.6) we get,

$$-\left(\frac{\partial^2}{\partial x^2} + \frac{\partial^2}{\partial y^2}\right)u(x, y) = \chi^2 u(x, y) \quad (\text{A1.8})$$

Let the plane at air-earth interface in discretized into n_{xy} cells, the LHS of equation (A1.8) after use of finite differences, gets transformed to a matrix \mathbf{F} which is symmetric and positive semi-definite. The discretized version of equation (A1.8) can be written as

$$\mathbf{F}\mathbf{u}_j = \chi_j^2 \mathbf{u}_j, \quad j = 1, n_{xy}. \quad (\text{A1.9})$$

Here, \mathbf{u}_j is the eigenvector corresponding to the eigenvalue χ_j^2 of the coefficient matrix.

Any vector can be expressed as linear superposition of orthogonal eigenvectors as

$$\mathbf{u} = \sum_j c_j \mathbf{u}_j. \quad (\text{A1.10})$$

The coefficient c_j 's can be evaluated using the known value of $\dot{\mathbf{b}}_z$ at air-earth interface ($z=0$) which can be described as

$$\dot{\mathbf{b}}_z = -\phi''(z=0) = \chi_j^2 u(x, y), \quad (\text{A1.11})$$

and

$$\mathbf{u} = \frac{1}{\chi_j^2} \cdot \dot{\mathbf{b}}_z(z=0). \quad (\text{A1.12})$$

Using equations (A1.12) and (A1.10), the coefficient of superposition can be evaluated as

$$c_j = \frac{1}{\chi_j^2} \cdot \dot{\mathbf{b}}_z(z=0) \cdot \mathbf{u}_j. \quad (\text{A1.13})$$

Finally, $\phi(x, y, z)$ can recast using (A1.7), (A1.10) and (A1.13) as

$$\phi(x, y, z) = \sum_{j=1}^{n_{xy}} \frac{1}{\chi_j^2} \dot{\mathbf{b}}_z(z=0) u_j u_j^T \exp(\chi_j z). \quad (\text{A1.14})$$

This integral boundary condition relation (A1.14) provides the matrix coefficients due to electric field continuation in the air. Here, n_{xy} is the number of horizontal electric field components at air-earth interface.

MATRIX COEFFICIENTS AND SIGMA ORTHONORMALIZATION

The eigenmode algorithm, using FDM, is described in Chapter 3. The components of the electric field are described here along with the average volume and the average conductivity definitions. The 13 non-zero coefficient values for all the three electric field components are given. The eigenvectors are not simple orthogonal, rather these follow sigma orthogonality and its implementation in terms of a constant factor multiplication to the simply orthogonal eigenvector is discussed.

A2.1 Matrix Coefficients

The average conductivities $\bar{\sigma}_x$, $\bar{\sigma}_y$ and $\bar{\sigma}_z$ associated with the points of cell (i, j, k), where e_x , e_y and e_z components are evaluated, are given by the following relations,

$$\begin{aligned}\bar{\sigma}_x(i, j, k) &= \frac{a(i)}{4V_x(i, j, k)} \left[\begin{array}{l} b(j)c(k)\sigma(i, j, k) + b(j-1)c(k)\sigma(i, j-1, k) \\ + b(j-1)c(k-1)\sigma(i, j-1, k-1) + b(j)c(k-1)\sigma(i, j, k-1) \end{array} \right], \\ \bar{\sigma}_y(i, j, k) &= \frac{b(j)}{4V_y(i, j, k)} \left[\begin{array}{l} a(i)c(k)\sigma(i, j, k) + a(i-1)c(k)\sigma(i-1, j, k) \\ + a(i-1)c(k-1)\sigma(i-1, j, k-1) + a(i)c(k-1)\sigma(i, j, k-1) \end{array} \right], \\ \bar{\sigma}_z(i, j, k) &= \frac{c(k)}{4V_z(i, j, k)} \left[\begin{array}{l} a(i)b(j)\sigma(i, j, k) + a(i-1)b(j)\sigma(i-1, j, k) \\ + a(i-1)b(j-1)\sigma(i-1, j-1, k) + a(i)b(j-1)\sigma(i, j-1, k) \end{array} \right] \end{aligned}$$

----- (A2.1)

Here, the volumes V_x , V_y and V_z are

$$V_x(i, j, k) = a(i)bh(j)ch(k) ,$$

$$V_y(i, j, k) = ah(i)b(j)ch(k) ,$$

$$V_z(i, j, k) = ah(i)bh(j)c(k). \quad (\text{A2.2})$$

The matrix symmetry is conserved by the transformations

$$\begin{aligned} \bar{e}_x(i, j, k) &= \sqrt{\mu_0 V_x(i, j, k) \bar{\sigma}_x(i, j, k)} e_x(i, j, k), \\ \bar{e}_y(i, j, k) &= \sqrt{\mu_0 V_y(i, j, k) \bar{\sigma}_y(i, j, k)} e_y(i, j, k), \\ \bar{e}_z(i, j, k) &= \sqrt{\mu_0 V_z(i, j, k) \bar{\sigma}_z(i, j, k)} e_z(i, j, k). \end{aligned} \quad (\text{A2.3})$$

This transformation is valid only for points with non-zero $\bar{\sigma}_x(i, j, k)$, $\bar{\sigma}_y(i, j, k)$ and $\bar{\sigma}_z(i, j, k)$. Using the abbreviations

$$\begin{aligned} d_x(i, j, k) &= 1/\sqrt{\mu_0 V_x(i, j, k) \bar{\sigma}_x(i, j, k)}, \\ d_y(i, j, k) &= 1/\sqrt{\mu_0 V_y(i, j, k) \bar{\sigma}_y(i, j, k)}, \\ d_z(i, j, k) &= 1/\sqrt{\mu_0 V_z(i, j, k) \bar{\sigma}_z(i, j, k)}, \end{aligned} \quad (\text{A2.4})$$

the system equations for the transformed electric components become

$$\lambda \bar{e}_x(i, j, k) = d_x(i, j, k) \cdot \left[\begin{aligned} & \left[\frac{a(i)ch(k)}{b(j)} + \frac{a(i)ch(k)}{b(j-1)} + \frac{a(i)bh(j)}{c(k)} + \frac{a(i)bh(j)}{c(k-1)} \right] d_x(i, j, k) \bar{e}_x(i, j, k) \\ & - \frac{a(i)ch(k)}{b(j-1)} d_x(i, j-1, k) \bar{e}_x(i, j-1, k) - \frac{a(i)ch(k)}{b(j)} d_x(i, j+1, k) \bar{e}_x(i, j+1, k) \\ & - \frac{\mathbf{a(i)bh(j)}}{\mathbf{c(k-1)}} \mathbf{d_x(i, j, k-1)} \bar{\mathbf{e}}_x(\mathbf{i, j, k-1}) - \frac{a(i)bh(j)}{c(k)} d_x(i, j, k+1) \bar{e}_x(i, j, k+1) \\ & + ch(k) d_y(i, j-1, k) \bar{e}_y(i, j-1, k) - ch(k) d_y(i+1, j-1, k) \bar{e}_y(i+1, j-1, k) \\ & - ch(k) d_y(i, j, k) \bar{e}_y(i, j, k) + ch(k) d_y(i+1, j, k) \bar{e}_y(i+1, j, k) \\ & + \mathbf{bh(j)d_z(i, j, k-1)} \bar{\mathbf{e}}_z(\mathbf{i, j, k-1}) - \mathbf{bh(j)d_z(i+1, j, k-1)} \bar{\mathbf{e}}_z(\mathbf{i+1, j, k-1}) \\ & - bh(j) d_z(i, j, k) \bar{e}_z(i, j, k) + bh(j) d_z(i+1, j, k) \bar{e}_z(i+1, j, k) \end{aligned} \right] \quad \text{----- (A2.5)}$$

$$\lambda \bar{e}_y(i, j, k) = d_y(i, j, k) \cdot \left\{ \begin{aligned} & \left[\frac{ah(i)b(j)}{c(k)} + \frac{ah(i)b(j)}{c(k-1)} + \frac{b(j)ch(k)}{a(i)} + \frac{b(j)ch(k)}{a(i-1)} \right] d_y(i, j, k) \bar{e}_y(i, j, k) \\ & - \frac{\mathbf{ah(i)b(j)}}{\mathbf{c(k-1)}} d_y(i, j, k-1) \bar{e}_y(i, j, k-1) - \frac{ah(i)b(j)}{c(k)} d_y(i, j, k+1) \bar{e}_y(i, j, k+1) \\ & - \frac{b(j)ch(k)}{a(i-1)} d_y(i-1, j, k) \bar{e}_y(i-1, j, k) - \frac{b(j)ch(k)}{a(i)} d_y(i+1, j, k) \bar{e}_y(i+1, j, k) \\ & + \mathbf{ah(i)d_z(i, j, k-1)} \bar{\mathbf{e}}_z(i, j, k-1) - \mathbf{ah(i)d_z(i, j+1, k-1)} \bar{\mathbf{e}}_z(i, j+1, k-1) \\ & - ah(i)d_z(i, j, k) \bar{e}_z(i, j, k) + ah(i)d_z(i, j+1, k) \bar{e}_z(i, j+1, k) \\ & + ch(k)d_x(i-1, j, k) \bar{e}_x(i-1, j, k) - ch(k)d_x(i-1, j+1, k) \bar{e}_x(i-1, j+1, k) \\ & - ch(k)d_x(i, j, k) \bar{e}_x(i, j, k) + ch(k)d_x(i, j+1, k) \bar{e}_x(i, j+1, k) \end{aligned} \right\}$$

----- (A2.6)

$$\lambda \bar{e}_z(i, j, k) = d_z(i, j, k) \cdot \left\{ \begin{aligned} & \left[\frac{bh(j)c(k)}{a(i-1)} + \frac{bh(j)c(k)}{a(i)} + \frac{ah(i)c(k)}{b(j-1)} + \frac{ah(i)c(k)}{b(j)} \right] d_z(i, j, k) \bar{e}_z(i, j, k) \\ & - \frac{bh(j)c(k)}{a(i-1)} d_z(i-1, j, k) \bar{e}_z(i-1, j, k) - \frac{bh(j)c(k)}{a(i)} d_z(i+1, j, k) \bar{e}_z(i+1, j, k) \\ & - \frac{ah(i)c(k)}{b(j-1)} d_z(i, j-1, k) \bar{e}_z(i, j-1, k) - \frac{ah(i)c(k)}{b(j)} d_z(i, j+1, k) \bar{e}_z(i, j+1, k) \\ & + bh(j)d_x(i-1, j, k) \bar{e}_x(i-1, j, k) - bh(j)d_x(i-1, j, k+1) \bar{e}_x(i-1, j, k+1) \\ & - bh(j)d_x(i, j, k) \bar{e}_x(i, j, k) + bh(j)d_x(i, j, k+1) \bar{e}_x(i, j, k+1) \\ & + ah(i)d_y(i, j-1, k) \bar{e}_y(i, j-1, k) - ah(i)d_y(i, j-1, k+1) \bar{e}_y(i, j-1, k+1) \\ & - ah(i)d_y(i, j, k) \bar{e}_y(i, j, k) + ah(i)d_y(i, j, k+1) \bar{e}_y(i, j, k+1) \end{aligned} \right\}$$

----- (A2.7)

In the above equations the bold terms do not contribute in the first layer, bounded by air-earth interface, and these are replaced with field continuation coefficients given by equation (A1.14) of Appendix A1. The complete system of equations can be represented as

$$\mathbf{A}\bar{\mathbf{e}} = \lambda\bar{\mathbf{e}}. \quad (\text{A2.8})$$

Here, \mathbf{A} matrix contains elements due to field continuation as well as due to FD approximation of equations (A2.5), (A2.6) and (A2.7).

The e_z components are replaced with the horizontal components using the current divergence relation (equation 3.19). This leads to a non-symmetric matrix as shown in Figure 3.5. Now the reduced system of equation can be written as

$$\mathbf{A}_R\check{\mathbf{e}} = \lambda\check{\mathbf{e}}, \quad (\text{A2.9})$$

where, \mathbf{A}_R denotes the reduced matrix and $\check{\mathbf{e}}$ denotes the reduced eigenvector having only horizontal components. These reduced eigenvectors, $\check{\mathbf{e}}$, are orthogonal. The full eigenvectors, $\bar{\mathbf{e}}$, are now reconstructed from these reduced eigenvectors, $\check{\mathbf{e}}$, using the divergence relation again. These full eigenvectors are sigma-orthonormalized as discussed below.

A2.2 Sigma Orthogonality of Eigenvectors

The full eigenvectors, $\bar{\mathbf{e}}$, are transformed, using equation (A2.3), into eigenvectors, \mathbf{e} . These transformed eigenvectors must be σ -orthonormal as stated in Chapter 2. The σ -orthonormality relation as described in equation (2.24) is

$$\int \sigma(r) \hat{\mathbf{e}}_n \hat{\mathbf{e}}_m d^3 r = \delta_{nm}. \quad (\text{A2.10})$$

Let the final σ -orthogonal eigenvectors, $\hat{\mathbf{e}}_n$, with weighted norm η_n be defined as

$$\hat{\mathbf{e}}_n(r) = \eta_n \mathbf{e}_n(r). \quad (\text{A2.11})$$

The orthogonality relation (A2.10) in discrete form can be written as

$$\sum_{r=1}^{N_A} \bar{\sigma}(r) \hat{\mathbf{e}}_n(r) \hat{\mathbf{e}}_m(r) V(r) = \delta_{nm}. \quad (\text{A2.12})$$

The norm factor η_n is obtained by applying weighted normalization as follows

$$\begin{aligned} \sum_{r=1}^{N_A} \bar{\sigma}(r) \hat{\mathbf{e}}_n^2(r) V(r) &= \sum_{r=1}^{N_A} \bar{\sigma}(r) \eta_n^2 \mathbf{e}_n^2(r) V(r) = 1, \\ \sum_{r=1}^{N_A} \bar{\sigma}(r) \mathbf{e}_n^2(r) V(r) &= 1/\eta_n^2. \end{aligned} \quad (\text{A2.13})$$

Using the relation (A2.3), the eigenvectors \mathbf{e}_n transformed into eigenvectors $\bar{\mathbf{e}}_n$, the norm factor simplifies to

$$\eta_n = \frac{1}{\sqrt{\frac{1}{\mu_0} \sum_{r=1}^{N_A} \bar{\mathbf{e}}_n^2(r)}} = \frac{\sqrt{\mu_0}}{\sqrt{\sum_{r=1}^{N_A} \bar{\mathbf{e}}_n^2(r)}} = \sqrt{\mu_0}, \quad (\text{A2.15})$$

assuming $|\bar{\mathbf{e}}_n| = 1$.

Thus, the eigenvectors $\hat{\mathbf{e}}_n$ with weighted norm, which are needed for eigenmode synthesis, are determined directly from the orthonormal eigenvectors $\bar{\mathbf{e}}_n$ by

$$\hat{\mathbf{e}}_n(r) = \eta_n \mathbf{e}(r) = \sqrt{\mu_0} d(r) \bar{\mathbf{e}}_n(r). \quad (\text{A2.16})$$

ALGORITHM PARAMETERS AND SUBPROGRAMS

The algorithm description is given in Chapter 4. The input data and other parameters are controlled by several counters. The details of these counters along with their default values and descriptions are presented in Table A3.1. The grid control parameters are given in Table A3.2. In Table A3.3, the list of subprograms is presented along with their purposes.

Table A3.1: Description of control parameters.

Parameter	Controls	Value	Description
irx	Grid generation in x-direction	0	Manual grid
		1	Logarithmic grid
iry	Grid generation in y-direction	0	Manual grid
		1	Logarithmic grid
irz	Grid generation in z- direction	0	Manual grid
		1	Logarithmic grid
irt	No of time periods in decades	0	Manual time period
		1	Logarithmic time period
irun	Generation of eigenmodes	0	Generate eigenmodes
		1	Reused eigenmodes
mode_type	Response computation corresponding to 2D	0	corresponding to 2D TE mode
		1	Corresponding to 2D TM mode
preconditioner	Which preconditioner	0	No preconditioner
		1	9-diag preconditioner
		2	Block preconditioner

.....Table A3.1 continued

restart	Eigenmode computation	0 1	All eigenmodes Desired Eigenmodes
---------	-----------------------	--------	--------------------------------------

Table A3.2: Grid parameters description.

Parameter	Description
nx	Number of cells in x-direction
ny	Number of cells in y-direction
nz	Number of cells in z-direction
ne	Number of $\mathbf{e}_x + \mathbf{e}_y$ components
nef	Total number of unknowns ($\mathbf{e}_x + \mathbf{e}_y + \mathbf{e}_z$ components)
np	Number of anomalous prisms
nt	Total number of time periods
qx (irx.eq.1)	Logarithmic grid control parameter in x-direction
qy (iry.eq.1)	Logarithmic grid control parameter in y-direction
qz (irz.eq.1)	Logarithmic grid control parameter in z-direction
tz (irt.eq.1)	Logarithmic time distribution control parameter
rho0	Half space resistivity
rho1,...np	Anomalous resistivity
ixa	Starting cell number of anomalous prism in x-direction
ixb	Ending cell number of anomalous prism in x-direction

.....Table A3.2 continued

iya	Starting cell number of anomalous prism in y-direction
iyb	Ending cell number of anomalous prism in y-direction
iza	Starting cell number of anomalous prism in z-direction
izb	Ending cell number of anomalous prism in z-direction
kev	Number of eigenmodes to be calculated
npv	In restarting > kev
Bicg_itmax	Maximum number of iterations for BiCGStab convergence
Lancz_tolr	Threshold value for accurate eigenmodes during a subset computation

Table A3.3: Various subprograms and their purpose.

Subprogram	Purpose	Called by	Calls
ae1	Matrix-vector multiplication	eigenstep, bicgstab	fpres0, conti1, conti2, conti3, conti4
ae1_reduced	Multiplication of reduced elements with vector	Precondi_3D	-----
bicgstab	To solve inverse of matrix	eigenstep	ae1, preconditioner_3D, block_pre, Precondi_3D
CGS	Block preconditioner	block_pre	local_pre
conti1	Integral boundary condition when x- and y- grids are non-uniform	ae1	tridi
conti2	Integral Boundary	ae1	tridi, fft

.....Table A3.3 continued

	condition when x-is non-uniform and y-is uniform		
conti3	Integral boundary condition when x-is uniform and Y-is non-uniform	ae1	tridi, fft
conti4	Integral boundary condition when both x- and y- are uniform	ae1	fft
dlahqr	Eigenmode computation of 3D	eigenmode_3d	-----
dnapps	Updation of a subset of eigenmodes	eigenmode_3d	Adepted/taken from ARPACK
eigenmode_1D	Eigenmode computation for 1D layered structure	Main	Tridi
eigenmode_3D	Computing 3D eigenmodes	Main	dnapps, eigenstep, dlahqr, gramsmtd, get_ez
eigenstep	Generation of Heisenberg matrix and new starting vector	eigenmode_3d	ae1, bicgstab
extremal	Limits of eigenvalues computation	Main	-----
fft	Forward/Inverse Fourier transform	conit2, conti3, conti4	-----
fpres0	Surface field computation	ae1	printr
get_ez	Solving e_z components of eigenvectors from reduced	eigenmode_3d	-----

.....Table A3.3 continued

	eigenvectors		
gramsmdt	Orthogonalization of new eigenvector with previous eigenvectors	eigenmode_3d	-----
grid	Generation of logarithmic grid	input	-----
init	Initialization of starting vector	Main	-----
input	Read input and control parameters	Main	grid, sigma0, sigma1, sigma2
local_pre	Local (block wise)	CGS	-----
method	Identification of uniform or non-uniform grid	Main	-----
output_1d	Primary field computation	Main	-----
output_3d	Total E-field, Impedance, Apparent resistivity and Phase computation for 3D	Main	-----
Pre_1	To multiply continuation element for preconditioning	block_pre	conti1, conti2, conti3, conti4
Pre_2	Multiplication of Reduced components for preconditioning	block_pre	-----
Pre_3	Multiplying each block with the vector element	CGS	-----
Pre_4	Preconditioner element	Pre_1	-----

.....Table A3.3 continued

Precondi_3D	First 9-diagonal preconditioner the reduces element iteratively	bicgstab	Preconditioner_3D, ae1_reduced
Preconditioner_3D	9-diag preconditioner	bicgstab, Pre_3	-----
printi	Print 3D integer array	sigma0	-----
printr	Print resistivity 3D array	sigma1, sigma2	-----
sigma0	Defining half space resistivity to all nodes	input	printr
sigma1	Defining anomalous nodal resistivity values	input	printr
sigma2	Average resistivity computation	input	printr
tridi	Eigenmodes computation of Symmetric tridiagonal matrix	conti1, conti2, conti3, eigenmode_1d	-----
weight	Coefficient computation for \mathbf{e}_x , \mathbf{e}_y and \mathbf{e}_z components	Main	-----
weight_ez	Coefficient corresponding to replacing \mathbf{e}_z into \mathbf{e}_x and \mathbf{e}_y components	Main	-----

SAMPLE INPUT AND OUTPUT FILES

Input.dat

*** title (max 75 characters):

sfd: large horizontal grid

*** grid:(1260+567)

0 !irx

10 !nx

0.

1000.

1500.

2000.

2250.

2500.

2750.

3000.

3500.

4000.

5000. !x(nx+1)

0 !iry

10 !ny

0.

1000.

1500.

2000.

2250.

2500.

2750.

3000.

3500.

4000.

5000. !y(ny+1)

0 !irz

7 !nz

0.

100.

350.

600.

850.

1100.

1500.

2500. !z(nz+1)

```

*** resistivity:
1.0                !rho00 (half space resistivity)
1                  !np (number of anomalous prisms)
0.1                !rho01 (resistivity of prisms)
005 006 005 006 002 003 !ixa,ixb,iya,iyb,iza,izb
9                  !iws0
0                  !iws1
0                  !iws2
*** time lags:
0                  !irt
1                  !nt
1.0                !it
*** error bounds
1.0E-16            !lancz_tolr
14000              !bicg_itmax
1.0E-06            !bicg_tol
1.0E-16            !bicg_stol
*** parameters controlling the Lanczos process:
1                  !restart (0-> computing all eigenvalues, 1-> computing desired eigenvalues)
0                  !preconditioner (0-> no pre, 1-> 9 diag pre, 2-> block pre)
1300               !mmax
1260,0            !kev,npv
0                  !irun (0-> regenerate, 1-> reused eigenvectors)
0                  !mode_type (1-> corresponds to 2D TE, 0-> 2D TM)

```


Output_main.dat

```
*** title (max 75 characters):
  sfd: large horizontal grid
*** grid:(1260+567)
0          !irx
10         !nx
0.
1000.
1500.
2000.
2250.
2500.
2750.
3000.
3500.
4000.
5000.     !x(nx+1)
0         !iry
10        !ny
0.
1000.
1500.
2000.
2250.
2500.
2750.
3000.
3500.
4000.
5000.     !y(ny+1)
0         !irz
7         !nz
0.
100.
350.
600.
850.
1100.
1500.
2500.     !z(nz+1)
*** resistivity:
1.0       !rho00 (half space resistivity)
1         !np (number of anomalous prisms)
0.1      !rho01 (resistivity of prisms)
005 006 005 006 002 003 !ixa,ixb,iya,iyb,iza,izb
```

```

9          liws0
0          liws1
0          liws2
*** time lags:
0          !irt
1          !nt
1.0       !it
*** error bounds
1.0E-16   !lancz_tolr
14000     !bicg_itmax
1.0E-06   !bicg_tol
1.0E-16   !bicg_stol
*** parameters controlling the Lanczos process:
1          !restart (0-> computing all eigenvalues, 1-> comput
0          !preconditioner (0-> no pre, 1-> 9 diag pre, 2-> bl
1300      !mmax
1260,0    !kev,npv
0          !irun (0-> regenerate, 1-> reused eigenvectors)
0          !mode_type (1-> corresponds to 2D TE, 0-> 2D TM)

```

sfd: large horizontal grid

nx= 10, tx= 5000.00, dxmin= 250.00

i	x(i)	a(i)	xc(i)	ah(i)
1	0.00	1000.00	500.00	1000.00
2	1000.00	500.00	1250.00	750.00
3	1500.00	500.00	1750.00	500.00
4	2000.00	250.00	2125.00	375.00
5	2250.00	250.00	2375.00	250.00
6	2500.00	250.00	2625.00	250.00
7	2750.00	250.00	2875.00	250.00
8	3000.00	500.00	3250.00	375.00
9	3500.00	500.00	3750.00	500.00
10	4000.00	1000.00	4500.00	750.00
11	5000.00		1000.00	

ny= 10, ty= 5000.00, dymin= 250.00

j	y(j)	b(j)	yc(j)	bh(j)
1	0.00	1000.00	500.00	1000.00
2	1000.00	500.00	1250.00	750.00
3	1500.00	500.00	1750.00	500.00
4	2000.00	250.00	2125.00	375.00
5	2250.00	250.00	2375.00	250.00
6	2500.00	250.00	2625.00	250.00
7	2750.00	250.00	2875.00	250.00
8	3000.00	500.00	3250.00	375.00

```

9 3500.00 500.00 3750.00 500.00
10 4000.00 1000.00 4500.00 750.00
11 5000.00          1000.00

```

nz= 7, tz= 2500.00, dzmin= 100.00

```

k   z(k)   c(k)   zc(k)  ch(k)
1   0.00  100.00  50.00  100.00
2  100.00  250.00  225.00 175.00
3  350.00  250.00  475.00 250.00
4  600.00  250.00  725.00 250.00
5  850.00  250.00  975.00 250.00
6 1100.00  400.00 1300.00 325.00
7 1500.00 1000.00 2000.00 700.00
8 2500.00          1000.00

```

dhmin= 250.00, dmin= 100.00

background resistivity rho0= 1.0000E+00 Ohm*m

relative position of prisms:

```

-----
i  ixa  ixb  iya  iyb  iza  izb
1  5    6    5    6    2    3

```

resistivity and absolute position of prisms:

```

-----
i rho[Ohm*m] xa[m]  xb[m]  ya[m]  yb[m]  za[m]  zb[m]
1  0.10000 2250.0 2750.0 2250.0 2750.0 100.0 600.0

```

iws0= 7: symbolic display of resistivity in the uppermost 7 levels

iws1=0: no display of resistivity

iws2=0: no display of averaged conductivity

smin= 1.000E+00 S/m, smax= 1.000E+01 S/m

is

is - level 1:

```

   1 2 3 4 5 6 7 8 9 10
10  0 0 0 0 0 0 0 0 0 0
 9  0 0 0 0 0 0 0 0 0 0
 8  0 0 0 0 0 0 0 0 0 0
 7  0 0 0 0 0 0 0 0 0 0
 6  0 0 0 0 0 0 0 0 0 0
 5  0 0 0 0 0 0 0 0 0 0
 4  0 0 0 0 0 0 0 0 0 0
 3  0 0 0 0 0 0 0 0 0 0
 2  0 0 0 0 0 0 0 0 0 0
 1  0 0 0 0 0 0 0 0 0 0

```

is - level 2:

```
  1 2 3 4 5 6 7 8 9 10
10 0 0 0 0 0 0 0 0 0 0
 9 0 0 0 0 0 0 0 0 0 0
 8 0 0 0 0 0 0 0 0 0 0
 7 0 0 0 0 0 0 0 0 0 0
 6 0 0 0 0 1 1 0 0 0 0
 5 0 0 0 0 1 1 0 0 0 0
 4 0 0 0 0 0 0 0 0 0 0
 3 0 0 0 0 0 0 0 0 0 0
 2 0 0 0 0 0 0 0 0 0 0
 1 0 0 0 0 0 0 0 0 0 0
```

is - level 3:

```
  1 2 3 4 5 6 7 8 9 10
10 0 0 0 0 0 0 0 0 0 0
 9 0 0 0 0 0 0 0 0 0 0
 8 0 0 0 0 0 0 0 0 0 0
 7 0 0 0 0 0 0 0 0 0 0
 6 0 0 0 0 1 1 0 0 0 0
 5 0 0 0 0 1 1 0 0 0 0
 4 0 0 0 0 0 0 0 0 0 0
 3 0 0 0 0 0 0 0 0 0 0
 2 0 0 0 0 0 0 0 0 0 0
 1 0 0 0 0 0 0 0 0 0 0
```

is - level 4:

```
  1 2 3 4 5 6 7 8 9 10
10 0 0 0 0 0 0 0 0 0 0
 9 0 0 0 0 0 0 0 0 0 0
 8 0 0 0 0 0 0 0 0 0 0
 7 0 0 0 0 0 0 0 0 0 0
 6 0 0 0 0 0 0 0 0 0 0
 5 0 0 0 0 0 0 0 0 0 0
 4 0 0 0 0 0 0 0 0 0 0
 3 0 0 0 0 0 0 0 0 0 0
 2 0 0 0 0 0 0 0 0 0 0
 1 0 0 0 0 0 0 0 0 0 0
```

is - level 5:

```
  1 2 3 4 5 6 7 8 9 10
10 0 0 0 0 0 0 0 0 0 0
 9 0 0 0 0 0 0 0 0 0 0
 8 0 0 0 0 0 0 0 0 0 0
 7 0 0 0 0 0 0 0 0 0 0
```

```

6 0 0 0 0 0 0 0 0 0 0
5 0 0 0 0 0 0 0 0 0 0
4 0 0 0 0 0 0 0 0 0 0
3 0 0 0 0 0 0 0 0 0 0
2 0 0 0 0 0 0 0 0 0 0
1 0 0 0 0 0 0 0 0 0 0

```

is - level 6:

```

  1 2 3 4 5 6 7 8 9 10
10 0 0 0 0 0 0 0 0 0 0
 9 0 0 0 0 0 0 0 0 0 0
 8 0 0 0 0 0 0 0 0 0 0
 7 0 0 0 0 0 0 0 0 0 0
 6 0 0 0 0 0 0 0 0 0 0
 5 0 0 0 0 0 0 0 0 0 0
 4 0 0 0 0 0 0 0 0 0 0
 3 0 0 0 0 0 0 0 0 0 0
 2 0 0 0 0 0 0 0 0 0 0
 1 0 0 0 0 0 0 0 0 0 0

```

is - level 7:

```

  1 2 3 4 5 6 7 8 9 10
10 0 0 0 0 0 0 0 0 0 0
 9 0 0 0 0 0 0 0 0 0 0
 8 0 0 0 0 0 0 0 0 0 0
 7 0 0 0 0 0 0 0 0 0 0
 6 0 0 0 0 0 0 0 0 0 0
 5 0 0 0 0 0 0 0 0 0 0
 4 0 0 0 0 0 0 0 0 0 0
 3 0 0 0 0 0 0 0 0 0 0
 2 0 0 0 0 0 0 0 0 0 0
 1 0 0 0 0 0 0 0 0 0 0

```

explanation:

0: rho= 1.00 Ohm*m

1: rho= 0.10 Ohm*m

time lags and extremal diffusion lengths:

```

-----
it  t[s] d_min[m] d_max[m] d_bgr[m]
 1 1.000E+00 2.821E+02 8.921E+02 8.921E+02

```

bgr=background

convergence check after mstep=1260 iterations

alphmin= 7.8540E-03, alphmax= 1.6000E+02

meth=1: no-fft grid in x- and y-direction

1D eigenvalues: no., value

```

 1 6.95E+01  2 4.33E+01  3 2.75E+01  4 1.34E+01  5 5.13E+00
 6 1.15E+00

```

Final eigenvalues of 3D problem

8.62E-01	8.62E-01	9.01E-01	1.25E+00	1.74E+00	1.74E+00	1.87E+00	1.87E+00	2.19E+00	2.19E+00
2.60E+00	3.09E+00	3.12E+00	3.13E+00	3.24E+00	3.24E+00	3.25E+00	3.35E+00	3.35E+00	3.65E+00
3.65E+00	3.82E+00	3.97E+00	3.97E+00	4.03E+00	4.03E+00	4.46E+00	4.46E+00	4.52E+00	4.54E+00
4.87E+00	4.87E+00	4.96E+00	5.30E+00	5.39E+00	5.48E+00	5.48E+00	5.49E+00	5.60E+00	5.79E+00
5.88E+00	5.94E+00	5.94E+00	5.94E+00	6.11E+00	6.11E+00	6.26E+00	6.26E+00	6.37E+00	6.38E+00
6.52E+00	6.52E+00	6.56E+00	6.83E+00	6.83E+00	6.96E+00	7.15E+00	7.15E+00	7.34E+00	7.64E+00
7.76E+00	7.76E+00	7.93E+00	7.93E+00	8.02E+00	8.19E+00	8.19E+00	8.36E+00	8.40E+00	8.45E+00
8.45E+00	8.69E+00	8.74E+00	8.74E+00	8.74E+00	8.78E+00	8.94E+00	8.99E+00	8.99E+00	9.06E+00
9.10E+00	9.15E+00	9.15E+00	9.22E+00	9.22E+00	9.40E+00	9.40E+00	9.80E+00	9.83E+00	9.83E+00
9.98E+00	1.00E+01	1.00E+01	1.01E+01	1.03E+01	1.03E+01	1.04E+01	1.05E+01	1.05E+01	1.06E+01
1.06E+01	1.06E+01	1.06E+01	1.08E+01	1.08E+01	1.08E+01	1.09E+01	1.09E+01	1.09E+01	1.10E+01
1.11E+01	1.11E+01	1.11E+01	1.11E+01	1.11E+01	1.12E+01	1.12E+01	1.13E+01	1.14E+01	1.14E+01
1.14E+01	1.15E+01	1.15E+01	1.15E+01	1.16E+01	1.16E+01	1.17E+01	1.17E+01	1.18E+01	1.18E+01
1.21E+01	1.21E+01	1.21E+01	1.22E+01	1.22E+01	1.23E+01	1.24E+01	1.24E+01	1.24E+01	1.25E+01
1.28E+01	1.28E+01	1.28E+01	1.29E+01	1.29E+01	1.30E+01	1.30E+01	1.30E+01	1.31E+01	1.31E+01
1.32E+01	1.32E+01	1.34E+01	1.36E+01	1.36E+01	1.37E+01	1.37E+01	1.37E+01	1.37E+01	1.38E+01
1.41E+01	1.41E+01	1.41E+01	1.41E+01	1.42E+01	1.43E+01	1.44E+01	1.44E+01	1.45E+01	1.46E+01
1.47E+01	1.47E+01	1.49E+01	1.49E+01	1.50E+01	1.53E+01	1.53E+01	1.54E+01	1.54E+01	1.54E+01
1.54E+01	1.54E+01	1.55E+01	1.55E+01	1.55E+01	1.56E+01	1.58E+01	1.59E+01	1.60E+01	1.60E+01
1.60E+01	1.60E+01	1.61E+01	1.65E+01	1.66E+01	1.66E+01	1.67E+01	1.67E+01	1.68E+01	1.70E+01
1.70E+01	1.73E+01	1.73E+01	1.74E+01	1.76E+01	1.76E+01	1.76E+01	1.78E+01	1.78E+01	1.78E+01
1.79E+01	1.80E+01	1.81E+01	1.81E+01	1.81E+01	1.83E+01	1.83E+01	1.83E+01	1.83E+01	1.83E+01
1.85E+01	1.85E+01	1.86E+01	1.87E+01	1.87E+01	1.87E+01	1.87E+01	1.88E+01	1.88E+01	1.88E+01
1.88E+01	1.90E+01	1.90E+01	1.91E+01	1.91E+01	1.92E+01	1.93E+01	1.94E+01	1.94E+01	1.96E+01
1.96E+01	1.98E+01	1.98E+01	1.98E+01	1.99E+01	2.01E+01	2.01E+01	2.02E+01	2.02E+01	2.02E+01
2.03E+01	2.05E+01	2.05E+01	2.05E+01	2.07E+01	2.07E+01	2.08E+01	2.08E+01	2.09E+01	2.09E+01
2.09E+01	2.09E+01	2.10E+01	2.10E+01	2.11E+01	2.11E+01	2.12E+01	2.12E+01	2.12E+01	2.13E+01
2.13E+01	2.13E+01	2.14E+01	2.14E+01	2.14E+01	2.14E+01	2.15E+01	2.16E+01	2.17E+01	2.17E+01
2.19E+01	2.19E+01	2.19E+01	2.19E+01	2.20E+01	2.20E+01	2.22E+01	2.22E+01	2.22E+01	2.23E+01
2.23E+01	2.24E+01	2.25E+01	2.25E+01	2.26E+01	2.27E+01	2.27E+01	2.28E+01	2.29E+01	2.29E+01
2.31E+01	2.31E+01	2.31E+01	2.32E+01	2.32E+01	2.34E+01	2.35E+01	2.35E+01	2.37E+01	2.37E+01
2.37E+01	2.37E+01	2.37E+01	2.38E+01	2.38E+01	2.39E+01	2.39E+01	2.39E+01	2.40E+01	2.42E+01

2.44E+01 2.44E+01 2.46E+01 2.46E+01 2.46E+01 2.51E+01 2.51E+01 2.51E+01 2.54E+01 2.54E+01
2.54E+01 2.54E+01 2.54E+01 2.55E+01 2.62E+01 2.63E+01 2.63E+01 2.64E+01 2.64E+01 2.64E+01
2.64E+01 2.65E+01 2.65E+01 2.67E+01 2.67E+01 2.67E+01 2.67E+01 2.68E+01 2.68E+01 2.70E+01
2.70E+01 2.70E+01 2.71E+01 2.73E+01 2.74E+01 2.74E+01 2.77E+01 2.77E+01 2.79E+01 2.79E+01
2.79E+01 2.80E+01 2.80E+01 2.82E+01 2.85E+01 2.85E+01 2.85E+01 2.87E+01 2.87E+01 2.87E+01
2.89E+01 2.90E+01 2.90E+01 2.91E+01 2.91E+01 2.92E+01 2.93E+01 2.93E+01 2.94E+01 2.94E+01
2.96E+01 2.96E+01 2.96E+01 2.96E+01 2.97E+01 2.97E+01 2.97E+01 2.99E+01 2.99E+01 3.01E+01
3.01E+01 3.04E+01 3.04E+01 3.04E+01 3.06E+01 3.08E+01 3.08E+01 3.12E+01 3.12E+01 3.12E+01
3.13E+01 3.17E+01 3.17E+01 3.18E+01 3.18E+01 3.20E+01 3.20E+01 3.20E+01 3.23E+01 3.23E+01
3.23E+01 3.24E+01 3.26E+01 3.26E+01 3.26E+01 3.27E+01 3.27E+01 3.28E+01 3.29E+01 3.29E+01
3.29E+01 3.29E+01 3.30E+01 3.32E+01 3.36E+01 3.36E+01 3.36E+01 3.37E+01 3.40E+01 3.40E+01
3.42E+01 3.42E+01 3.42E+01 3.42E+01 3.43E+01 3.43E+01 3.44E+01 3.45E+01 3.46E+01 3.46E+01
3.47E+01 3.49E+01 3.49E+01 3.49E+01 3.50E+01 3.51E+01 3.51E+01 3.52E+01 3.53E+01 3.53E+01
3.54E+01 3.54E+01 3.54E+01 3.55E+01 3.56E+01 3.57E+01 3.58E+01 3.59E+01 3.60E+01 3.60E+01
3.61E+01 3.62E+01 3.62E+01 3.62E+01 3.62E+01 3.64E+01 3.64E+01 3.64E+01 3.65E+01 3.66E+01
3.67E+01 3.67E+01 3.67E+01 3.67E+01 3.69E+01 3.71E+01 3.71E+01 3.71E+01 3.73E+01 3.73E+01
3.73E+01 3.73E+01 3.73E+01 3.75E+01 3.75E+01 3.78E+01 3.78E+01 3.78E+01 3.78E+01 3.78E+01
3.81E+01 3.81E+01 3.83E+01 3.84E+01 3.84E+01 3.87E+01 3.87E+01 3.87E+01 3.89E+01 3.89E+01
3.89E+01 3.90E+01 3.90E+01 3.90E+01 3.90E+01 3.93E+01 3.95E+01 3.95E+01 3.95E+01 3.95E+01
3.96E+01 3.97E+01 3.99E+01 4.00E+01 4.00E+01 4.01E+01 4.01E+01 4.04E+01 4.06E+01 4.06E+01
4.07E+01 4.07E+01 4.08E+01 4.08E+01 4.08E+01 4.08E+01 4.11E+01 4.12E+01 4.12E+01 4.12E+01
4.12E+01 4.12E+01 4.13E+01 4.14E+01 4.14E+01 4.15E+01 4.15E+01 4.17E+01 4.17E+01 4.19E+01
4.20E+01 4.20E+01 4.20E+01 4.21E+01 4.21E+01 4.23E+01 4.23E+01 4.23E+01 4.26E+01 4.27E+01
4.29E+01 4.29E+01 4.29E+01 4.32E+01 4.32E+01 4.33E+01 4.33E+01 4.34E+01 4.35E+01 4.35E+01
4.35E+01 4.37E+01 4.37E+01 4.37E+01 4.37E+01 4.37E+01 4.38E+01 4.38E+01 4.38E+01 4.42E+01
4.42E+01 4.42E+01 4.43E+01 4.43E+01 4.46E+01 4.47E+01 4.47E+01 4.48E+01 4.48E+01 4.49E+01
4.52E+01 4.52E+01 4.54E+01 4.54E+01 4.54E+01 4.54E+01 4.58E+01 4.59E+01 4.59E+01 4.59E+01
4.61E+01 4.61E+01 4.61E+01 4.62E+01 4.62E+01 4.62E+01 4.64E+01 4.64E+01 4.64E+01 4.64E+01
4.65E+01 4.66E+01 4.67E+01 4.67E+01 4.67E+01 4.67E+01 4.67E+01 4.67E+01 4.68E+01 4.68E+01
4.68E+01 4.68E+01 4.70E+01 4.70E+01 4.70E+01 4.74E+01 4.74E+01 4.74E+01 4.74E+01 4.74E+01
4.75E+01 4.77E+01 4.77E+01 4.79E+01 4.79E+01 4.79E+01 4.79E+01 4.79E+01 4.81E+01 4.81E+01
4.81E+01 4.81E+01 4.82E+01 4.85E+01 4.85E+01 4.85E+01 4.86E+01 4.87E+01 4.87E+01 4.87E+01
4.88E+01 4.88E+01 4.88E+01 4.89E+01 4.89E+01 4.89E+01 4.90E+01 4.90E+01 4.91E+01 4.91E+01

4.92E+01 4.92E+01 4.93E+01 4.93E+01 4.93E+01 4.93E+01 4.96E+01 4.96E+01 4.97E+01 4.97E+01
4.98E+01 4.98E+01 5.01E+01 5.01E+01 5.01E+01 5.02E+01 5.02E+01 5.03E+01 5.03E+01 5.05E+01
5.05E+01 5.06E+01 5.06E+01 5.06E+01 5.07E+01 5.09E+01 5.09E+01 5.10E+01 5.11E+01 5.11E+01
5.12E+01 5.12E+01 5.14E+01 5.14E+01 5.15E+01 5.15E+01 5.16E+01 5.16E+01 5.16E+01 5.16E+01
5.17E+01 5.18E+01 5.18E+01 5.19E+01 5.19E+01 5.20E+01 5.20E+01 5.20E+01 5.21E+01 5.21E+01
5.21E+01 5.23E+01 5.23E+01 5.24E+01 5.24E+01 5.24E+01 5.27E+01 5.27E+01 5.28E+01 5.29E+01
5.30E+01 5.30E+01 5.30E+01 5.32E+01 5.32E+01 5.32E+01 5.33E+01 5.33E+01 5.36E+01 5.36E+01
5.36E+01 5.38E+01 5.39E+01 5.39E+01 5.39E+01 5.41E+01 5.41E+01 5.44E+01 5.44E+01 5.44E+01
5.45E+01 5.45E+01 5.47E+01 5.47E+01 5.48E+01 5.49E+01 5.49E+01 5.50E+01 5.50E+01 5.50E+01
5.50E+01 5.51E+01 5.51E+01 5.51E+01 5.52E+01 5.52E+01 5.54E+01 5.54E+01 5.55E+01 5.56E+01
5.56E+01 5.57E+01 5.57E+01 5.57E+01 5.57E+01 5.57E+01 5.58E+01 5.58E+01 5.59E+01 5.59E+01
5.60E+01 5.60E+01 5.60E+01 5.60E+01 5.61E+01 5.61E+01 5.62E+01 5.62E+01 5.62E+01 5.68E+01
5.69E+01 5.69E+01 5.70E+01 5.70E+01 5.72E+01 5.72E+01 5.73E+01 5.73E+01 5.74E+01 5.74E+01
5.75E+01 5.75E+01 5.75E+01 5.75E+01 5.75E+01 5.75E+01 5.76E+01 5.77E+01 5.77E+01 5.78E+01
5.78E+01 5.78E+01 5.79E+01 5.79E+01 5.79E+01 5.79E+01 5.80E+01 5.83E+01 5.83E+01 5.84E+01
5.84E+01 5.84E+01 5.85E+01 5.86E+01 5.86E+01 5.86E+01 5.86E+01 5.91E+01 5.92E+01 5.92E+01
5.93E+01 5.93E+01 5.96E+01 5.96E+01 5.97E+01 5.97E+01 5.97E+01 5.98E+01 5.99E+01 5.99E+01
6.00E+01 6.00E+01 6.02E+01 6.02E+01 6.07E+01 6.08E+01 6.11E+01 6.11E+01 6.14E+01 6.14E+01
6.16E+01 6.16E+01 6.17E+01 6.17E+01 6.17E+01 6.19E+01 6.22E+01 6.27E+01 6.27E+01 6.27E+01
6.28E+01 6.28E+01 6.30E+01 6.32E+01 6.32E+01 6.35E+01 6.35E+01 6.35E+01 6.36E+01 6.36E+01
6.39E+01 6.43E+01 6.43E+01 6.43E+01 6.43E+01 6.44E+01 6.46E+01 6.46E+01 6.47E+01 6.48E+01
6.48E+01 6.49E+01 6.49E+01 6.51E+01 6.54E+01 6.54E+01 6.54E+01 6.54E+01 6.55E+01 6.56E+01
6.56E+01 6.56E+01 6.56E+01 6.56E+01 6.57E+01 6.58E+01 6.59E+01 6.60E+01 6.60E+01 6.60E+01
6.61E+01 6.61E+01 6.61E+01 6.63E+01 6.63E+01 6.66E+01 6.67E+01 6.69E+01 6.70E+01 6.70E+01
6.77E+01 6.77E+01 6.78E+01 6.78E+01 6.81E+01 6.81E+01 6.85E+01 6.87E+01 6.87E+01 6.93E+01
6.96E+01 6.97E+01 6.97E+01 6.97E+01 7.00E+01 7.01E+01 7.01E+01 7.02E+01 7.02E+01 7.02E+01
7.03E+01 7.03E+01 7.04E+01 7.04E+01 7.05E+01 7.06E+01 7.09E+01 7.09E+01 7.09E+01 7.09E+01
7.10E+01 7.11E+01 7.13E+01 7.13E+01 7.16E+01 7.19E+01 7.24E+01 7.25E+01 7.25E+01 7.26E+01
7.28E+01 7.29E+01 7.29E+01 7.29E+01 7.30E+01 7.31E+01 7.31E+01 7.31E+01 7.34E+01 7.38E+01
7.43E+01 7.46E+01 7.46E+01 7.51E+01 7.52E+01 7.52E+01 7.58E+01 7.58E+01 7.60E+01 7.67E+01
7.72E+01 7.72E+01 7.75E+01 7.75E+01 7.78E+01 7.79E+01 7.79E+01 7.79E+01 7.82E+01 7.84E+01
7.85E+01 7.87E+01 7.87E+01 7.89E+01 7.89E+01 7.92E+01 7.93E+01 7.97E+01 7.98E+01 7.99E+01
7.99E+01 8.00E+01 8.03E+01 8.03E+01 8.05E+01 8.05E+01 8.06E+01 8.08E+01 8.08E+01 8.08E+01

8.12E+01 8.12E+01 8.17E+01 8.20E+01 8.21E+01 8.21E+01 8.23E+01 8.31E+01 8.31E+01 8.31E+01
8.37E+01 8.37E+01 8.37E+01 8.39E+01 8.40E+01 8.44E+01 8.44E+01 8.46E+01 8.46E+01 8.46E+01
8.50E+01 8.50E+01 8.52E+01 8.52E+01 8.52E+01 8.60E+01 8.60E+01 8.66E+01 8.66E+01 8.69E+01
8.69E+01 8.71E+01 8.73E+01 8.76E+01 8.83E+01 8.83E+01 8.90E+01 8.94E+01 8.94E+01 9.03E+01
9.05E+01 9.05E+01 9.06E+01 9.06E+01 9.08E+01 9.12E+01 9.24E+01 9.24E+01 9.24E+01 9.25E+01
9.26E+01 9.28E+01 9.28E+01 9.29E+01 9.30E+01 9.31E+01 9.31E+01 9.43E+01 9.44E+01 9.44E+01
9.47E+01 9.51E+01 9.53E+01 9.53E+01 9.56E+01 9.61E+01 9.68E+01 9.68E+01 9.74E+01 9.77E+01
9.77E+01 9.78E+01 9.80E+01 9.81E+01 9.81E+01 9.90E+01 9.95E+01 1.00E+02 1.00E+02 1.03E+02
1.03E+02 1.03E+02 1.03E+02 1.03E+02 1.03E+02 1.03E+02 1.04E+02 1.06E+02 1.07E+02 1.07E+02
1.09E+02 1.10E+02 1.10E+02 1.14E+02 1.14E+02 1.16E+02 1.17E+02 1.17E+02 1.25E+02 1.26E+02
1.96E+02 1.96E+02 2.08E+02 2.10E+02 2.11E+02 2.12E+02 2.12E+02 2.12E+02 2.13E+02 2.13E+02
2.13E+02 2.13E+02 2.15E+02 2.15E+02 2.15E+02 2.16E+02 2.16E+02 2.17E+02 2.17E+02 2.17E+02
2.18E+02 2.18E+02 2.18E+02 2.19E+02 2.19E+02 2.19E+02 2.20E+02 2.20E+02 2.20E+02 2.21E+02
2.21E+02 2.21E+02 2.21E+02 2.22E+02 2.22E+02 2.22E+02 2.24E+02 2.25E+02 2.25E+02 2.25E+02
2.26E+02 2.26E+02 2.27E+02 2.27E+02 2.27E+02 2.27E+02 2.28E+02 2.28E+02 2.29E+02 2.29E+02
2.29E+02 2.32E+02 2.32E+02 2.33E+02 2.33E+02 2.34E+02 2.35E+02 2.35E+02 2.35E+02 2.35E+02
2.37E+02 2.37E+02 2.37E+02 2.38E+02 2.39E+02 2.40E+02 2.40E+02 2.42E+02 2.42E+02 2.42E+02
2.43E+02 2.45E+02 2.45E+02 2.45E+02 2.45E+02 2.46E+02 2.46E+02 2.46E+02 2.46E+02 2.46E+02
2.48E+02 2.48E+02 2.48E+02 2.49E+02 2.50E+02 2.51E+02 2.53E+02 2.55E+02 2.55E+02 2.56E+02
2.56E+02 2.56E+02 2.56E+02 2.56E+02 2.57E+02 2.58E+02 2.58E+02 2.58E+02 2.58E+02 2.60E+02
2.60E+02 2.61E+02 2.62E+02 2.62E+02 2.62E+02 2.63E+02 2.64E+02 2.65E+02 2.65E+02 2.66E+02
2.66E+02 2.66E+02 2.67E+02 2.68E+02 2.69E+02 2.70E+02 2.73E+02 2.73E+02 2.74E+02 2.74E+02
2.76E+02 2.76E+02 2.80E+02 2.80E+02 2.81E+02 2.82E+02 2.87E+02 2.87E+02 2.89E+02 2.89E+02
2.89E+02 2.89E+02 2.90E+02 2.90E+02 2.95E+02 2.95E+02 2.96E+02 3.01E+02 3.01E+02 3.09E+02
3.10E+02 3.15E+02 3.15E+02 3.20E+02 3.23E+02 3.27E+02 3.27E+02 3.28E+02 3.28E+02 3.33E+02
3.33E+02 3.33E+02 3.36E+02 3.37E+02 3.45E+02 3.45E+02 3.50E+02 3.51E+02 3.52E+02 3.52E+02
3.61E+02 3.61E+02 3.62E+02 3.62E+02 3.66E+02 3.66E+02 3.66E+02 3.66E+02 3.70E+02 3.70E+02
3.78E+02 3.78E+02 3.83E+02 3.83E+02 3.94E+02 3.98E+02 3.98E+02 4.26E+02 4.26E+02 4.50E+02
time period= 1.00000000000000

output_response.dat

one-dimer primary no.	z-coord	model e-field	fields: h-field			
2	1.00E+02	8.07E-01	-1.70E-01	1.46E+02	-2.84E+02	
3	3.50E+02	3.83E-01	-3.18E-01	3.15E+01	-2.06E+02	
4	6.00E+02	1.16E-01	-2.76E-01	-3.56E+01	-1.01E+02	
5	8.50E+02	-1.48E-02	-1.77E-01	-4.83E+01	-4.41E+01	
6	1.10E+03	-5.81E-02	-8.56E-02	-3.93E+01	-5.45E+00	
7	1.50E+03	-3.95E-02	1.26E-03	-3.39E+01	7.24E+00	

number of cells in x-direction: nx= 10
 number of cells in y-direction: ny= 10
 number of cells in z-direction: nz= 7
 reduced matrix size= 1260
 number of desired eigenmodes: kevm= 1260
 mode_type e= 1 1

**** VALUES AT THE SURFACE ****

** output with x/y varying along row/col **

* Re(Ex) :	*											
x-node nos.:		1	2	3	4	5	6	7	8	9	10	
x-coord values:		5.00E+02	1.25E+03	1.75E+03	2.12E+03	2.38E+03	2.62E+03	2.88E+03	3.25E+03	3.75E+03	4.50E+03	
iy y-coordRe(Ex)-values....											
1	1.00E+03	9.94E-01	9.90E-01	9.93E-01	9.93E-01	9.94E-01	9.94E-01	9.93E-01	9.93E-01	9.89E-01	9.94E-01	
2	1.50E+03	9.91E-01	9.88E-01	9.86E-01	9.85E-01	9.85E-01	9.85E-01	9.85E-01	9.86E-01	9.87E-01	9.90E-01	
3	2.00E+03	9.88E-01	9.82E-01	9.77E-01	9.65E-01	9.71E-01	9.71E-01	9.64E-01	9.77E-01	9.82E-01	9.88E-01	
4	2.25E+03	9.87E-01	9.81E-01	9.69E-01	9.36E-01	9.69E-01	9.69E-01	9.36E-01	9.69E-01	9.81E-01	9.87E-01	
5	2.50E+03	9.87E-01	9.82E-01	9.66E-01	9.27E-01	9.60E-01	9.60E-01	9.27E-01	9.66E-01	9.82E-01	9.87E-01	
6	2.75E+03	9.87E-01	9.81E-01	9.69E-01	9.36E-01	9.69E-01	9.69E-01	9.36E-01	9.69E-01	9.81E-01	9.87E-01	
7	3.00E+03	9.88E-01	9.82E-01	9.77E-01	9.64E-01	9.71E-01	9.71E-01	9.65E-01	9.77E-01	9.82E-01	9.88E-01	
8	3.50E+03	9.90E-01	9.87E-01	9.86E-01	9.85E-01	9.85E-01	9.85E-01	9.85E-01	9.86E-01	9.88E-01	9.91E-01	
9	4.00E+03	9.94E-01	9.89E-01	9.93E-01	9.93E-01	9.94E-01	9.94E-01	9.93E-01	9.93E-01	9.91E-01	9.94E-01	

* Im(Ex) :	*											
x-node nos.:		1	2	3	4	5	6	7	8	9	10	

8	3.75E+03	-2.37E+02	-2.35E+02	-2.36E+02	-2.36E+02	-2.35E+02	-2.35E+02	-2.36E+02	-2.36E+02	-2.35E+02	-2.37E+02
9	4.50E+03	-2.36E+02	-2.35E+02	-2.36E+02	-2.35E+02	-2.36E+02	-2.36E+02	-2.35E+02	-2.36E+02	-2.35E+02	-2.36E+02

```

*      Re(Zxy)  :      *
x-node  nos.:      1      2      3      4      5      6      7      8      9      10
x-coord values:      5.00E+02  1.25E+03  1.75E+03  2.12E+03  2.38E+03  2.62E+03  2.88E+03  3.25E+03  3.75E+03  4.50E+03
iy      y-coord  ....Re(Zxy)-values....
1  1.00E+03      2.07E-03  2.09E-03  2.09E-03  2.10E-03  2.10E-03  2.10E-03  2.10E-03  2.09E-03  2.10E-03  2.07E-03
2  1.50E+03      2.07E-03  2.08E-03  2.07E-03  2.07E-03  2.08E-03  2.08E-03  2.07E-03  2.07E-03  2.08E-03  2.07E-03
3  2.00E+03      2.08E-03  2.04E-03  2.01E-03  2.04E-03  2.11E-03  2.11E-03  2.04E-03  2.01E-03  2.04E-03  2.08E-03
4  2.25E+03      2.08E-03  2.04E-03  1.98E-03  1.90E-03  2.23E-03  2.24E-03  1.90E-03  1.98E-03  2.04E-03  2.08E-03
5  2.50E+03      2.08E-03  2.04E-03  1.97E-03  1.82E-03  2.26E-03  2.26E-03  1.82E-03  1.97E-03  2.04E-03  2.08E-03
6  2.75E+03      2.08E-03  2.04E-03  1.98E-03  1.90E-03  2.24E-03  2.23E-03  1.90E-03  1.98E-03  2.04E-03  2.08E-03
7  3.00E+03      2.08E-03  2.04E-03  2.01E-03  2.04E-03  2.11E-03  2.11E-03  2.04E-03  2.01E-03  2.04E-03  2.08E-03
8  3.50E+03      2.07E-03  2.08E-03  2.07E-03  2.07E-03  2.08E-03  2.08E-03  2.07E-03  2.07E-03  2.08E-03  2.07E-03
9  4.00E+03      2.07E-03  2.10E-03  2.09E-03  2.10E-03  2.10E-03  2.10E-03  2.10E-03  2.09E-03  2.09E-03  2.07E-03

```

```

*      Im(Zxy)  :      *
x-node  nos.:      1      2      3      4      5      6      7      8      9      10
x-coord values:      5.00E+02  1.25E+03  1.75E+03  2.12E+03  2.38E+03  2.62E+03  2.88E+03  3.25E+03  3.75E+03  4.50E+03
iy      y-coord  ....Im(Zxy)-values....
1  1.00E+03      1.86E-03  1.83E-03  1.83E-03  1.83E-03  1.84E-03  1.84E-03  1.83E-03  1.83E-03  1.82E-03  1.86E-03
2  1.50E+03      1.83E-03  1.83E-03  1.83E-03  1.82E-03  1.82E-03  1.82E-03  1.83E-03  1.83E-03  1.83E-03  1.83E-03
3  2.00E+03      1.82E-03  1.80E-03  1.82E-03  1.78E-03  1.79E-03  1.79E-03  1.78E-03  1.82E-03  1.80E-03  1.82E-03
4  2.25E+03      1.81E-03  1.81E-03  1.80E-03  1.61E-03  1.52E-03  1.52E-03  1.61E-03  1.80E-03  1.81E-03  1.81E-03
5  2.50E+03      1.81E-03  1.84E-03  1.79E-03  1.59E-03  1.44E-03  1.44E-03  1.59E-03  1.79E-03  1.84E-03  1.81E-03
6  2.75E+03      1.81E-03  1.81E-03  1.80E-03  1.61E-03  1.52E-03  1.52E-03  1.61E-03  1.80E-03  1.81E-03  1.81E-03
7  3.00E+03      1.82E-03  1.80E-03  1.82E-03  1.78E-03  1.79E-03  1.79E-03  1.78E-03  1.82E-03  1.80E-03  1.82E-03
8  3.50E+03      1.83E-03  1.83E-03  1.83E-03  1.83E-03  1.82E-03  1.82E-03  1.82E-03  1.83E-03  1.83E-03  1.83E-03
9  4.00E+03      1.86E-03  1.82E-03  1.83E-03  1.83E-03  1.84E-03  1.84E-03  1.83E-03  1.83E-03  1.83E-03  1.86E-03

```

```

*      (RHOxy)  :      *
x-node  nos.:      1      2      3      4      5      6      7      8      9      10
x-coord values:      5.00E+02  1.25E+03  1.75E+03  2.12E+03  2.38E+03  2.62E+03  2.88E+03  3.25E+03  3.75E+03  4.50E+03
iy      y-coord  ....(RHOxy)-values....
1  1.00E+03      9.83E-01  9.78E-01  9.79E-01  9.82E-01  9.86E-01  9.86E-01  9.82E-01  9.78E-01  9.76E-01  9.81E-01
2  1.50E+03      9.68E-01  9.73E-01  9.64E-01  9.66E-01  9.67E-01  9.67E-01  9.65E-01  9.64E-01  9.71E-01  9.67E-01

```

3	2.00E+03	9.65E-01	9.41E-01	9.34E-01	9.31E-01	9.70E-01	9.70E-01	9.31E-01	9.34E-01	9.41E-01	9.64E-01
4	2.25E+03	9.62E-01	9.40E-01	9.05E-01	7.87E-01	9.26E-01	9.24E-01	7.87E-01	9.05E-01	9.41E-01	9.62E-01
5	2.50E+03	9.62E-01	9.54E-01	9.00E-01	7.42E-01	9.07E-01	9.07E-01	7.42E-01	9.00E-01	9.54E-01	9.62E-01
6	2.75E+03	9.62E-01	9.41E-01	9.05E-01	7.87E-01	9.24E-01	9.26E-01	7.87E-01	9.05E-01	9.40E-01	9.62E-01
7	3.00E+03	9.64E-01	9.41E-01	9.34E-01	9.31E-01	9.70E-01	9.70E-01	9.31E-01	9.34E-01	9.41E-01	9.65E-01
8	3.50E+03	9.67E-01	9.71E-01	9.64E-01	9.65E-01	9.67E-01	9.67E-01	9.66E-01	9.64E-01	9.73E-01	9.68E-01
9	4.00E+03	9.81E-01	9.76E-01	9.78E-01	9.82E-01	9.86E-01	9.86E-01	9.82E-01	9.79E-01	9.78E-01	9.83E-01

* PHASExy : *

x-node nos.:	1	2	3	4	5	6	7	8	9	10	
x-coord values:	5.00E+02	1.25E+03	1.75E+03	2.12E+03	2.38E+03	2.62E+03	2.88E+03	3.25E+03	3.75E+03	4.50E+03	
iy y-coordPHASExy-values....										
1	1.00E+03	4.19E+01	4.11E+01	4.11E+01	4.10E+01	4.13E+01	4.13E+01	4.11E+01	4.12E+01	4.10E+01	4.19E+01
2	1.50E+03	4.15E+01	4.14E+01	4.15E+01	4.13E+01	4.11E+01	4.12E+01	4.14E+01	4.15E+01	4.14E+01	4.16E+01
3	2.00E+03	4.12E+01	4.14E+01	4.21E+01	4.11E+01	4.02E+01	4.02E+01	4.11E+01	4.22E+01	4.14E+01	4.12E+01
4	2.25E+03	4.10E+01	4.16E+01	4.22E+01	4.03E+01	3.43E+01	3.41E+01	4.03E+01	4.22E+01	4.17E+01	4.10E+01
5	2.50E+03	4.10E+01	4.20E+01	4.23E+01	4.12E+01	3.25E+01	3.25E+01	4.12E+01	4.23E+01	4.20E+01	4.10E+01
6	2.75E+03	4.10E+01	4.17E+01	4.22E+01	4.03E+01	3.41E+01	3.43E+01	4.03E+01	4.22E+01	4.16E+01	4.10E+01
7	3.00E+03	4.12E+01	4.14E+01	4.22E+01	4.11E+01	4.02E+01	4.02E+01	4.11E+01	4.21E+01	4.14E+01	4.12E+01
8	3.50E+03	4.16E+01	4.14E+01	4.15E+01	4.14E+01	4.12E+01	4.11E+01	4.13E+01	4.15E+01	4.14E+01	4.15E+01
9	4.00E+03	4.19E+01	4.10E+01	4.12E+01	4.11E+01	4.13E+01	4.13E+01	4.10E+01	4.11E+01	4.11E+01	4.19E+01

Output_time.dat

date time_mainstart=
20090823

105149.921

date and time start_eigenstep1=
20090823

105149.984

date and time end_eigenstep1=
20090823

105302.953

date and time start_eigenstep2=
20090823

105302.953

date and time end_eigenstep2=
20090823

105302.953

date and time start_dlahqr=
20090823

105303.015

date and time end_dlahqr=
20090823

105319.015

date time_mainend=
20090823

105409.328

REFERENCES

- Abdul Azeez, K. K., and Harinarayana, T., 2007. Magnetotelluric evidence of potential geothermal resource in Puga, Ladakh, NW Himalaya. *Current Sci.*, **93**, 323-329.
- Adam, A., 1997. Magnetotelluric phase anisotropy above extensional structures of the Neogene Pannonian Basin. *J. Geomag. Geoelec.*, **49**, 1549-1557.
- Arnoldi, W. E., 1951. The principle of minimized iteration in the solution of the matrix eigenproblem. *Quart. Appl. Math.*, **9**, 17-29.
- Asaue, H., Koike, K., Yoshinaga, T., and Takakura, S., 2006. Magnetotelluric resistivity modeling for 3D characterization of geothermal reservoirs in the Western side of Mt. Aso, SW Japan. *J. App. Geophys.*, **18**, 296-312.
- Avdeev, D. B., 2005. Three-dimensional electromagnetic modelling and inversion from theory to application. *Sur. Geophys.*, **26**, 767-799.
- Backus, G. E., and Gilbert, J. E., 1970. Uniqueness in the inversion of inaccurate gross earth data. *Phil. Trans. Roy. Soc. London*, **266**, 123-192.
- Baglama, J., Calvetti, D., and Reichel, L., 1996. Iterative methods for the computation of a few eigenvalues of a large symmetric matrix. *BIT*, **36**, 400-421.
- Baglama, J., Calvetti, D., and Reichel, L., 1998. Fast leja points. *Elect. Trans. Num. Anal.*, **7**, 124-140.
- Barrett, R., Berry, M., Chan, T. F., Demmel, J., Donato, J., Dongarra, J., Eijkhout, V., Pozo, R., Romine, C., and van der Vorst, H., 1994. *Templates for the solution of linear systems: building blocks for iterative methods*. Society for industrial and applied mathematics, Philadelphia, PA.

- Beattie, C. A., Embree, M., and Sorensen, D. C., 2005. Convergence of polynomial restart krylov methods for eigenvalue computations. *SIAM review*, **47**, 492-515.
- Berdichevsky, M. N., and Zhdanov, M. S., 1984. *Advanced theory of deep geomagnetic sounding*. Elsevier, Amsterdam, pp. 408.
- Bhattacharya, B. B., and Sen, M. K., 1981. Depth of investigation of collinear electrode arrays over homogeneous, anisotropic half-space in direct current method. *Geophys.*, **46**, 768-780.
- Bhattacharya, B. B., Mukherjee, D. S., and Chatterjee, D., 1983. Enhancement of EM anomaly: A circuit theory approach. *Geophys.*, **48**, 1248-1251.
- Blome, M., Maurer, H. R., and Schmidt, K., 2009. Advances in three-dimensional geoelectric forward solver techniques. *Geophys. J. Int.*, **176**, 740-752.
- Born, M., and Wolf, E., 2005. *Principles of optics*, 7th edition. Cambridge University Press, UK, pp. 952.
- Brewitt-Taylor, C. R., and Weaver, J. T., 1976. On the finite difference solution of two-dimensional induction problems. *Geophys. J. R. Astr. Soc.*, **47**, 375-396.
- Brezinski, C., Redivo-Zaglia, M., and Sadok, H., 2001. The matrix and polynomial approaches to Lanczos-type algorithms. *J. Comp. Appl. Math.*, **123**, 241-260.
- Cagniard, L., 1953. Basic theory of the magnetotelluric method of geophysical prospecting. *Geophys.*, **18**, 605-635.
- Calvetti, D., Reichel, L., and Sorensen, D. C., 1994. An implicitly restarted Lanczos method for large symmetric eigenvalue problems. *Elect. Trans. Num. Anal.*, **2**, 1-21.

- Cantwell, T., 1960. Detection and analysis of low frequency magnetotelluric signal. Ph.D. Thesis, Dept. of Geol. and Geophys., M. L. T., Cambridge, Mass.
- Cerv, V., and Pek, J., 1990. Modeling and analysis of electromagnetic fields in 3D inhomogeneous media. *Sur. Geophys.*, **11**, 205-229.
- Cerv, V., Menvielle, M., and Pek, J., 2007. Stochastic interpretation of magnetotelluric data, comparison of methods. *Ann. Geophys.*, **50**, 7-19.
- Changsheng, L., Zhengyong, R., Jingtian, T., and Yan, Y., 2008. Three-dimensional magnetotellurics modeling using edge based finite-element unstructured meshes. *App. Geophys.*, **5**, 170-180.
- Chen, C., C., Chen, C., Chiang, C., Shu, H., Chiu, W., Unsworth, M. J., and Bertrand, E., 2007. Crustal resistivity anomalies beneath Central Taiwan imaged by a broadband magnetotelluric transect. *Terr. Atmos. Ocean. Sci.*, **18**, 19-30.
- Chen, L., Booker, J. R., Jones, A. G., Wu, N., Unsworth, M. J., Wenbo, W., and Tan, H., 1996. Electrically conductive crust in southern Tibet from INDEPTH magnetotelluric surveying. *Sci.*, **274**, 1694-1696.
- Chen, P., Hou, Z., and Fan, G., 1998. Three-dimensional topographic responses in MT using finite difference method. *Acta Seis. Sinica*, **11**, 631-635.
- Coggon, J. H., 1971. Electromagnetic and electrical modeling by the finite element method. *Geophys.*, **36**, 132-155.
- Commer, M., and Newman, G. A., 2008. New advances in three-dimensional controlled-source electromagnetic inversion. *Geophys. J. Int.*, **172**, 513-535.
- Constable, S., and Cox, C. S., 1996. Marine controlled source electromagnetic sounding. The PEGASUS experiment. *J. Geophys. Res.*, **101**, 5519-5530.

- Constable, S., and Srnka, L. J., 2007. An introduction to marine controlled-source electromagnetic methods for hydrocarbon exploration. *Geophys.*, **72**, WA3-WA12.
- Constable, S., and Weiss, C. J., 2006. Mapping thin resistors and hydrocarbons with marine EM methods: Insights from 1D modeling. *Geophys.*, **71**, G43-G51.
- Constable, S., Orange, A., Hoversten, G. M., and Morrison, H. F., 1998. Marine magnetotellurics for petroleum exploration. A seafloor instrument system. *Geophys.*, **63**, 816-825.
- Cox, C. S., 1981. On the electrical conductivity of the oceanic lithosphere. *Phys. Earth Planet. Int.*, **25**, 196-201.
- Cox, C. S., Filloux, J. H., Gough, D. I., Larson, J. C., Poehls, K. A., Von Herzen, R. P., and Winter, R., 1980. Atlantic lithosphere sounding. *J. Geomag. Geoelec.*, **32**, Suppl. I, SI 13– SI 32.
- Cullum, J. K., and Willoughby, R. A., 1985. Lanczos algorithms for large symmetric eigenvalue computations; Vol. I, Theory. Birkhauser, Printed in Germany, pp. 268.
- Cullum, J. K., and Willoughby, R. A., 1985. Lanczos algorithms for large symmetric eigenvalue computations; Vol. II, Programs. Birkhauser, Printed in Germany, pp. 496.
- Daniel, J., Gragg, W. B., Kaufman, L., and Stewart, G. W., 1976. Reorthogonalization and stable algorithms for updating the Gram-Schmidt QR factorization. *Math. Comp.*, **30**, 772-795.
- Das, U. C., and Verma, S. K., 1981. Numerical considerations on computing the EM response of three dimensional inhomogeneities in a layered earth. *Geophys. J. R. Astr. Soc.*, **66**, 733-740.

- Das, U. C., and Verma, S. K., 1982. Electromagnetic response of an arbitrary strapped three dimensional conductor in a layered earth - numerical results. *Geophys. J. R. Astr. Soc.*, **68**, 55-66.
- deGroot-Hedlin, C., and Constable, S., 1990. Occam's inversion to generate models form magnetotelluric data. *Geophys.*, **55**, 1613-1624.
- deGroot-Hedlin, C., and Constable, S., 2004. Inversion of magnetotelluric data for 2D structure with sharp resistivity contrast. *Geophys.*, **69**, 78-86.
- de Lima, O. A. L., Sato, H. K., and Porsani, M. J., 1995. Imaging industrial contaminant plumes with resistivity techniques. *J. App. Geophys.*, **34**, 93-108.
- Dmitriev, V. I., and Berdichevsky, M. N., 1979. Fundamental model of magnetotelluric sounding. *Proc. IEEE*, **67**, 1034-1043.
- Druskin, V., and Knizhnerman, L., 1994. Spectral approach to solving three-dimensional diffusion Maxwell's equations in the time and frequency domains. *Radio Sci.*, **29**, 937-953.
- Druskin, V. L., Knizhnerman, L. A., and Lee, P., 1999. New spectral Lanczos decomposition method for induction modeling in arbitrary 3-D geometry. *Geophys.*, **64**, 701-706.
- Duff, I. S., and Scott, J. A., 1993. Computing selected eigenvalues of sparse unsymmetric matrices using subspace iteration. Internal Report, RAL-91-056.
- Eidsmo, T., Ellingsrud, S., MacGregor, L. M., Constable, S., Sinha, M. C., Johanson, S., Kong, F. N., and Westerdahl, H., 2002. Sea Bed Logging (SBL), a new method for remote and direct identification of hydrocarbon filled layers in deepwater areas. *First Break*, **20**, 144-152.

- Ellingsrud, S., Eidsmo, T., Johansen, S., Sinha, M. C., MacGregor, L. M., and Constable, S., 2002. Remote sensing of hydrocarbon layers by seabed logging (SBL): Results from a cruise offshore Angola. *The Leading Edge*, **21**, 972-982.
- Emad, N., Petiton, S., and Edjlali, G., 2005. Multiple explicitly restarted Arnoldi method for solving large eigenproblems. *SIAM J. Sci. Comp.*, **27**, 253-277.
- Ericsson, T., and Ruhe, A., 1980. The spectral transformation Lanczos method for the numerical solution of large sparse generalized symmetric eigenvalue problems. *Math. Comp.*, **35**, 1251-1268.
- Farquharson, C. G., and Oldenburg, D. W., 2002. Three-dimensional forward- modeling and inversion algorithms for magnetotelluric data. 16th workshop on electromagnetic induction on the earth, June 16-22, College of Santa Fe, Santa Fe, New Mexico, USA.
- Fomenko, E. Y., and Mogi, T., 2002. A new computation method for a staggered grid of 3D EM field conservative modeling. *Earth Planets Space*, **54**, 499-509.
- Forsythe, G. E. and Wasow, W. A., 1964. Finite difference method for partial differential equations. Wiley, New York, pp. 444.
- Fox, L., and Ingerov, O., 2007. Natural source EM for offshore hydrocarbon detection offers potential cost savings. *First Break*, **25**, 87-96.
- Giraud, L., Langou, J., and Rozloznik, M., 2003. On the loss of orthogonality in the Gram-Schmidt orthogonalization process. CERFACS Technical Report No. TR/PA/03/25. URL http://www.cerfacs.fr/algorithm/reports/2003/TR_PA_03_25.pdf.
- Golub, G. H., and VanLoan, C. F., 1983. Matrix computations. The John Hopkins University Press, Baltimore, Maryland.

- Grant, F. S., and West, G. F., 1965. Interpretation theory in applied geophysics. McGraw-Hill Book Company, New York, pp. 584.
- Groom, R. W., and Bailey, R. C., 1989. Decomposition of magnetotelluric impedance tensors in the presence of local three-dimensional galvanic distortion. *J. Geophys. Res.*, **94**, 1913-1925.
- Gupta, P. K., Bennett, L. A., and Raiche, A. P., 1987. Hybrid calculation of the three-dimensional electromagnetic response of buried conductors. *Geophys.*, **52**, 301-306.
- Gupta, P. K., Niwas, S., and Gaur, V. K., 1996. Straightforward inversion scheme (SIS) for one-dimensional magnetotelluric data. *J. Earth Sys. Sci.*, **105**, 413-429.
- Gupta, P. K., Niwas, S., and Gaur, V. K., 1997. Straightforward inversion of vertical electrical sounding data. *Geophys.*, **62**, 775-785.
- Harinarayana, T., Murthy, D. N., Eknath Rao, S. P., Manoj, C., Veeraswamy, K., Naganjaneyulu, K., Abdul Azeed, K. K., Sastry, R. S., and Virupakshi, G., 2002. Magnetotelluric field investigations in Puga geothermal region, Jammu and Kashmir, India: 1-D modeling results. *Geotherm. Resour. Counc. Trans.*, **26**, 393-397.
- Hernandez, V., Roman, J. E., and Tomas, A., 2007. Evaluation of several variants of explicitly restarted Lanczos eigensolvers and their parallel implementations. *LNCS*, **4395**, 403-416.
- Hetmaniuk, U., and Lehoucq, R. B., 2006. Uniform accuracy of eigenpairs from a shift-invert Lanczos method. *SIAM J. Matrix Anal. Appl.*, **28**, 927-948.
- Hildebrand, F. B., 1974. Introduction to numerical analysis, Tata-McGraw Hill, New Delhi, pp. 669.

- Hochstenbach, M. E., 2003. Subspace methods for eigenvalue problems. Ph. D. Thesis, Department of Information and Computing Sciences, Utrecht University, Netherlands.
- Hohmann, G. W., 1975. Three-dimensional induced polarization and electromagnetic modeling. *Geophys.*, **40**, 309-324.
- Hohmann, G. W., 1983. Three-dimensional EM modeling. *Geophys. Sur.*, **6**, 27-53.
- Hohmann, G. W., and Ting, S. C., 1978, Three-dimensional magnetotelluric modeling: ESL Final Rep. 77-15, DOE contract EY-76-S-07- 1601, July, pp. 48.
- Hoover, D. B., Long, C. L., and Senterfit, R. M., 1978. Some results from audiomagnetotellurics investigations in geothermal areas. *Geophys.*, **43**, 1501-1514.
- Ipsen, I. C. F., and Meyer, C. D., 1998. The idea behind Krylov methods. *Am. Math. Mon.*, **105**, 889-899.
- Israil, M., Tyagi, D. K., Gupta, P. K., and Niwas, S., 2008. Magnetotelluric investigations for imaging electrical structure of Garhwal Himalayan corridor, Uttarakhand, India. *J. Earth. Syst. Sci.*, **117**, 189-200.
- Jackson, J. D., 1975. *Classical electrodynamics*. John Wiley and Sons, New York.
- Jacobs, D. A. H., 1981a. The exploitation of sparsity by iterative methods. In: *Sparse matrices and their uses*, Ian S. Duff (Ed.), Springer-Verlag, 191-221.
- Jacobs, D. A. H., 1981b. Preconditioned conjugate gradient algorithm for solving finite difference system. In: *Sparse matrices and their uses*. Ian S. Duff (Ed.), Springer-Verlag, 509-535.

- Johansen, S. E., Amundsen, H. E. F., Røsten, T., Ellingsrud, S., Eidesmo, T., and Bhuyian, A. H., 2005. Subsurface hydrocarbons detected by electromagnetic sounding. *First Break*, **23**, 31-36.
- Jones, F. W. and Pascoe, L. J., 1971. A general computer program to determine the perturbation of alternating electric currents in a two-dimensional model of a region of uniform conductivity with an embedded inhomogeneity. *Geophys. J. R. Astr. Soc.*, **24**, 3-30.
- Jones, F. W., and Pascoe, L. J., 1972. The perturbation of geomagnetic fields by three-dimensional conductive inhomogeneities. *Geophys. J. R. Astr. Soc.*, **27**, 479-485.
- Jones, F. W., and Vozoff, K., 1978. The calculation of magnetotelluric quantities for three-dimensional conductivity inhomogeneities. *Geophys.*, **43**, 1167-1175.
- Joubert, W., 1992. Lanczos methods for the solution of nonsymmetric system of linear equations. *Siam J. Matrix Anal. Appl.*, **13**, 926-943.
- Kaufman, A. A., and Keller, G. V., 1981. *The magnetotelluric sounding method*. Elsevier, Amsterdam.
- Khattri, K. N., 1992. Local seismic investigations in the Garhwal-Kumaun Himalaya. *Mem. Geol. Soc. India*, **23**, 45-66.
- Kong, F. N., Westerdahl, H., Ellingsrud, S., Eidesmo, T., and Johansen, J., 2002. 'Seabed logging': A possible direct hydrocarbon indicator for deep sea prospects using EM energy. *Oil and Gas Journal*, **100**, 30-38.
- Kumar, R., Ghosh, S. K., Sangode, S. J., and Thakur, V. C., 2002. manifestation of Intra-Foreland thrusting in the Neogene Himalaya foreland basin fill. *J. Geo. Soc. India*, **59**, 547-560.

- Lagios, E., Galanapoulos, D., Hobbs, B. A., Dawes, G. J. K., 2002. Two-dimensional magnetotelluric modeling of the Kos Island geothermal region (Greece). *Tectonophys.*, **287**, 157-172.
- Lanczos, C., 1950. An iterative method for the solution of the eigenvalue problem of linear differential and integral operators. *J. Res. Natl. Bur. Stand.*, **45**, 225-280.
- Langou, M. J., 2003. Iterative methods for solving linear systems with multiple right hand sides. Ph.D. Dissertation, INSA, Toulouse, France.
- Ledo, J., 2005. 2-D verses 3-D magnetotelluric data interpretation. *Sur. Geophys.*, **26**, 511-543.
- Lee, K. H., Pridmore, D. F., and Morrison H. F., 1981. A hybrid three-dimensional electromagnetic modeling scheme. *Geophys.*, **46**, 796-805.
- Lee, T. J., Song, Y., and Uchida, T., 2007. Three-dimensional magnetotelluric surveys for geothermal development in Pohang, Korea. *Expl. Geophys.*, **38**, 89-97.
- Lehoucq, R. B., 1997. Truncated QR algorithms and the solution of large-scale eigenvalue problems. Preprint MCS-P648-0297, Mathematics and Computer Science Division, Argonne National Laboratory, Argonne, Ill.
- Lehoucq, R. B., and Scott, J. A., 1996. An evaluation of Arnoldi based software for sparse nonsymmetric eigenproblems. Internal Report, RAL-TR-96-023.
- Lehoucq, R. B., and Scott, J. A., 1997. Implicitly restarted Arnoldi methods and eigenvalues of the discretized Navier Stokes equations. *SIAM J. Matrix Anal. Appl.*, **23**, 551-562.
- Lehoucq, R. B., and Sorensen, D. C., 1996. Deflation techniques for an implicitly re-started Arnoldi iteration. *SIAM J. matrix Anal. Appl.*, **17**, 789-821.

- Lehoucq, R. B., Sorensen, D. C., and Yang, C., 1997. ARPACK Users' Guide: Solution of Large Scale Eigenvalue Problems with Implicitly Restarted Arnoldi Methods. <http://www.caam.rice.edu/software/ARPACK/UG/ug.html>.
- Livelybrooks, D., 1993. Program 3D feem: a multidimensional electromagnetic finite element model. *Geophys. J. Int.*, **114**, 443-458.
- MacGregor, L., and Sinha, S., 2000. Use of marine controlled-source electromagnetic sounding for sub-basalt exploration. *Geophys. Prosp.*, **48**, 1091-1106.
- MacGregor, L., Sinha, M., and Constable, S., 2001. Electrical resistivity structure of the Valu Fa Ridge, Lau Basin, from marine controlled-source electromagnetic sounding. *Geophys. J. Int.*, **146**, 217-236.
- Mackie, R. L., Madden, T. R., and Wannamaker, P. E., 1993. Three-dimensional magnetotelluric modeling using difference equations- Theory and comparisons to integral equation solutions. *Geophys.*, **58**, 215-226.
- Madden, T. R., and Mackie, R. L., 1989. Three-Dimensional Magnetotelluric Modeling and Inversion. *Proceedings of the IEEE*, **77**, 318-333.
- Manteuffel, T. A., 1978. Adaptive procedure for estimating parameters for the nonsymmetric Tchebyshev iteration. *Numer. Math.*, **31**, 183-208.
- Mauro, D. D., Volpi, G., Manzella, A., Zaja, A., Praticelli, N., Cerv, V., Pek, J., and Santis, A. D., 1999. Magnetotelluric investigations of the seismically active region of Northwest Bohemia: preliminary results. *Ann. Geofis.*, **42**, 39-48.
- McNeice, G. W., and Jones, A. G., 2001. Mutisite, multifrequency tensor decomposition of magnetotelluric data. *Geophys.*, **66**, 158-173.

- Meerbergen, K., Scott, J., 2000. The design of a block rational Lanczos code with partial reorthogonalization and implicit restarting, RAL-TR-2000-011.
- Meerbergen, K., Spence, A., and Roose, D., 1994. Shift-invert and Cayley transforms for detection of rightmost eigenvalues of nonsymmetric matrices. BIT, **34**, 409-423.
- Meurant, G., and Strakos, Z., 2006. The Lanczos and conjugate gradient algorithms in finite precision arithmetic. Acta Num., **15**, 471-542.
- Mitchell, A. R., and Griffiths, D. F., 1980. The finite difference method in partial differential equations. Wiley-Interscience publication, Chichester, Wiley.
- Mitra, R., 1973. Computer techniques for electromagnetics. Pergamon, New York.
- Mitra, R., 1975. Numerical and asymptotic techniques in electromagnetics. Springer-Verlag, New York.
- Mitsuhata, Y., and Uchida, T., 2004, Three-dimensional magnetotelluric modeling using the T- Ω finite element method. Geophys., **69**, 108-119.
- Mogi, T., 1996. Three-dimensional modeling of magnetotelluric data using finite element method. J. App. Geophys., **35**, 185-189.
- Monk, P., and Suli, E., 1994. A convergence analysis of Yee's scheme on nonuniform grids. SIAM J. Num. Anal., **31**, 393-412.
- Morgan, M. A., (Ed.), 1990. Finite element and finite difference methods in electromagnetic scattering. Elsevier, New York.
- Morgan, R. B., 1996. On restarting the Arnoldi method for large nonsymmetric eigenvalue problems. Math. Comp., **65**, 1213-1230.
- Morgan, R. B., and Zeng, M., 2006. A harmonic restarted Arnoldi algorithm for calculating eigenvalues and determining multiplicity. Linear Alg. Appl., **415**, 96-113.

- Morse, P. M., and Feshbach, H., 1953. *Methods of theoretical physics*. McGraw-Hill Book Co., Inc., Tokyo.
- Nabighian, M. N. (Ed.), 1988. *Electromagnetic methods in applied geophysics, Vol. I, Theory*. Soc. Expl. Geophys.
- Nabighian, M. N. (Ed.), 1991. *Electromagnetic methods in applied geophysics, Vol. II, Applications*. Soc. Expl. Geophys.
- Najman, Y., 2006. The detrital record of orogenesis: a review of approaches and techniques used in the Himalayan Sedimentary Basins. *Earth Sci. Rev.*, **74**, 1-72.
- Nam, M. J., Kim, H. J., Song, Y., Lee, T. J., Son, J.-S., and Suh, J. H., 2007. 3D magnetotelluric modelling including surface topography. *Geophys. Pros.*, **55**, 277-287.
- Newman, G. A., and Alumbaugh, D. L., 1997. 3D electromagnetic modeling using staggered finite differences. *IEEE: Geoscience and Remote Sensing*, **2**, 929-932.
- Oldenburg, D. W., 1979. One-dimensional inversion of natural source magnetotelluric observations. *Geophys.*, **44**, 1218-1244.
- Oldenburg, D. W., and Ellis, R. G., 1993. Efficient inversion of magnetotelluric data in two-dimensions. *Phys. Earth Planet. Int.*, **81**, 177-200.
- Paige, C. C., 1970. Practical use of the symmetric Lanczos process with re-orthogonalization. *BIT*, **10**, 183-195.
- Pak, J., 1985. Linearization methods of interpreting magnetotelluric and magnetic variation data. *Travaux Inst. Geophys. Acad. Tchecosl. Sci.*, **609**, 199-326.

- Pandey, R. K., and Bhattacharya, B. B., 1983. Correction factor for determining depth to the basement from H-type magnetotelluric sounding curves. GSI special Publication Series, **2**, 505 – 512.
- Park, J., and Chave, A. D., 1984. On the estimation of magnetotelluric response functions using the singular value decomposition. Geophys. J. R. Astr. Soc., **77**, 683-709.
- Park, S. K. and Torres-Verdin, C., 1988. A Systematic Approach to the Interpretation of Magnetotelluric Data in Volcanic Environments with Applications to the Quest for Magma in Long Valley, California. J. Geophys. Res., **93**, 13265-13283.
- Parker, R. L., 1977. Understanding inverse theory. Annu. Rev. Earth Planet. Sci., **5**, 35-64.
- Parlett, B. N., and Scott, D. S., 1979. The Lanczos algorithm with selective orthogonalization. Math. Comp., **33**, 311-328.
- Patricia, P. D. L., Francesco, L. E., Berthold, K., and Sergio, F., 2002. Magnetotelluric studies of the Caldas Novas geothermal reservoir, Brazil. J. App. Geophys., **49**, 33-46.
- Pedersen, L. B., and Engels, M., 2005. Routine 2D inversion of magnetotelluric data using the determinant of impedance tensor. Geophys., **70**, G33-G41.
- Pellerin, L., Johnston, J. M., and Hohmann, G. W., 1996. A numerical evaluation of electromagnetic methods in geothermal exploration. Geophys., **61**, 121-130.
- Petrick, W. R., 2005. A new passive technique to monitor and discover agricultural groundwater resources. Industrial Imaging Co., Inc., Salt Lake city, UT 84103.
- Porsani, M. J., and Ulrych, T. J., 1989. Discrete convolution by means of forward and backward modeling. IEEE Trans. Acous. Speech and signal Proc., **37**, 1680-1686.
- Porstendorfer, G., 1975. Principles of magnetotelluric prospecting. Borntraeger, Berlin.

- Pous, J., Ledo, J., Marcuello, A., and Daignières, M., 2007. Electrical resistivity model of the crust and upper mantle from a magnetotelluric survey through the central Pyrenees. *Geophys. J. Int.*, **121**, 750-762.
- Press, W. H., Teukolsky, S. A., Vetterling, W. T., and Flannery, B. P., 1993. Numerical recipes in FORTRAN. Second Edition, in arrangement with Cambridge University Press, Foundation Books, Delhi, India.
- Price, A. T., 1962. The theory of magnetotelluric methods when the source field is considered. *J. Geophys. Res.*, **67**, 1907-1918.
- Pridmore, D. F., Hohmann, G. W., Ward, S. H., and Sill, W. R., 1981. An investigation of finite element modeling for electrical and electromagnetic data in three-dimensions. *Geophys.*, **46**, 1009-1024.
- Raiche, A. P., 1974. An integral equation approach to three-dimensional modeling. *Geophys. J. R. Astr. Soc.*, **36**, 363-376.
- Rao, I. B. R. R., Chary, M. V., and Mathur, R. R., 2003. EM studies over suspected seismic zones in peninsular India, *Mem. Geol. Soc. India*, **54**, 23-42.
- Rao, I. B. R. R., Nagendra, R., Rao, S. L. N., and Venkatramaiah, J., 2008. Very low frequency electromagnetic prospecting method-A few field applications in India. *J. Earth Syst. Sci.*, **92**, 165-177.
- Rastogi, A., Gupta, P. K., and Niwas, S., 1997. Multigrid inversion of two-dimensional EM data using bi-conjugate gradient method. *J. Assoc. Expl. Geophys., India*, **18**, 43-49.

- Reddy, I. K., Rankin, D., and Phillips, R. J., 1977. Three-dimensional modeling in magnetotelluric and magnetic variational sounding. *Geophys. J. R. Astr. Soc.*, **51**, 313-325.
- Rikitake, T., 1966. *Electromagnetism and the earth's interior*. Elsevier, Amsterdam, pp. 308.
- Rokityansky, I. I., 1982. *Goelectromagnetic investigations of the earth's crust and mantle*. Springer-Verlag, Berlin, pp. 381.
- Ruhe, A., 1979. Implementation aspects of band Lanczos algorithms for computation of eigenvalues of large sparse symmetric matrices. *Math. Comp.*, **33**,680-687.
- Saad, Y., 1980. Variations on Arnoldi's method for computing eigenelements of large unsymmetric matrices. *Lin. Alg. Appl.*, **34**, 269-295.
- Saad, Y., 1984. Chebyshev acceleration technique for solving nonsymmetric eigenvalue problems. *Math. Comp.*, **42**, 567-588.
- Saad, Y., 1994. SPARSKIT: A basic tool kit for sparse matrix calculations, version 2. Technical report, CSRD, University of Illinois and RIACS (NASA Ames Research Centre). URL [http:// www-users.cs.umn.edu/ ~saad/software/ /SPARSKIT/ sparskit.html](http://www-users.cs.umn.edu/~saad/software/SPARSKIT/sparskit.html).
- Sarkar, T. K., Siarkiewicz, K. R., and Stratton, R. F., 1981. Survey of numerical methods for solution of large system of linear equations for electromagnetic field problems. *IEEE Trans. Antennas Propagat.*, **AP-29**, 847-856.
- Sasaki, Y., 2001. Full 3-D inversion of electromagnetic data on PC. *J. App. Geophys.*, **46**, 45-54.

- Schnegg, P.-A., 1999. A computing method for 3D magnetotelluric modelling directed by polynomials. *Earth Planets Space*, **51**, 1005-1012.
- Scott, J. A., 1993. An Arnoldi code for computing selected eigenvalues of sparse real unsymmetric matrices. Council for the Central Laboratory of the Research Councils, Internal Report RAL-93-097, Rutherford Appleton Laboratory, Chilton Didcot, Oxfordshire, UK.
- Semenov, V. Y., Adam, A., Jozwiak, W., Ladanyvskyy, B., Logvinov, I. M., Pek, J., Pushkarev, P., Vozar, J. and Experimental Team of CEMES, 2008. Electrical structure of the upper mantle beneath Central Europe: Results of the CEMES project. *Acta Geophys.*, **56**, 957-981.
- Shalivahan, Sinharay, R. K., and Bhattachary, B. B., 2006. Remote reference (RR) magnetotelluric (MT) impedance estimation of wideband data using hybrid algorithm. *J. Geophys. Res.*, **111**, B11103.
- Shi, X., Utada, H., Wang, J., Siripunvaraporn, W., and Wu, W., 2004. Three dimensional magnetotelluric forward modeling using vector finite element method combined with divergence corrections (VFE++). IAGA WG 1.2 on Electromagnetic Induction in the Earth, Proceedings of the 17th Workshop, Hyderabad, India.
- Singh, R. P., and Lal, T., 1980a. Wave-tilt characteristics of EM waves over a homogeneous earth model. *IEEE Trans. on Geoscience and Remote Sensing*, **GE-18**, 285-288.
- Singh, R. P., and Lal, T., 1980b. Reflection characteristics of EM waves over homogeneous earth model. *Ann. di Geofis.*, **33**, 247-258.

- Singh, R. P., Kant, Y., and Rastogi, A., 1992. Magnetotelluric sounding in indo-Gangatic plains and Himalayan foothills region. *Indian J. Pet. Geol.*, **1**, 258-271.
- Siripunvaraporn, W., Egbert, G., and Lenbury, Y., 2002. Numerical accuracy of magnetotelluric modeling: A comparison of finite difference approximations. *Earth Planets Space*, **54**, 721-725.
- Smith, J. T., 1996a. Conservative modeling of 3-D electromagnetic fields, Part I: Properties and error analysis. *Geophys.*, **61**, 1308-1318.
- Smith, J. T., 1996b. Conservative modeling of 3-D electromagnetic fields, Part II: Biconjugate gradient solution and an accelerator. *Geophys.*, **61**, 1319-1324.
- Smith, J. T., and Booker, J. R., 1991. Rapid inversion of two- and three-dimensional magneto-telluric data. *J. Geophys. Res.*, **96**, 3905-3922.
- Smythe, W. R., 1950. *Static and dynamic electricity*. McGraw-Hill Book Co., Inc., Tokyo, pp. 616.
- Sommerfield, A., 1909. Propagation of waves in wireless telegraphy. *Ann. Phys.*, (Germany), **28**, 665-736.
- Sommerfield, A., 1926. Propagation of waves in wireless telegraphy. *Ann. Phys.*, (Germany), **81**, 1135-1153.
- Sorensen, D. C., 1992. Implicit application of polynomial filters in a k-step Arnoldi method. *J. Matrix Anal. Appl.*, **13**, 357-385.
- Sorensen, D. C., 1995. Implicitly restarted Arnoldi/Lanczos method for large scale eigenvalue calculations. *Parallel Numerical Algorithms: Proceedings of an ICASE/LaRC Workshop*, Edited by Keyes, D. E., A. Sameh, A., and Venkatakrisnan, V., Kluwer.

- Sorkhabi, R. B., Stump, E., Foland, K., and Jain, A. K., 1999. Tectonic and cooling history of the Garhwal Higher Himalaya (Bhagirathi Valley): constraints from thermochronological data. *Gondwana Research Group Memoir*, **6**, 217-235.
- Srivastava, S. P., Douglass, J. L., and Ward, S. H., 1963. The application of magnetotelluric and telluric methods in central Alberta. *Geophys.*, **28**, 426-466.
- Stratton, J. A., 1941. *Electromagnetic theory*. McGraw-Hill Book Co., Inc., Tokyo.
- Stuntebeck, C., 2003. Three-dimensional electromagnetic modeling by free-decay mode superposition. Ph.D. Thesis, Braunschweig University, Germany.
- Tabbagh, A., 1985. The response of a three-dimensional magnetic and conductive body in shallow depth electromagnetic prospecting. *Geophys. J. R. Astr. Soc.*, **81**, 215-230.
- Taflove, A., 1995. *Computational electrodynamics: The finite-differentiation time-domain method*. Artech House, Inc., Morwood, pp. 599.
- Tezkan, B., 1994a. On the detectability of a highly conductive layer in the upper mantle beneath the Black Forest crystalline using magnetotelluric methods. *Geophys. J. Int.*, **118**, 185-200.
- Tezkan, B., Hördt, A., and Gobashy, M., 2000. Two dimensional inversion of radiomagnetotelluric data: selected case histories for waste site exploration. *J. App. Geophys.*, **44**, 237-256.
- Tikhonov, A. N., 1950. On investigation of electrical characteristics of deep strata of Earth's crust (in Russian). *Dokl. Acad. Nauk USSR*, **73**, 295-297.
- Ting, S. C., and Hohmann, G. W., 1981. Integral equation modeling of three-dimensional magnetotelluric response. *Geophys.*, **46**, 182-197.

- Tong, C. H., and Ye, Q., 1999. Analysis of the finite precision Bi-Conjugate gradient algorithm for nonsymmetric linear systems. *Math. Comp.*, **69**, 1559-1575.
- Tremblay, J. C., and Carrington, T., 2007. A refined unsymmetric Lanczos eigensolver for computing accurate eigentriplets of a real unsymmetric matrix. *Elec. Trans. Num. Anal.*, **28**, 95 .
- Tyagi, D. K., 2007. 2D modeling and inversion of magnetotelluric data acquired in Garhwal Himalaya. Ph.D. thesis, Indian institute of Technology Roorkee, India.
- Unsworth, M. J., Jones, A. G., Wei, W., Marquis, G., Gokarn, S. G., Spratt, J. E., Bedrosian, P., Booker, J., Leshou, C., Clarke, G., Shenghui, L., Chanhong, L., Ming, D., Sheng, J., Solon, K., Handong, T., Ledo, J., and Roberts, B. for The INDEPTH-MT team, 2005. Crustal rheology of the Himalaya and Southern Tibet inferred from magnetotelluric data. *Nature*, **438**, 78-81.
- Van der Vorst, H. A., 2003. Iterative Krylov methods for large linear systems. First edition, Cambridge monograph on applied and computational mathematics, Cambridge University Press, UK.
- Virdi, N. S., 1988. Pre-Tertiary geotectonic events in the Himalaya. *Z. Geol. Wiss, Berlin*, **16**, 571-585.
- Vozoff, K., Hasegawa, H., and Ellis, R. M., 1963. Results and limitations of magnetotelluric surveys in simple geological situations. *Geophys.*, **28**, 778-792.
- Wait, J. R., 1982. *Geo-Electromagnetism*. Academic Press Inc., New York.
- Wannamaker, P. E., 1991. Advances in three-dimensional magnetotelluric modeling using integral equations. *Geophys.*, **56**, 1716-1728.

- Wannamaker, P. E., Hohmann, G. W., and San Filippo, W. A., 1984a. electromagnetic modeling of three-dimensional bodies in layered earth using integral equations. *Geophys.*, **49**, 60-74.
- Wannamaker, P. E., Hohmann, G. W., and Ward, S. H., 1984b. Magnetotelluric responses of three-dimensional bodies in layered earths. *Geophys.*, **49**, 1517-1533.
- Ward, S. H., 1967. Electromagnetic theory for geophysical application. In: *Mining Geophysics, Vol. II, Chap II, Part A*, Soc. Expl. Geophys., Tulsa, Oklahoma, 10-196.
- Ward, S. H., and Hohmann, G. H., 1988. Electromagnetic theory for geophysical application. In: *Electromagnetic methods in applied geophysics, Vol. 1*, M.N. Nabighian (Ed.), Soc. Expl. Geophys., 131-311.
- Weaver, J. T., 1971a. The general theory of electromagnetic induction in a conducting half space. *Geophys. J. R. Astr. Soc.*, **22**, 83-100.
- Weaver, J. T., 1971b. Image theory for an arbitrary quasi-static field in the presence of a conducting half-space. *Radio Sci.*, **6**, 647-653.
- Weaver, J. T., 1994. *Mathematical methods for geo-electromagnetic induction*. Research Studies Press Ltd., Taunton, Somerset, England.
- Weaver, J. T., and Brewitt-Taylor, C. R., 1978. Improved boundary condition for the numerical solution of E-polarization problems in geomagnetic induction. *Geophys. J. R. Astr. Soc.*, **54**, 309-317.
- Wei, W., Martyn, U., Alan, J., John, B., Tan, H., Doug, N., Chen, L., Li, S., Kurt, S., Paul, B., Jin, S., Deng, M., Juanjo, L., David, K., and Brian, R., 2001. Detection of

- widespread fluids in the Tibetan crust by magnetotelluric studies. *Sci.*, **292**, 716-718.
- Weidelt, P., 1975. Electromagnetic induction in three-dimensional structures. *Geophys. J. R. Astr. Soc.*, **41**, 85-109.
- Weidelt, P., 1995. Bounds on local averages of one-dimensional electrical conductivity distributions. *Geophys. J. Int.*, **123**, 683-714.
- Weidelt, P., 2007. Guided waves in marine CSEM. *Geophys. J. Int.*, **171**, 153-176.
- Weidelt, P., 2009. Personal communication.
- Weitemeyer, K. A., Constable, S. C., Key, K. W., and Behrens, J. P., 2006. First results from a marine controlled-source electromagnetic survey to detect gas hydrates offshore Oregon. *Geophys. Res. Lett.*, **33**, L03304.
- Wilkinson, J. H., 1965. *The algebraic eigenvalue problem*. Clarendon Press, Oxford.
- Wright, P. M., Ward, S. H., Ross, H. P., and West R. C., 1985. State of art geophysical exploration for geothermal resources. *Geophys.*, **50**, 2666-2696.
- Xiong, Z., 1992. EM modeling three-dimensional dtructures by the method of system iteration using integral equations. *Geophys.*, **57**, 1556–1561.
- Xiong, Z., 1999. Domain decomposition for 3D electromagnetic modeling. *Earth Planets Space*, **51**, 1013-1018.
- Xiong, Z., Luo, Y., Wang, S., and Wu, G., 1986. Induced polarization and electromagnetic modeling of a three-dimensional body embedded in a two-layered anisotropic earth. *Geophys.*, **51**, 2235-2246.
- Xiong, Z., Raiche, A., and sugeng, F., 2000. Efficient solution of full domain 3D electromagnetic modelling problems. *Explor. Geophys.*, **31**, 158-161.

- Xu, S., Ruan, B., Zhou, H., Chen, L., and Xu, S., 1997. Numerical modeling of 3-D terrain effect on MT field. *Science in China Series D: Earth Sciences*, **40**, 269-275.
- Yee, K. S., 1966. Numerical solution of initial boundary value problems involving Maxwell's equations in isotropic media. *IEEE Trans. Ant. Prop.*, **AP-14**, 302-307.
- Yuan, J., and Edwards, R. N., 2000. The assessment of marine gas hydrates through electrical remote sounding: Hydrate without a BSR?. *Geophys. Res. Let.*, **27**, 2397-2400.
- Zhdanov, M. S., 2009. *Geophysical electromagnetic theory and methods*. Elsevier, Amsterdam, pp. 848.
- Zhdanov, M. S., and Fang, S., 1996. Quasi-Linear Approximation in 3-D EM Modeling. *Geophys.*, **61**, 646–665.
- Zhdanov, M. S., and Fang, S., 1997. Quasi-Linear Series in Three-Dimensional Electromagnetic Modeling. *Radio Sci.*, **32**, 2167–2188.
- Zhdanov, M. S., Varentsov, I. M., Weaver, J. T., Golubev, N. G., and Krylov, V. A., 1997. Methods for modeling electromagnetic fields results from COMMEMI – the international project on the comparison of modeling methods for electromagnetic induction. *J. App. Geophys.*, **37**, 133-271.
- Zhou, P. B., 1993. *Numerical analysis of electromagnetic fields*. Springer-Verlag, pp. 406.